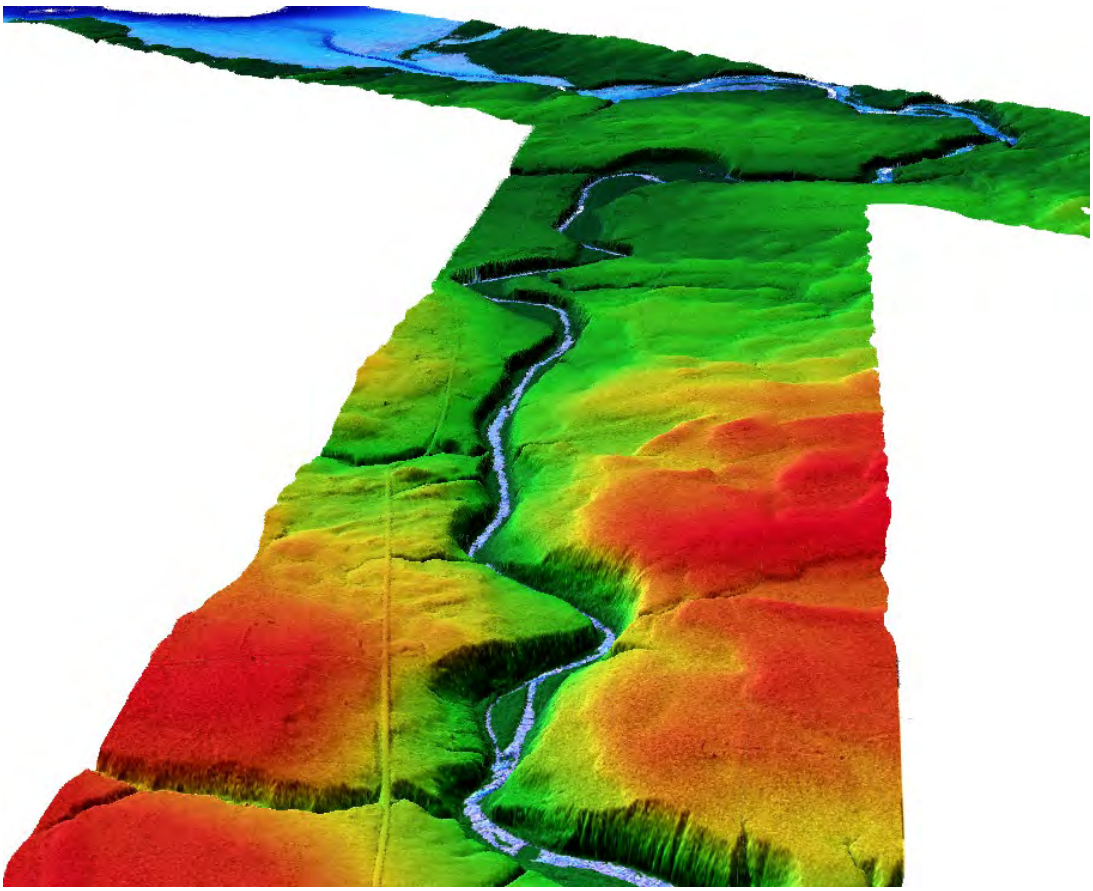

TOPO-BATHYMETRIC LIDAR

For Coastal and River Flood Assessment

The role and value of bathymetric lidar for inland and coastal flood mapping in Nova Scotia.

Timothy Webster, PhD, Nathan Crowell, Dedipya Kodavati, et al.
Applied Geomatics Research Group, NSCC, Tim.Webster@nscc.ca

Submitted to Nova Scotia Department of Municipal Affairs, March 2020.

Topo-bathymetric lidar for coastal and in-land flood assessment

How to cite this work and report:

Webster, T., Crowell, N. and Kodavati, D. 2020. Topo-bathyemtric lidar for coastal and in-land flood assessment. Nova Scotia Department of Municipal Affairs. Technical report, Applied Geomatics Research Group, NSCC Middleton, NS.

Contents

Table of Figures

List of Tables

Executive Summary

Topographic-bathymetric lidar (TB-lidar) systems typically utilize two lasers: a near infrared (NIR) laser for topographic data collection (land features and water surface) and a green laser for bathymetric data collection (seabed or river or lakebed). These systems generate high-resolution seamless digital elevation models (DEMs) that include land and submerged elevation. Most systems are equipped with a camera system, either a simple RGB or multispectral camera that can be utilized to generate coincident orthophoto mosaics from the same survey. There are shallow water TB-lidar systems that produce high density lidar points in water depths of 10s of centimeters to ca. 15 m depending on water clarity. There are deep-water systems that acquire data at a lower density and typically require special aircraft requirements (cooling of the laser and in some cases 2 camera holes). This document describes the background theory of TB-lidar and the requirements for relatively clear water for this technology to be affective. It also presents a brief description of project planning and data processing with some recommended specifications for TB-lidar surveys for the purpose of flood assessment.

TB-lidar can enhance flood mapping in many areas including coastal, estuarine and in-land flooding. Additional areas of enhanced capability include using the data from TB-lidar for coastal areas to begin to incorporate wave-runup into flood risk assessments. The most significant advancements of including TB-lidar in the flood assessment process are in the areas of enhanced hydrodynamic modelling, both for coastal inundation and for in-land flooding. The ability of TB-lidar to map the submerged terrain along the coast, in the riverbed and lakes, makes it an ideal tool to produce the seamless DEM's required for such modelling. In addition, the data can be used to estimate bed roughness so that bed friction parameters can be assigned which influence the velocity of the water. Some of the main advantages of a hydrodynamic (HD) modelling approach over the GIS based still water or the HAND (Height Above Nearest Drainage – River GIS inundation method) approach is that the HD approach produces both inundation levels and thus can derive flood water depth and current speeds which can be used together (depth X velocity) to build more complex hazard maps. Another advantage of HD modelling over the still water approach is that the still water approach tends to overestimate the flood extent, although more study is required to exactly quantify this. Comparisons are made between HD models and GIS still-water levels for two coastal sites in this report. The fact that most TB-lidar sensors are equipped with a camera system and aerial photos are acquired simultaneously with the lidar provides the ability to generate a high-resolution orthophoto for land use assessment which can be used for floodplain roughness mapping, aid in lidar error estimation and quantification and enhanced visualization of the flood event (depth & hazard).

In this study, an in-land survey was conducted for River John in Pictou County, NS. As a result of aircraft availability and delays the survey was conducted in late October when conditions were not as favorable as July and August when the water levels were lower, and the water was clearer. However, even with those limitations the TB-lidar survey was successful and is used to demonstrate how a seamless-DEM of the floodplain and river channel can be acquired and used as input into hydrodynamic models. In addition to the aerial survey, several river cross-sections were collected using survey grade GNSS equipment and compared to the lidar DEM. The differences in elevation on hard surfaces had a mean and standard deviation of 5 cm with a 7 cm respectively and for the river channel 8 cm and 19 cm respectively. Water level instruments were deployed along the Northumberland Strait and at two locations in River John. These instruments recorded the storm surge and river discharge associated with Hurricane Dorian in Sept. 2019. A storm surge of 1.5 m was associated with this event and the water levels were used in demonstrating how TB-lidar can be used for hydrodynamic flood risk assessment. Specifications are recommended for both coastal and in-land river surveys which include point densities, suitable water conditions, typical products, and vertical accuracies.

1. Topo-bathymetric theory

Topographic-bathymetric lidar (TB-lidar) systems typically utilize two lasers: a near infrared (NIR) laser for topographic data collection (land features and water surface) and a green laser for bathymetric data collection (seabed or river or lakebed). These systems generate high-resolution seamless digital elevation models (DEMs) that include land and submerged elevation. Most systems are equipped with a camera system, either a simple RGB or multispectral camera and in some cases a hyperspectral scanner that can be utilized to generate coincident orthophoto mosaics from the same survey. Although shallow water TB-lidar sensors are relatively new ca. 2012, deeper water airborne laser bathymetry sensors have been around since the late 80's and early 90's and have been used for hydrographic charting as well as to demonstrate a variety of coastal research applications ranging from bottom classification and bathymetric mapping for coastal management (Brock and Perkins, 2009). The United States Army Corps of Engineers (USACE) have established the Joint Airborne Lidar Bathymetry Technical Center of Expertise (JALBTCX) to perform operations, research, and development in airborne lidar bathymetry and have produced a new book on airborne topographic-bathymetric lidar (TB-lidar), entitled Airborne Laser Hydrography II that provides a detailed history of the technology and a review of the current systems and applications of TB-lidar and is free to download (Philpot and William, 2019).

Topo-bathymetric lidar works by emitting a near-infrared (NIR) and a green laser from an aircraft, typically in an elliptical or circular scan pattern, and measuring the travel time of the laser pulses to and from the land, water surface, and seabed (Figure 1-A, B). The NIR laser pulse reflects off the land or water, while some of the green laser pulse is reflected at the air-water interface and the rest is refracted and attenuated as it passes through the water column and reflected from the seabed to return to the detector (Figure 1-C). The travel path of the green laser is complex as it passes from air to water the speed of the light slows down by approximately 1/3 and thus is refracted. Once in the water column, the green light is scattered and losses its energy exponentially with depth until it reflects off the sea-river bed and returns to the detector. In order to compensate for the refraction angle and change in the speed of light from air to water, the system must be able to detect the water surface. The NIR laser returns and the green laser returns are used to detect the water surface in order to compensate for these optical path effects of the green laser changing media from air to water and the return path back to the detector. The beam divergence of the NIR laser is typical of that of topographic lidars on the order of 0.5 mrad whereas the green laser will have a larger beam divergence, for example the Leica Chiroptera-II is 3 mrad compared to the Riegl VQ-880-G is 1 mrad.

Unlike sonar, where the speed of sound in water is significantly affected by salinity and temperature, TB-lidar works equally well in fresh or saltwater. However, the water clarity is typically the limiting factor for a successful TB-lidar survey. The reflectance of seabed or river-lakebed also plays a role in addition to water clarity for determining how deep the green laser can penetrate and reflect back to the sensor.

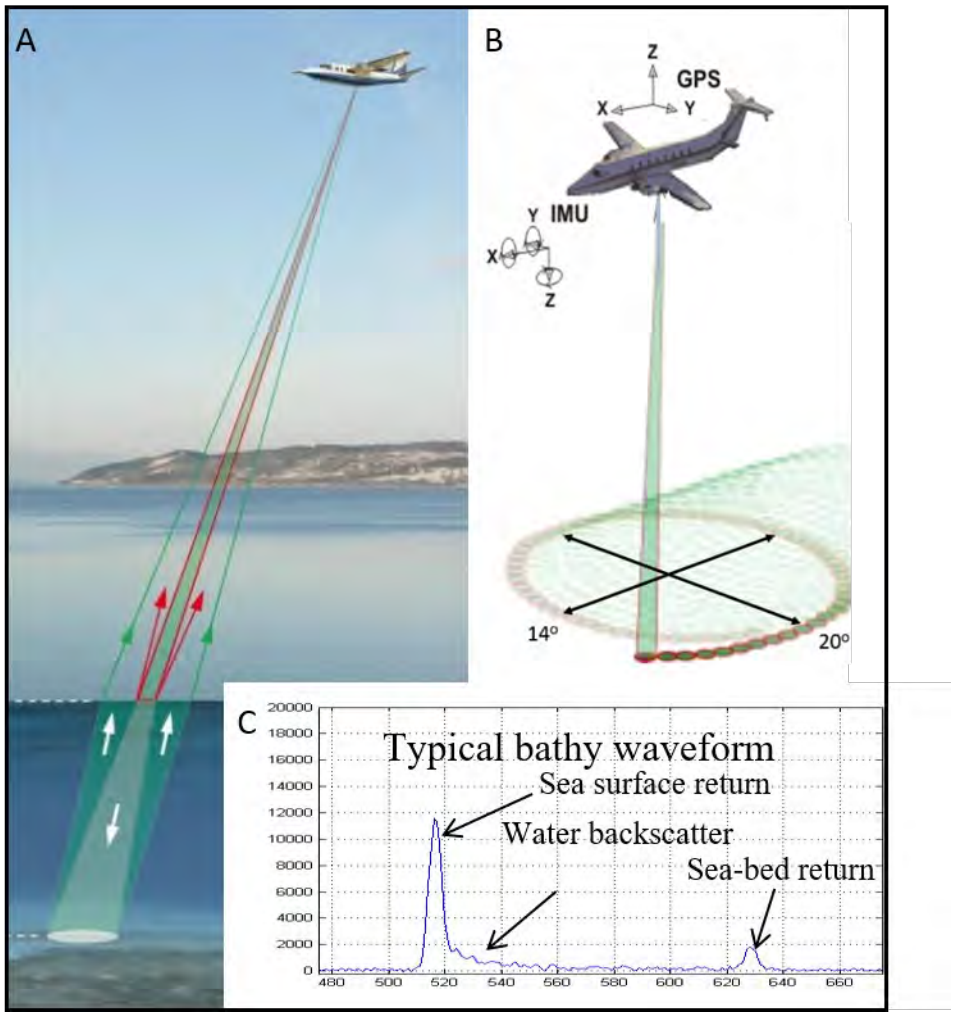

Figure 1 Topo-bathymetric lidar (TB-lidar) theory. A - Interaction of the NIR and green laser light when travelling between air and water, refraction and scattering take place. B - Typical elliptical scan patter for TB-LIDAR with navigation system GPS+IMU. C – Typical waveform captured from the green laser. (Source Leica)

2. Topo-bathymetric lidar processing

The processing of TB-lidar data after a mission is similar to topographic lidar data processing as the first step is to process the trajectory of the aircraft using a ground base station and the GSS and inertial measurement unit in the sensor. During a TB-lidar survey the waveforms of the NIR and green laser are recorded and are related to the trajectory by GNSS time. Once related to the trajectory, the waveforms and then post processed into discrete points. In some cases, for example the NIR waveforms are processed during the time of flight into discrete points. During the processing of the green laser waveforms, the water surface is detected and modelled in order for the green laser pulse path to be refracted at the water surface and the range adjusted by the change of the speed of light in water. One distinct advantage of surveying hydrography with TB-lidar to echo sounding is that the speed of the light in water is only marginally affected by changes in salinity and temperature compared to how these properties effect the speed of sound in water. This property makes TB-lidar ideal for surveying in estuarine environments where fresh and saltwater mix in a sometimes-complex fashion. The typical recorded waveform from the green laser consists of a large amplitude return from the water surface

followed by the volume backscatter of the laser pulse through the water column and then a peak representing reflection off the seabed or riverbed (Figure 1-C, Figure 2-F). The amplitude of the reflected seabed peak of the waveform is recorded as the lidar intensity and can reveal information on the cover type of the seabed or riverbed such as differences between sand and vegetation (Figure 2-F). The elliptical scan pattern offers a few advantages compared to the traditional saw-tooth pattern many topographic lidars use. The green laser does not penetrate air bubbles (white caps, surf zone, etc.) as a result of scattering, however if the forward scan does not penetrate a breaking wave, the backward part of the scan probably will as a result of the movement of the crest of the wave and bubbles. Another advantage is that most targets get surveyed twice from two angle, thus reducing and possible shadow effects, which is also very beneficial for capturing more points along steep slopes, for example coastal cliff faces (Figure 2-A).

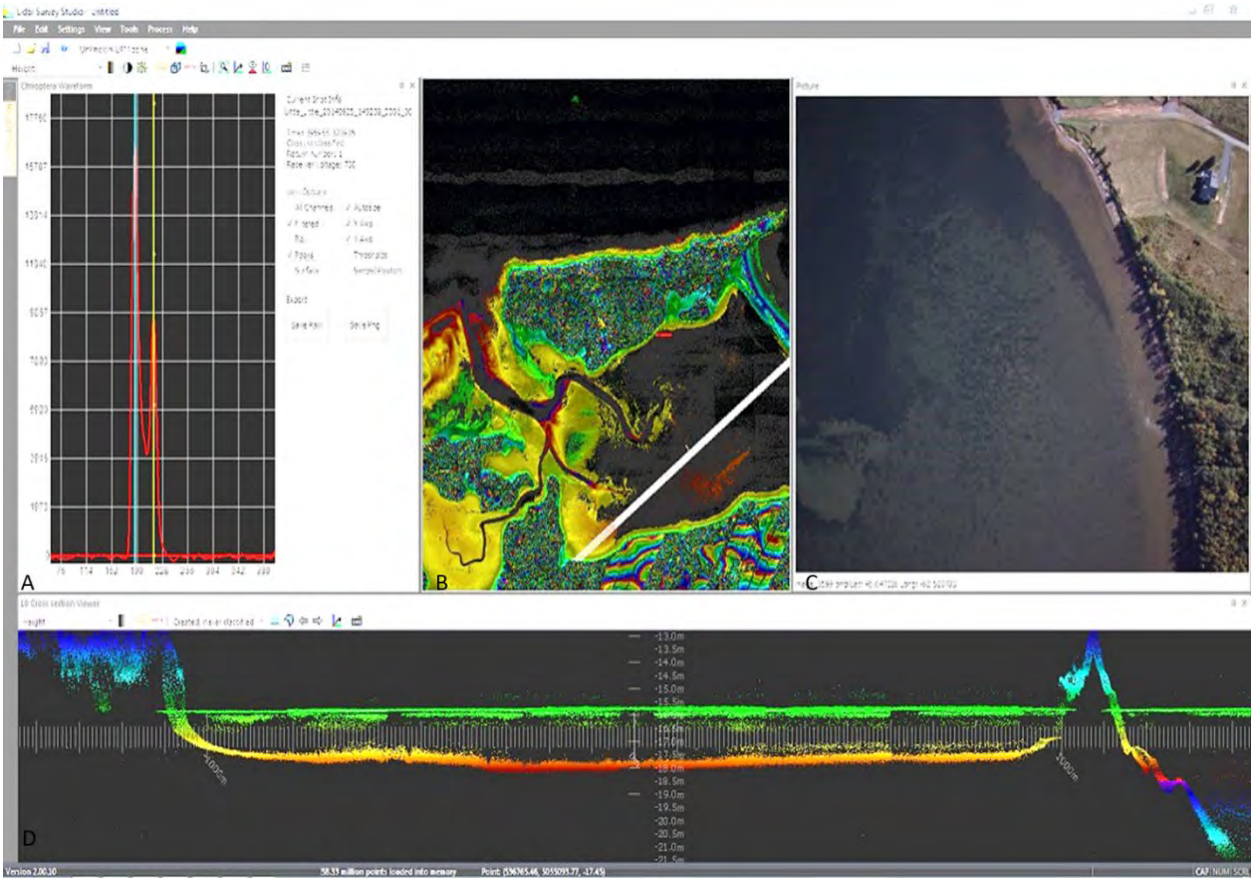

Figure 2 Examples of TB-lidar points across the land-water boundary, Little Harbour, NS. A – Shows the green laser waveform with discrete points (blue line-water surface, yellow line-bathymetry). B – Shows a cross-section cut through the seamless elevation points at Little Harbour. C – Shows a quality assurance photograph captured and linked to the lidar points. channel with multiple flight lines. D – Shows a cross-section extracted across the harbor with the water surface in green.

Once the waveform data have been processed into discrete points, the points are classified into broad categories of land, non-land (vegetation-buildings), water, bathymetry, submerged objects and noise. Further refinement of this initial classification if typically required using many of the standard tools that are used for topographic lidar processing such as Terrascan™. Once the point data have been classified various GIS raster products can be derived from one survey (Figure 3). Most TB-lidar system are equipped with a RGB or multispectral camera system, for example the Chiroptera-II is equipped with the

RCD30 camera which will capture RGB and NIR imagery that can be used to colourize the lidar point cloud and generate orthophotos (Figure 3-D). The coincident orthophoto can be very useful in assisting with the interpretation of some of the lidar returns. In addition to the production of a seamless DSM and DEM, the amplitude of the reflected laser pulses can be used to construct intensity images (Figure 3-E).

This intensity image can be merged with the elevation data to produce a hybrid image that is useful for visual interpretation (Figure 3-F). The light losses energy exponentially with depth in water, thus low bathymetric intensity levels can result from shallow dark objects (e.g. seagrass) or simply bright objects at greater depths (e.g. sand). The intensity can be sampled for a common cover type, such as sand, at different depths and used to build an empirical relationship where the intensity can be "depth normalized" to compensate for this decay of energy (Webster et al., 2016).

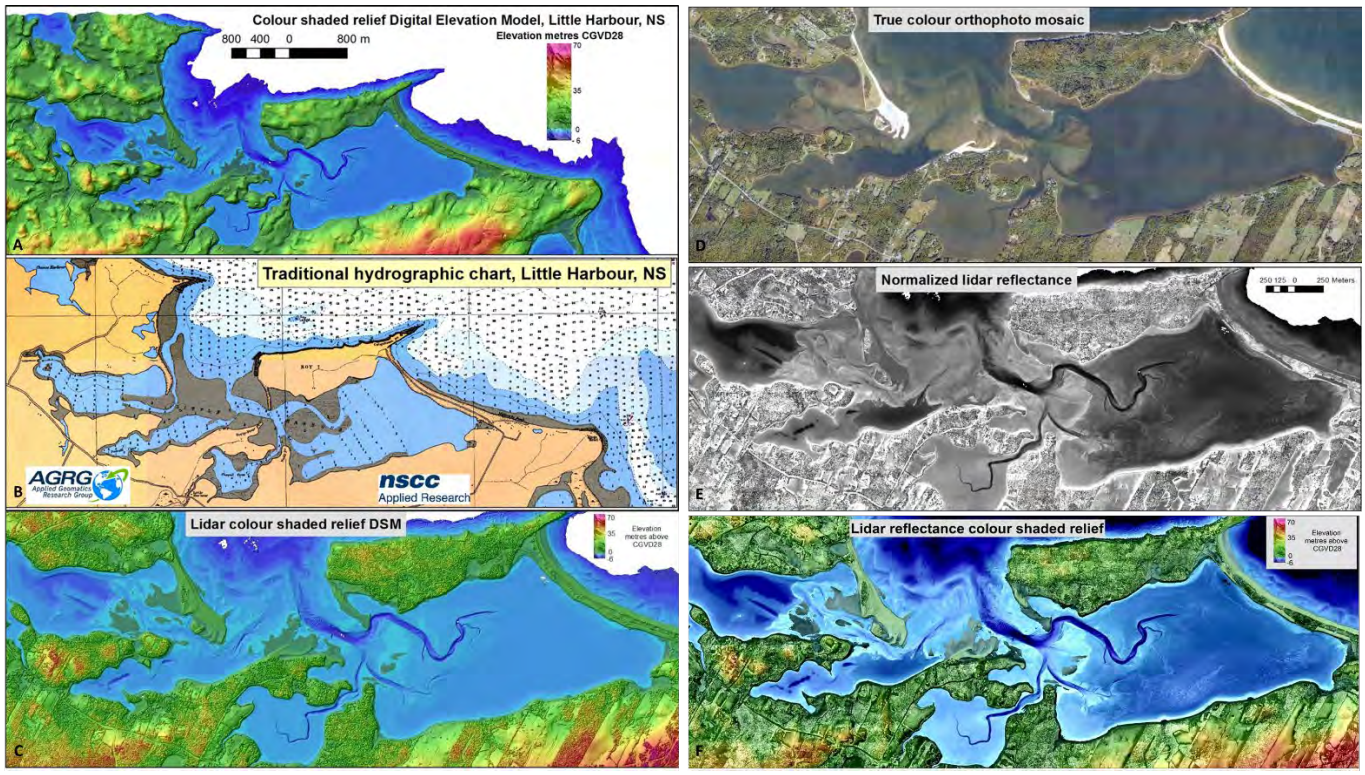

Figure 3 Examples of derived GIS raster layers from one TB-lidar survey, Little harbor, NS. Comparison between the A - TB-lidar seamless DEM and the B- nautical chart ca. 1946 from CHS. C - Seamless Digital Surface Model (DSM) from the TB-lidar . D – True colour orthophoto from the TB-lidar survey. E – Normalized lidar intensity-amplitude where the NIR returns are used for the land and the green returns for the seabed. F – Merged TB-lidar DSM with the intensity showing variations on the seabed materials (Figure adapted from Webster et al., 2016).

As previously mentioned, TB-lidar technology is ideally suited for surveying water bodies with variable salinity and temperature as the speed of light is virtually not affected as compared with the speed of sound used in echo sounding. An example of a freshwater lake surveyed with TB-lidar is presented in the following section. Zwickers Lake is approximately 26 km south of Middleton and was surveyed by AGRG-NSCC using the Leica Chiroptera-2 system in 2015 and 2016 (Figure 4, Figure 5). Depth contours have been generated for the lake and compared to those available from NS Department of Fisheries and Aquaculture (https://novascotia.ca/fish/documents/lake-inventory-maps/5-A-zwicker.pdf). Figure 4

shows the extra detail observed in the lake bathymetry utilizing the TB-lidar sensor. Figure 5 shows an esker on the land south of the lake which extends into the lake and eventually emerging back on land southeast of the lake.

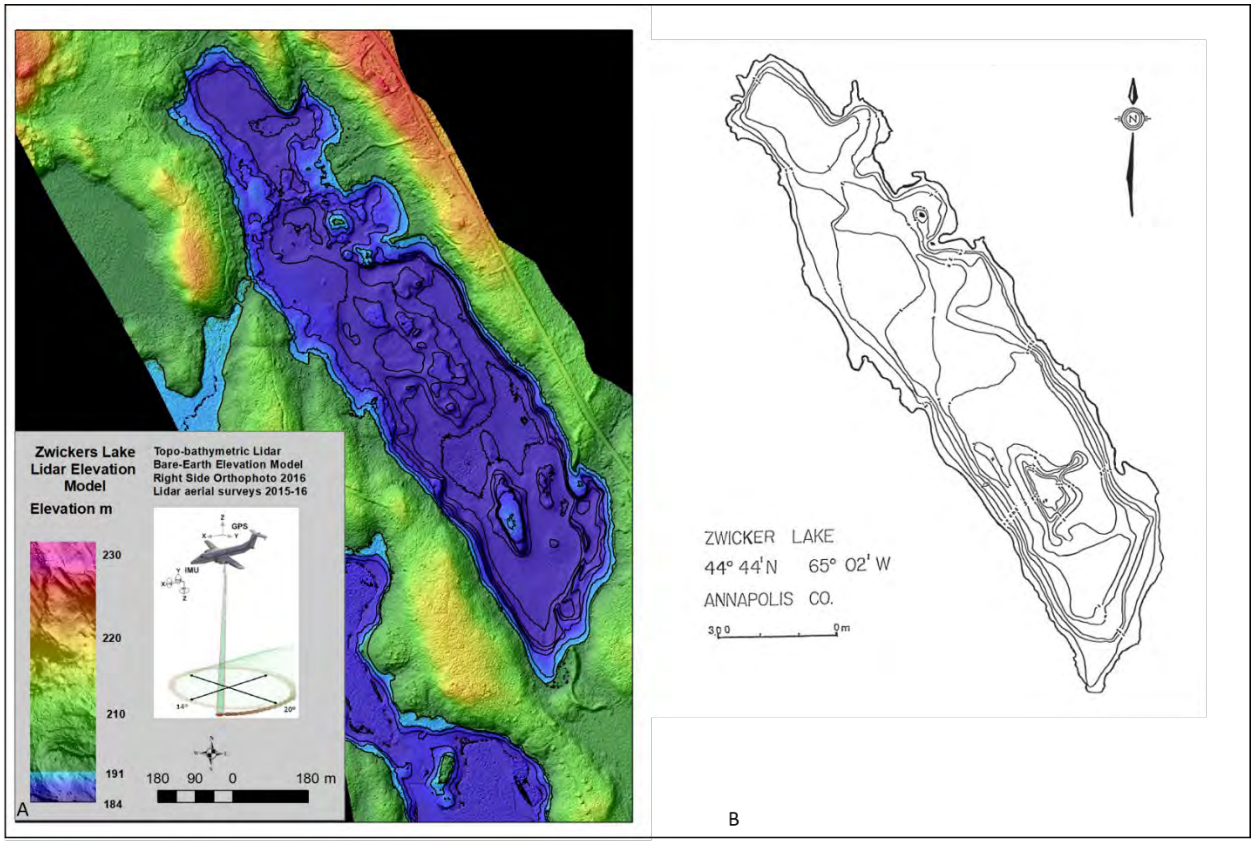

Figure 4 Example of a TB-lidar Zwickers Lake survey and NS Fisheries and Aquaculture lake contours. A – Example of the seamless DEM for Zwickers Lake, Annapolis County. B – Comparison to the previous elevation data for Zwickers Lake, note the enhanced detail of the 1 m contours.

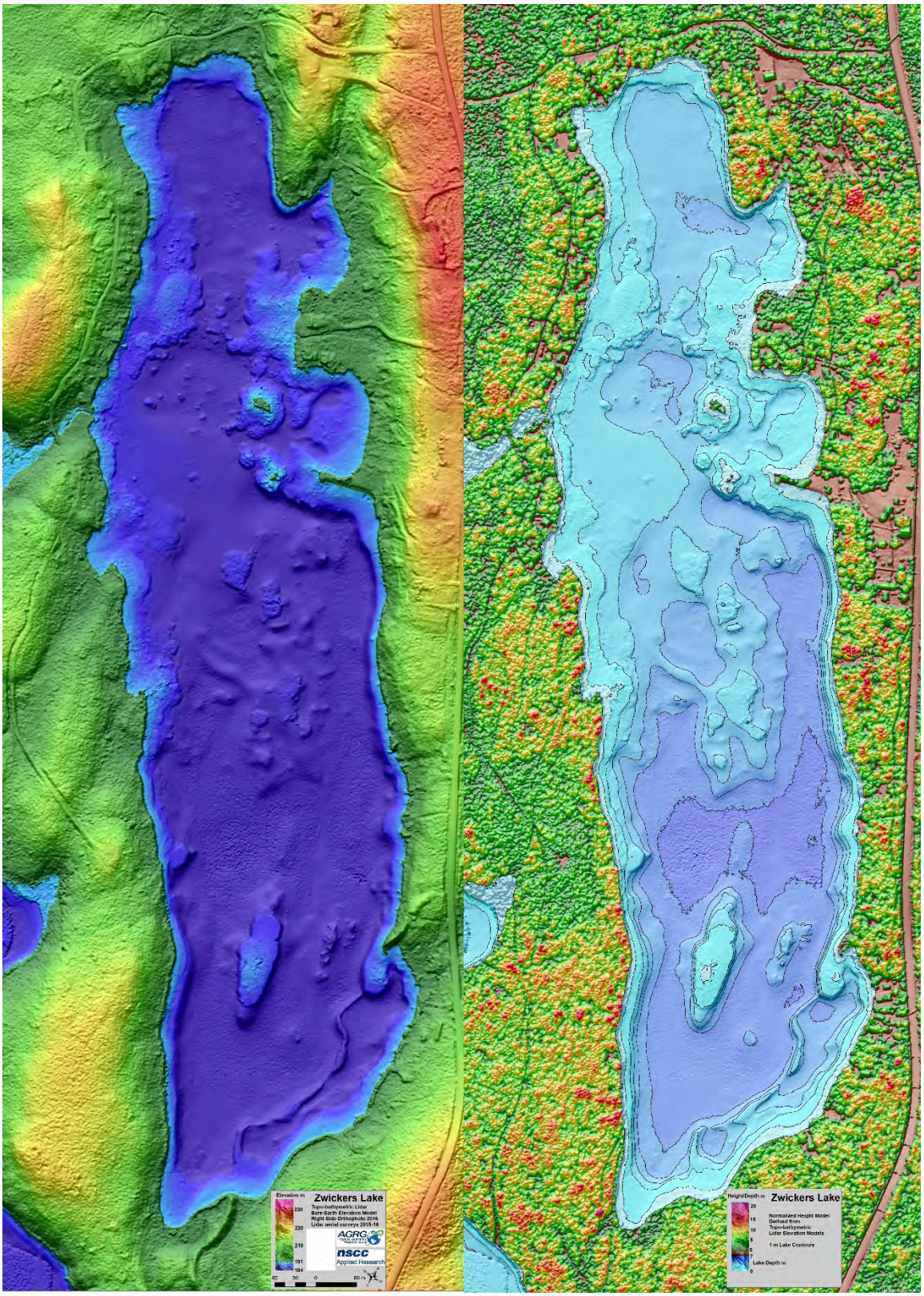

Figure 5 Example of TB lidar products for Zwickers Lake. One the left is a seamless DEM and on the right is a Normalized Height Model and Lake depth map with 1 m depth contours.

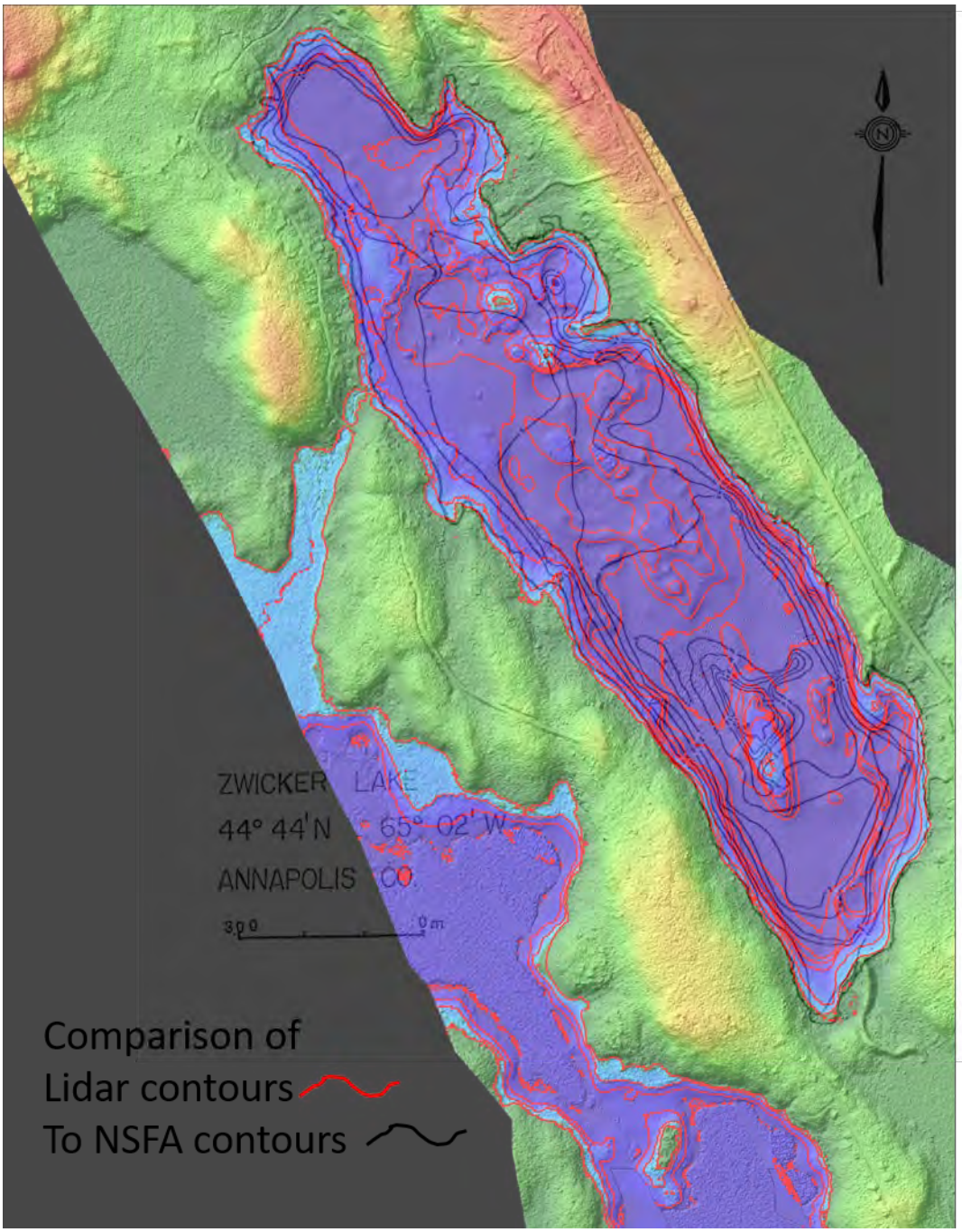

Figure 6 Comparison of the lake contours derived from TB-lidar (red) with those from NSFA (black).

3. Other TB-lidar Examples

The number of applications for TB-lidar has grown exponentially since the early systems became operational in the late 1980's and early 1990's, where the primary application was nautical charting. Since then, as more systems were developed and users gained access to the unique datasets, uses have expanded into a wide variety of coastal engineering and coastal zone management applications (Brock and Perkins, 2009). As previously mentioned, one of the main uses in the past of TB-lidar was for hydrographic charting. The Canadian Hydrographic Service (CHS), Department of Fisheries and Oceans

(DFO), contracts TB-lidar surveys to be conducted to update nautical charts in areas that are too shallow for ship-based echo sounding surveys to be conducted safely (CHS, 2019). TB-lidar has also been demonstrated in the Gulf of St. Lawrence along the Quebec coastline, where the Optech SHOALS 1000 system, classified as deep water system, was used to survey a section of the coastal zone and derive habitat classes from a combination of elevation and reflectance data (Collin et al. 2011, 2012). More recently the new generation of shallow water TB-lidar systems, such as the Leica Chiroptera-II, was used in the Maritime Canada coastal zone for multiple applications including: updating hydrographic charts, high-resolution bathymetric maps to support aquaculture site selection and monitoring, mapping seagrass beds and seaweed biomass, input into hydrodynamic models (ex. oil spill preparedness), and mapping near shore geological structures (e.g. Webster et al. (2016, 2019)). The technology has been used around the world for a variety of applications. The seabed substratum and vegetation were mapped for a study site within the Baltic Sea (Tulldahl et al., 2012; Velasco et al, 2014) and off the coast of Spain using the Hawkeye II deep water system. In Australia the Tenix LADS (laser airborne depth sounder) Mk II lidar was used for differentiating canopy structure of macroalgae communities (Zavalas et al., 2014). In the United States, JALBTCX used the Optech SHOALS to examined the evolution of large scale crescentic bars before and after hurricanes within the Gulf of Mexico (Arifin & Kennedy, 2011) and examined ephemeral sand waves in the response to hurricane forces in the surf zone (Kennedy et al., 2008) and to map regions of the Great lakes (Reif et al., 2013). The Chiroptera I sensor was used to map shallow lakes in Alaska (Paine et al., 2015). Other TB-lidar sensors on the market are produced by Optech known as the Coastal Zone Mapping and Imaging Lidar (CZMIL-Nova) and the Reigl VQ-880-G (Allouis et al., 2010). Other applications where TB-lidar has been used include: post storm response, geomorphological feature extraction, shorelines and shoreline change, dune and depositional coastal features, bluff and cliff edge detection, and environmental mapping (Brock & Perkins, 2009).

4. TB lidar Coverage and Applicable areas

Older deep water bathymetric lidar sensors could not resolve the water surface from bottom at depths less than 2 m, whereas the new shallow water sensors have a limit on the order of ca. 20 cm making the ability to generate seamless terrain models a reality. The main improvements to the latest generation of sensors is the shorter transmit pulse lengths of the green laser and better detection limits. The main limiting factor affecting depth of penetration of TB-lidar is water clarity. Thus, turbidity management is recommended for a successful survey. The main sources that can adversely affect the green laser from penetrating the water column come from suspended sediment, although algae blooms may also have negative impacts, and dissolved organic matter which can be common in some lakes and streams that originate in bogs. For coastal and riverine TB-lidar surveys, the weather proceeding a survey can greatly influence the conditions and probability of success. For example, in coastal areas an onshore wind can cause waves which intern cause sediment to become suspended and thus high turbidity conditions where the particles in the water cause the light to scatter and not penetrate to the seabed (Webster et al., 2016). In the case of riverine environments, heavy rain can cause sediment and organic materials to be transported into the river, thus degrading the water clarity. Turbidity management involves understanding the environmental conditions that cause high turbidity (e.g. wind and rain) and the length of time for the water to clear before it is suitable for a survey. A secondary factor affecting the depth penetration of the green laser is the brightness of the seabed or riverbed, darker objects have tendency to absorb the green light, while light objects, such as sand, reflect more of the green light and thus allow the signals to reflect back to the sensor at greater depths.

A Secchi disk is commonly divided into black and white quadrants in order to maximize contrast, and the depth at which the black and white disk disappears from view is called the "Secchi depth". Clear waters will have a larger Secchi depth than more turbid waters, and the size of the Secchi disk may need to be adjusted for different water clarity conditions. TB-lidar shallow water sensors typically have a depth rating of 1.5 times the Secchi Depth, and deep water systems have a rating of 2-3 times the Secchi Depth.

Water clarity is measured by the Diffuse Attenuation Coefficient (Kd) (Figure 7). The rate of change of the irradiance energy, E is a function of the depth (Ed) and is a measure of water clarity that is similar in concept to the Secchi depth in that the rate of change will be faster in turbid waters than in clear waters. The rate of change of Ed, or logarithmic derivative of Ed is the diffuse attenuation coefficient, Kd (Philpot & William, 2019).

$$K_d = -\frac{d \ln E_d(z,\lambda)}{dz} = -\frac{1}{E_d(z,\lambda)} \frac{dE_d(z,\lambda)}{dz} \qquad (m^{-1})$$

Figure 7 Diffuse Attenuation Coefficient Kd, E(λ) radiance distribution over a hemisphere at a certain wavelength of energy (λ) at depth z (from Philpot & William, 2019).

Kd values can change rapidly for a body of water as previously demonstrated with the change in turbidity levels over a few days, however the typical values of *Kd* range from 0.05 for clear water to 0.11 for turbid water for wavelengths used in TB-lidar. As will be discussed in the planning section of this document, satellites such as MODIS can estimate *Kd* for certain wavelengths which can aid to determine if a TB-lidar survey is feasible for an area or the best season to attempt a survey.

Ideally when conducting TB-lidar coastal surveys, there are multiple survey sites within the region that have different shoreline orientations such that not all sites will be turbid as a result of a regional wind event (Figure 8). It can be challenging to obtain Secchi depths leading up to a TB-lidar survey and thus ensure the conditions are suitable. There are numerous weather stations available on-line that can provide insights into the past and current wind and rain conditions, however it still can be challenging to predict the turbidity conditions, especially after a wind event when the water needs time to clear.

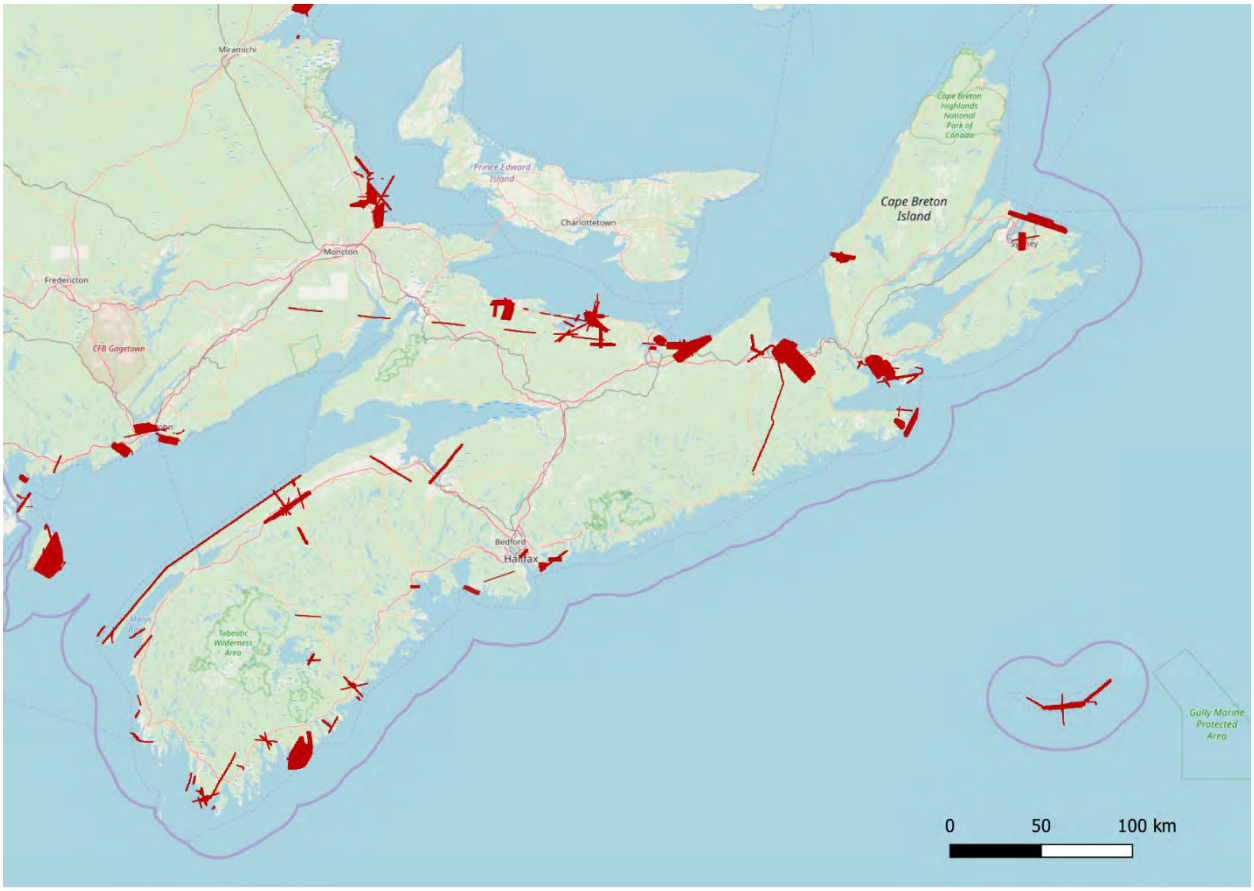

Figure 8 Example of topo-bathymetric lidar collected by AGRG-NSCC since 2014 (red areas) with their Leica Chiroptera 4X system.

There are areas around Nova Scotia such as the upper bay of Fundy (Minas Basin to Truro) and (Chignecto Bay near Amherst) where the water is turbid all the time as a result of the amount of fine grain sediment in the area. Other parts of Nova Scotia water systems (lakes and river) are known to have dark colour water “Mersey Tea” that are also not conducive to TB-lidar acquisitions. The dark water acts as a light trap and absorbs the green laser light, thus providing very little penetration. At the estuary mouth of these river like Liverpool for example, the water mixes with the cleaner ocean water and the lidar can penetrate again, but not up stream. The dark colour of the water is a result of tannins from the vegetation and dissolved organic matter thought to be originating from bogs in the watershed (source GeoNova) (Figure 9, Figure 10).

There are no direct measurements on water clarity, however there have been Secchi depth measurements taken for some lakes, although these can change over time (https://data.novascotia.ca/Environment-and-Energy/Nova-Scotia-Lake-Chemistry-Data/vn55-yjyi). Areas with Secchi depths greater than 3 m have good potential for a successful TB-lidar survey (Figure 9, Figure 10). With these surrogate measures of water clarity it is still recommended to visit the potential survey site to evaluate the water clarity conditions and variability.

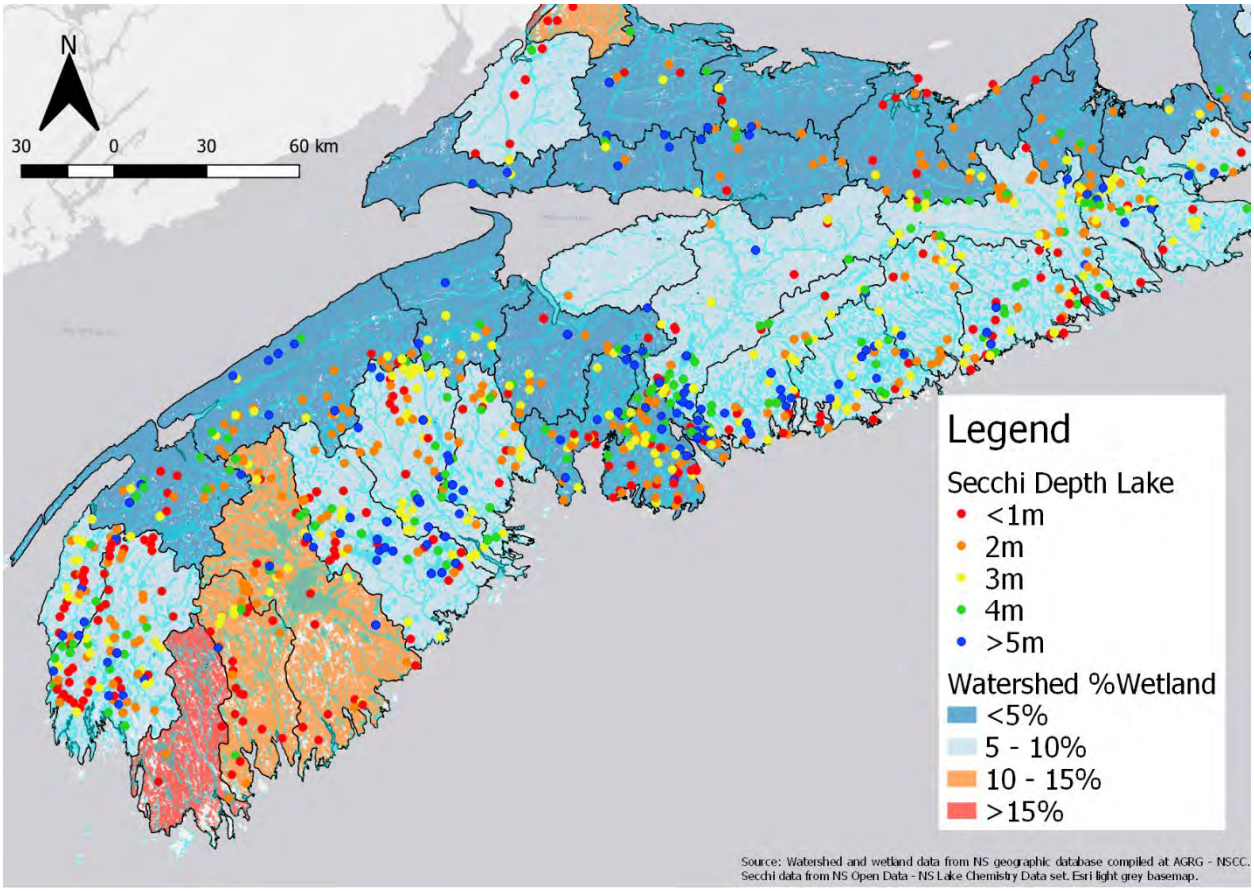

Figure 9 Example of Secchi depth measurements and the amount of wetlands per primary watershed for southern NS.

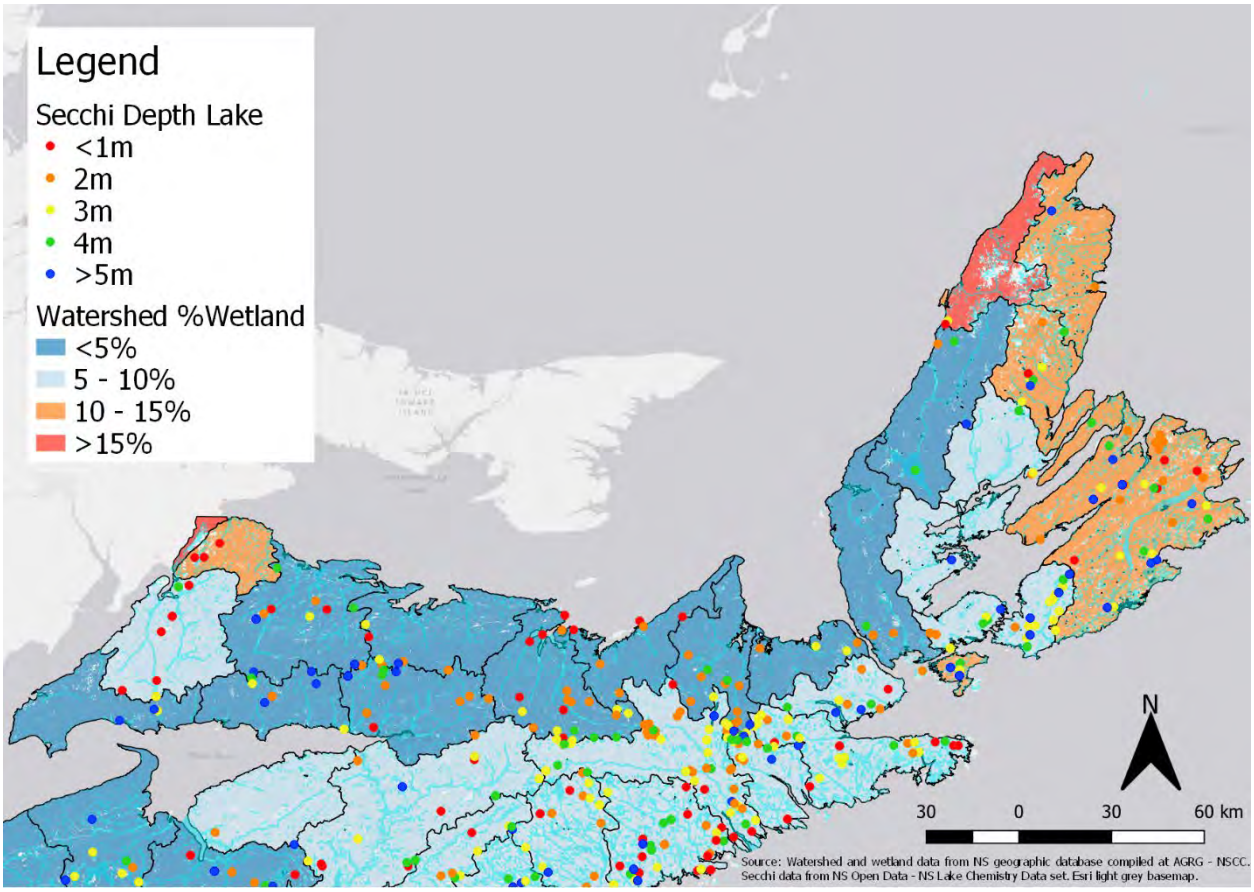

Figure 10 Example of Secchi depth measurements and the amount of wetlands per primary watershed for northern NS

Another approach has been used by researchers at the Bedford Institute of Oceanography where they have used medium resolution satellite data (MODIS at 250 m resolution) to calculate suspended sediment concentrations and to estimate Secchi depth (personal communication César Fuentes-Yaco, DFO). The MODIS imagery can be used to establish a time series where cloud free imagery is available. This can provide an estimate on how turbid the conditions are and the best time of year to attempt a survey. The 250 m resolution provides a synoptic view of the region and highlights the variable water clarity conditions for a given date (Figure 11).

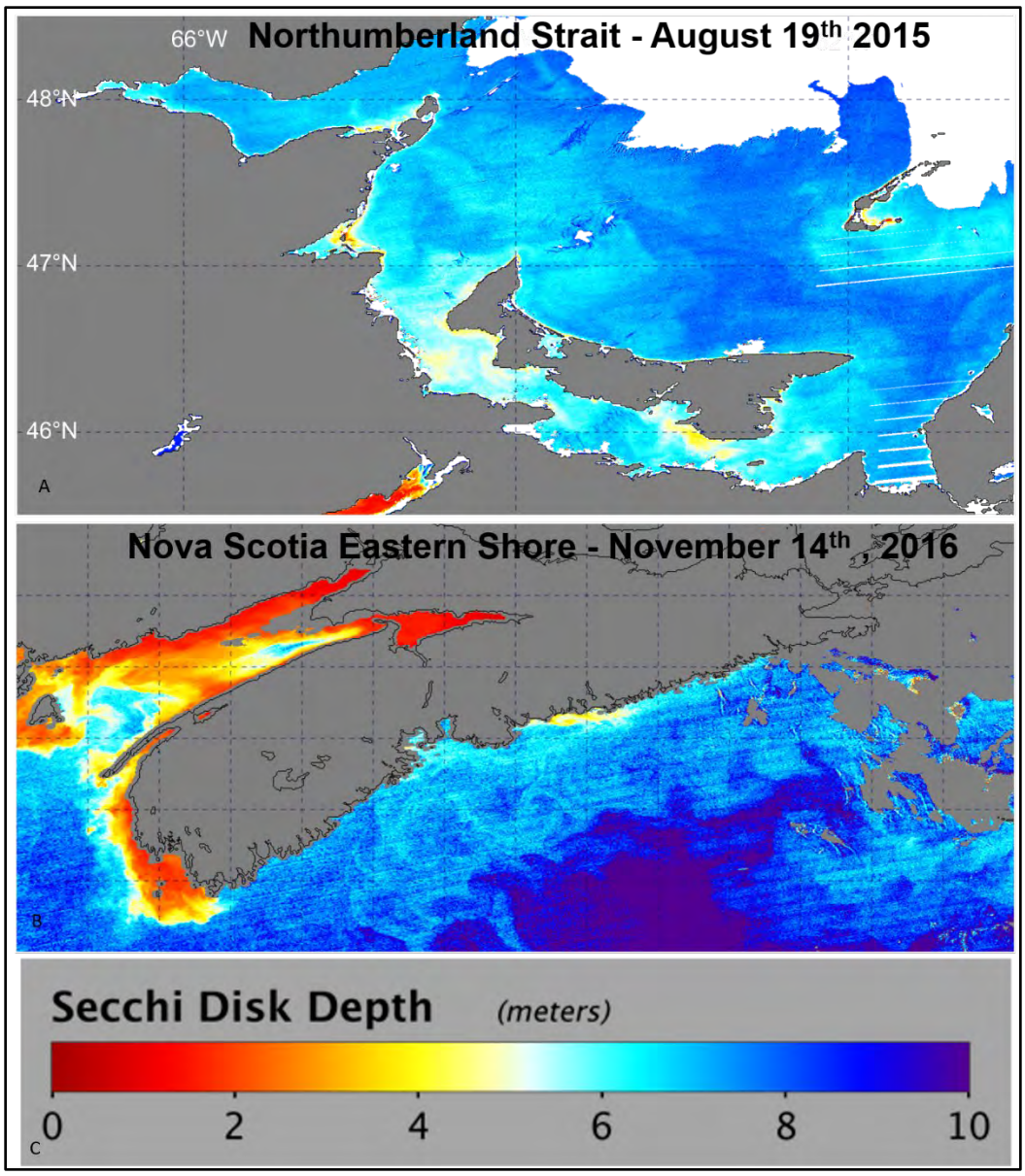

Figure 11 Example of MODIS derived images of water clarity estimates. A – Secchi depth estimates for the Northumberland Strait. B - Secchi depth estimates for the eastern shore and Bay of Fundy (Images courtesy of César Fuentes-Yaco, DFO).

The coastal water clarity conditions are highly variable and most effected by onshore winds and in some cases tide and land run off. In many areas high turbidity conditions can clear after a few days of calm weather which allows the suspended sediment to resettle on the bottom and the water clarity improves. An example of the variability of Total Suspended Matter (TSM) is demonstrated from analysis of MODIS satellite images where the bands are processed to produce a TSM index. The spatial and temporal variability along the Northumberland Strait demonstrates this (Figure 12). The Sentinal-2 satellite has optical data at a 10 m resolution and is freely available from the European Space Agency (ESA). ESA also provides the ability for a TSM index to be calculated and could provide a higher resolution approach to obtaining time series of water clarity conditions.

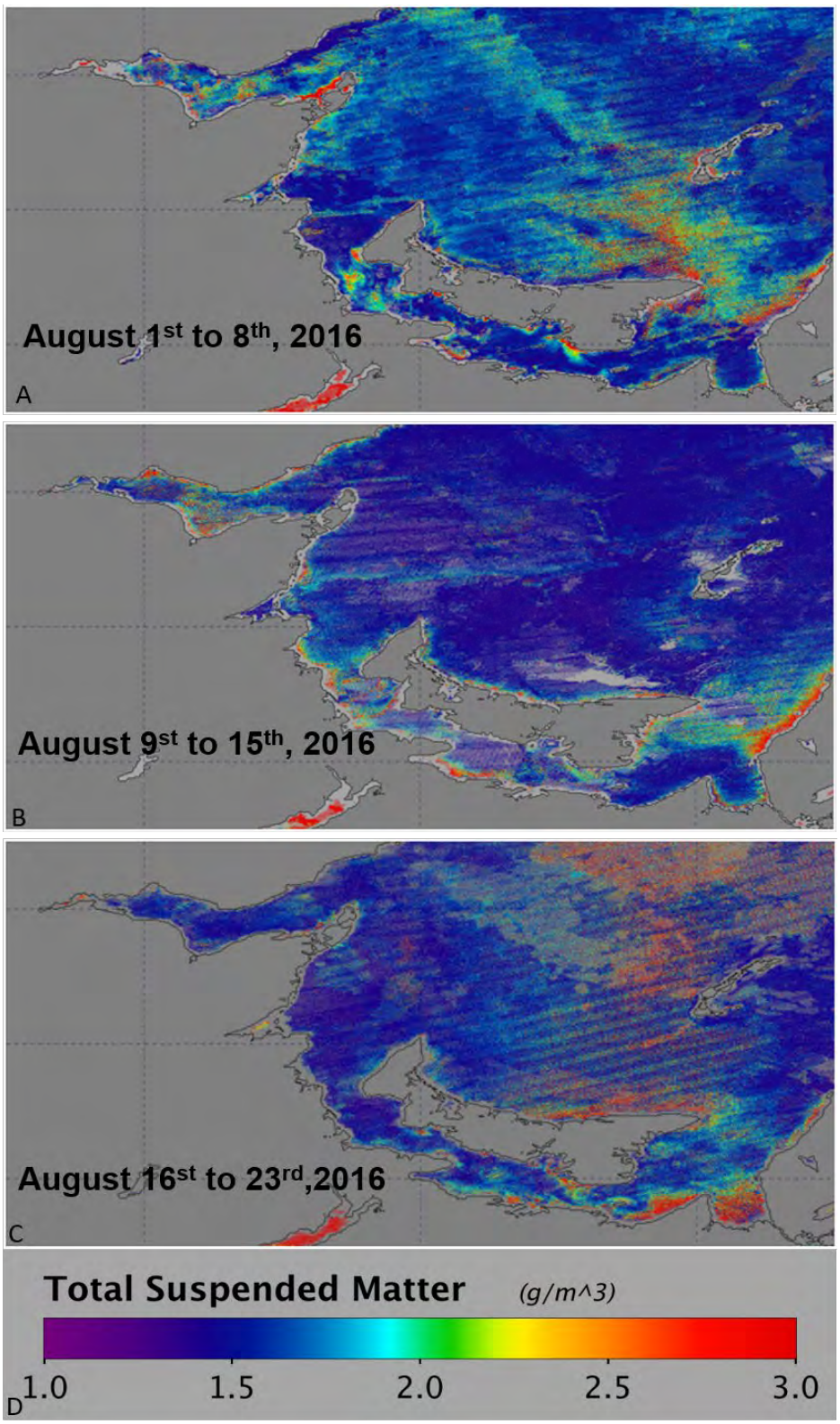

Figure 12 Example of Total Suspended Matter index derived from MODIS satellite imagery for the Northumberland Strait. A – Map derived from a composite image Aug. 1-8, 2016. B - Map derived from a composite image Aug. 9-15, 2016. C - Map derived from a composite image Aug. 16-23, 2016. (Images courtesy of César Fuentes-Yaco, DFO).

In general TB-lidar is applicable for any body of water with sufficient clarity. In the upper Bay of Fundy (Minas Channel and Cobequid Bay and Chignecto Bay) where the suspended sediment is always very high and the water very turbid, this technology would not be applicable. Similarly, in southwest Nova Scotia where the rivers and lakes often have very dark waters (Mersey Tea) as a result of the high concentration of tannins and dissolved organic carbon, this technology is not applicable. However, for the rest of coastal Nova Scotia including the Bay of Fundy south of Minas Passage, the Atlantic coastline and the Northumberland Strait conditions are suitable for successful TB-lidar surveys (Figure 8). As with any coastal water body, however, water clarity conditions can be affected by strong on-shore winds and wave conditions that stir up the bottom sediments. In the event of turbid conditions being cause in wind and waves, once the wind speeds lower to less than 15-20 km/hr the water can clear in 1-2 days for most of our coastline. In the lakes and rivers in central and Northern Nova Scotia the water clarity appears suitable for successful application of this technology. In these areas, intense rain events can wash materials into the river and lake systems (sediment and organic material) and cause the clarity to decrease. In some lakes, biological processes including algae blooms and vertical circulation can affect water clarity. In all situations, one should observe the water clarity of a potential survey site and monitor it during the survey operations.

5. Project planning

In general, for both tidal and riverine TB-lidar surveys, it is better to survey when the water is lower, this increases your likelihood of maximizing your coverage of the bottom. Once a study area has been determined, the main factors to consider after the water clarity issue, is pulse or point density, which can influence how many flight lines are required and the level of overlap between survey lines. In general, if the desired point density can be achieved with a single flight line, then 20-30% overlap is sufficient to ensure there are no gaps during the collection process. Special flight planning software is utilized which takes into account the flying altitude, the field of view of the sensor, the amount of overlap and flying speed. The normal flight operation involves initializing the navigation system (establishing GNSS lock and warming up the IMU) and flying close to or over the GNSS ground control station before starting the survey lines (Figure 13). Previously GNSS base stations were set up over known survey monuments (e.g. High Precision Network (HPN) monument) and observations were collected at 1 second epoch to be used for post processing positioning. Today, however there are many active control stations that are continuously recording at 1 second intervals that can be utilized for control of a TB-lidar survey. During the planning of the survey, a cross-line is usually included as a means of internally checking that the calibration of the sensor is sound and that all of the data line up, regardless of flight orientation (Figure 13-B). In the following figure the planned survey lines are shown as well as the actual trajectory that was flown for part of the survey (Figure 13). This includes flying over the GNSS base station, here depicted as HPN8650.

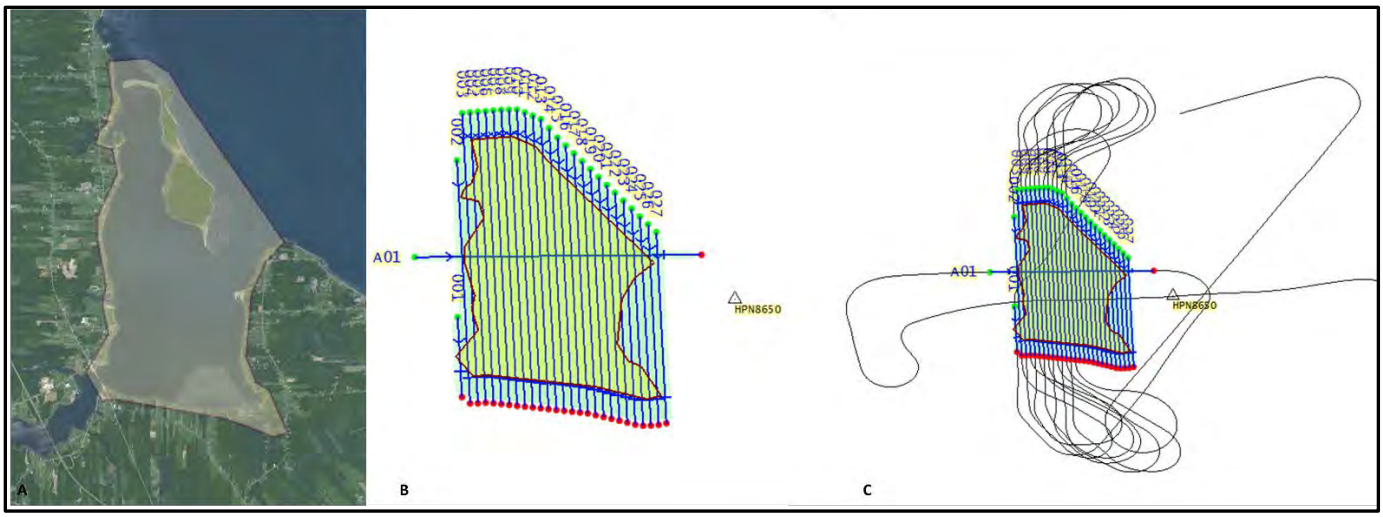

Figure 13 Example of a TB-lidar survey site. A - The area of interest is outlined initially. B - Flight planning software is used to optimize the flight line orientation to minimize the number of lines and turns. C – The actual flight trajectory of the aircraft for half of the survey.

5.1 Data collection

During the data collection phase of the project, most TB-lidar surveys are flown at approximately 400 m above ground level. If coastal surveys are being conducted and any islands need to be surveyed, a twin-engine aircraft must be used in order to be able to safety make a landing if there is an engine failure. In addition to this safety requirement, most TB-lidar sensors require a larger aircraft (twin engine typically) because of the increased power requirements for the green laser. Although not required, it is often desirable to have a field team on the water during the survey. The field team can collect Secchi depth readings to confirm the water clarity conditions, and depending on the end application of the data, collect bottom samples and photographs to determine the benthic cover material. The field team would also collect GNSS check points both of hard surfaces on land to check the topographic lidar and GNSS points directly on the seabed or utilize high-precision echo sounding and navigation equipment to obtain bathymetric check points.

5.2 Data processing and management

As previously mentioned, the first step in processing after the flight is to obtain the GNSS observations data from the base station, typically at 1 second epoch. These data are then used to process the aircraft GNSS data recorded at 1 second and the IMU data, typically recorded at 200 Hz. Processing the navigation data provides the aircraft trajectory which utilizes GNSS time that can then be linked to the laser ranges and camera events in order to position them. The lidar waveforms are either processed during the time of flight or in the case of the green laser, post processed into discrete points using proprietary software unique to the sensor. Once the waveforms are processed to discrete points, they can be inspected and if required integrated with the aerial photos and the RGB and or NIR spectral values attached to the lidar data as additional attributes. When the data are initially processed it is broadly classified into land, water and bathymetry but typically needs refinement. This refinement can utilize standard classification software that is used for topographic lidar, although the process of classifying valid bathymetric returns from noise requires different parameters than classifying ground from vegetation in the case of topographic lidar. However, the processes are generally the same, the LAS point data is tiled into 1 km blocks or whatever size is manageable, depending on point density, and

then the classification refinement is conducted. Figure 16 shows the standard classes that are used for bathymetric features. It is important to note that these classes do not include a submerged aquatic vegetation class, which is becoming an important product that can be derived from a TB-lidar survey. Once the classified LAS (ver. 1.4) is complete, then data validation can take place on the point cloud. It is important to note that GIS systems such as ESRI's Arc Map do not currently support these higher bathymetric classes (e.g. class 40 bathymetry) in LAS 1.4. Alternatively, raster GIS products can be constructed as outlined earlier and these be validated by comparing against check points or other data sources of a higher quality.

5.3 Data validation

Wherever possible it is always recommended that independent check points of a higher precision be collected to compare to both the topographic and bathymetric lidar points. The standard approach is to utilize Real Time Kinematic (RTK) GNSS to collect check points. An example of validation of a river survey is shown below where GNSS (GPS) points have been collected on the bridge surface as well in the floodplain and across the river channel (Figure 14).

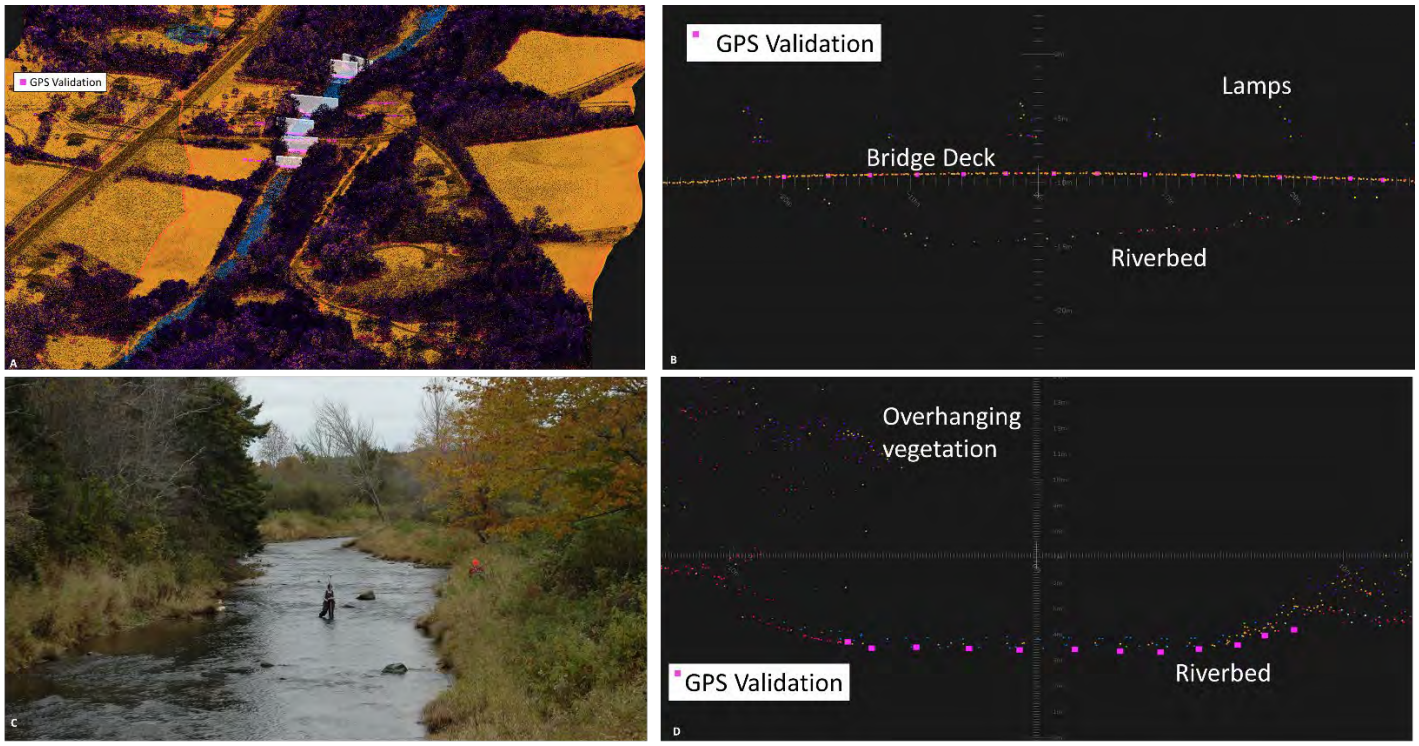

Figure 14 Validation of a TB-lidar river survey. A – point cloud showing cross-sections where validation check points have been collected. B GPS points collected on the bridge deck are compared to those of the lidar. Note that the river channel is captured even under the bridge as a result of the elliptical scan angle. C. Photo of GPS points being collected across the channel. D. Cross-section of GPS points (purple squares) and lidar points showing good agreement in the channel even with overhanging vegetation.

When the GNSS points are overlaid on the DEM, the difference in elevation DZ is calculated by subtracting the DEM elevation from the GNSS elevation. The difference in Z or delta Z (DZ) can be used to assess the accuracy of the seamless DEM (Figure 15).

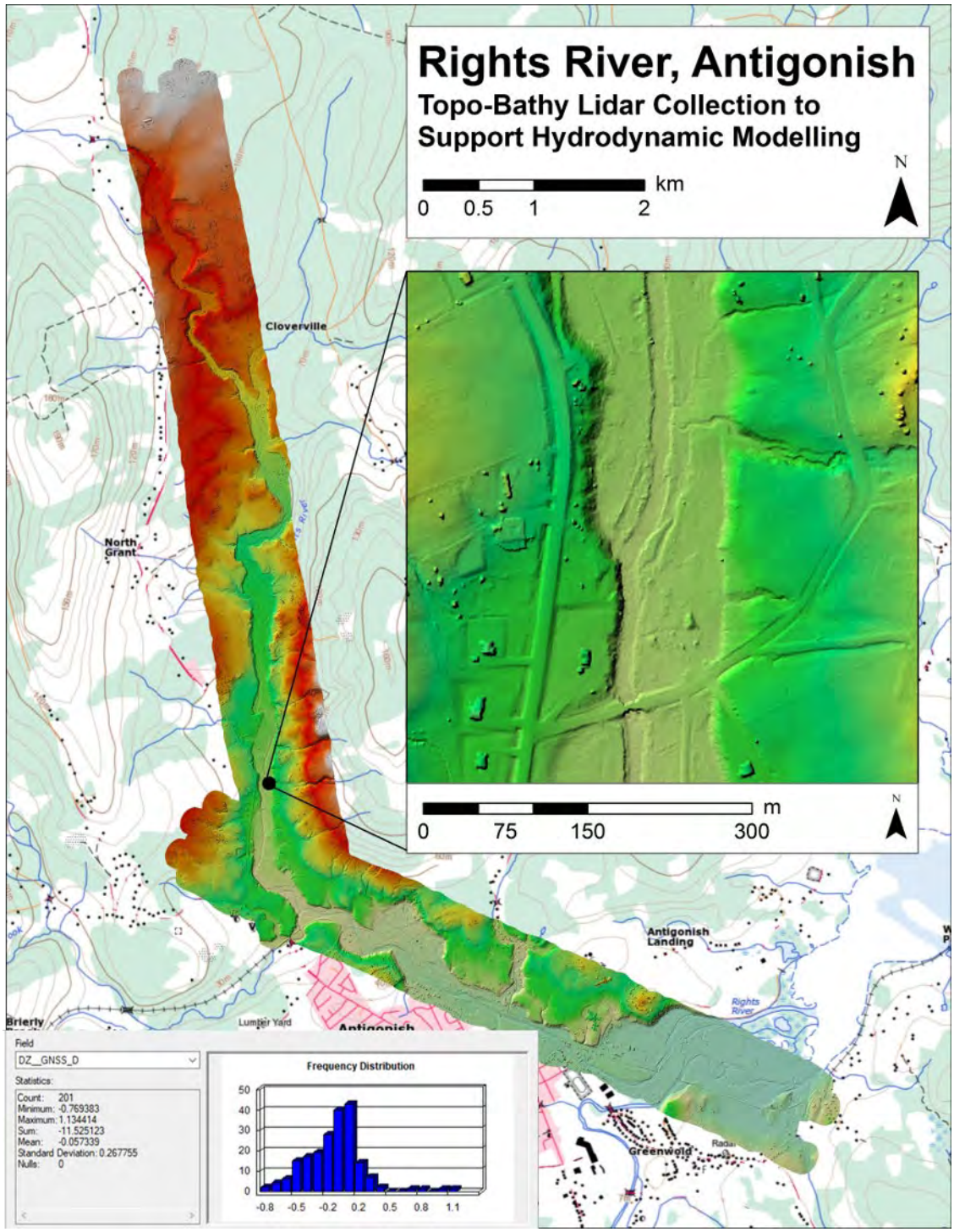

Figure 15 TB-lidar extent of Rights River, Antigonish, NS. Inset of histogram of DZ (GNSS-lidar DEM) for river cross-sections. The DZ mean =-0.06 m, and DZ standard deviation = 0.27 m.

6. NOAA and Canadian Hydrographic Service specifications

The National Oceanic and Atmospheric Administration's (NOAA) National Geodetic Survey (NGS) Remote Sensing Division (RSD) Coastal Mapping Program (CMP) requires the collection of airborne topographic/bathymetric lidar and digital camera imagery data to enable accurate and consistent measurement of the national shoreline. The NOAA specifications call for bathymetric lidar data to be collected from the water's edge to the specified extent as detailed in the provided project boundary shapefile or to laser extinction, whichever comes first. For shoreline mapping and modeling uses, it is particularly important to have good bathymetric data in the very shallow (0-4 m) areas. For this reason, the lidar systems, software, and processing procedures shall enable measurement of bathymetry in this very shallow region. The sensor used for this mapping shall have an operational measurement depth range equal to or greater than a 1.5 Secchi depth. Sensors with segmented beams, shall also comply with these specifications (National Science Technology Council, 2016).

A nominal density of 2 points per square meter shall be points, collections should be planned and executed to produce a first-return point cloud that approaches a regular lattice of points, rather than a collection of widely spaced high density profiles of the terrain. NOAA's overarching objective is to obtain clean, seamless (i.e., free of gaps or discontinuities) topographic-bathymetric data across the intertidal zone and shallow nearshore zone. With this overarching objective in mind, the following decision tree shall be used for determining when to collect shoreline flight lines: a. Optimal environmental conditions: If the mission crew encounters` optimal environmental conditions for nearshore topo-bathy mapping (defined here to mean exceptional water clarity relative to typical conditions in project site, as well as low wind and wave conditions in the surf and nearshore zones) at any met, to support the gridding of a 1 meter GSD DEM. The bathymetric or submerged topographic portion of the lidar collect shall be planned for a nominal density for 2 points per square meter, although it is understood that this density may not be met due to certain environmental conditions that cannot be controlled. Shoreline flight lines are tide-coordinated to ensure the highest probability of achieving clean, seamless topo-bathy coverage across the intertidal and shallow nearshore zones. This typically requires flying each shoreline flight line twice: once within 20 percent of the Mean Range of tide around Mean Lower Low Water and once within 30 percent of the Mean Range of tide around Mean High Water, as well as during favorable water clarity conditions. The Mean Range of tide is defined as the difference in height between Mean High Water and Mean Low Water. To clean, classify, and merge the collected topographic and bathymetric data acquired along the designated project boundaries. An integrated topographic-bathymetric point cloud dataset is an important component in understanding the land-sea interface and effectively adapting to sea level rise, mitigating impacts from natural hazards, storm surges, and flooding, as well as preserving the integrity of coastal habitats and resources. In addition to the proposed coastal strategy discussing specifications they also recognize the importance of research and development to advance the technology. "Given the rapid evolution of topographic and bathymetric lidar and other coastal mapping technologies, and with new applications of the data continually emerging, research and development (R&D) programs are important to mapping efforts." (National Science Technology Council, 2016).

Unlike NOAA that utilize shallow water TB-lidar sensors, the Canadian Hydrographic Service (CHS) requires deep water sensors capable of 2-3 Secchi depth penetration. The following is an excerpt of some of the specifications required by CHS for bathymetric lidar surveys. The Contractor must include the following mission planning parameters to maximize data collection efficiency and effectiveness.

These include low tide coordination, swath width, swath overlap, navigation, base station proximity and visibility. Contractor must account for; demonstrate; and implement strategies to mitigate the impact of the following parameters, during mission planning and execution of the survey: Topography of the survey area and surrounding area; such as mountainous terrain that could prevent or hinder flight operations. Weather, including but not limited to: water clarity and turbidity management. Native phenomenon; such as kelp growth and algae blooms during summer months. Maximum data acquisition around low tide, this is described as two hours prior and two hours after. Minimum 200 metres inland, horizontally. Include all bays, inlets, islands, peninsulas, inter tidal zones, flood plains, river deltas and land areas that are within the survey blocks. Plan flight lines to maximum expected depths, with the intention of collecting data to the point of extinction, not necessarily to the full extent of the survey blocks. The maximum flight altitude must be 400m. Adjacent swaths must have a minimum overlap of 20%. Flight lines pattern must be flown in alternate directions to help identify systematic errors. The regular system of lidar lines must be supplemented by a minimum of two check lines per survey zone for verifying and evaluating the accuracy and reliability of surveyed soundings and positions. Cross lines must be run across all planned lidar survey lines at angles ranging from 45 to 90 degrees more than the original survey line. Cross lines must be acquired and processed to the same accuracy and data quality standards as the main survey lines and shall be included in the grids submitted as the final bathymetric product of the survey. All data must be collected and recorded in Julian day and Coordinated Universal Time (UTC). It should be noted that the purpose of CHS flights is for hydrographic charting and not flood risk mapping.

The Contractor must deliver classified LAS 1.4 point cloud format using the classification (Figure 16).

Classification Value	Meaning
40	Bathymetric point (e.g., seafloor or riverbed; also known as submerged topography)
41	Water surface (sea/river/lake surface from bathymetric or topographicbathymetric lidar; distinct from Point Class 9, which is used in topographic-only lidar and only designates “water,” not “water surface”)
42	Derived water surface (synthetic water surface location used in computing refraction at water surface)
43	Submerged object, not otherwise specified (e.g., wreck, rock, submerged piling)
44	International Hydrographic Organization (IHO) S-57 object, not otherwise specified
45	No-bottom-found-at (bathymetric lidar point for which no detectable bottom return was received)
46-63	Reserved
64-255	User definable

Figure 16 Example of the bathymetric classes available in LAS 1.4.

As mentioned the use of LAS 1.4 with the bathymetric classes is somewhat problematic if using these data with ArcGIS. The ESRI platform does not recognize these higher number classes such as 40-45, thus making it impossible to derive a DEM from the LAS 1.4 data using that software.

The International Hydrographic Organization (IHO) specifies an Order 1 standard for bathymetric data shallower than 100 m and defines the maximum allowable total vertical uncertainty (TVU) at 2-σ

confidence interval (International Hydrographic Organization, 2008). The TVU varies with depth and is defined in the equation below, where 'a' represents the portion of uncertainty that does not vary with depth (e.g. airport position uncertainty from the trajectory processing), 'b' represents the coefficient of the portion of the uncertainty that varies with depth 'd'. All TBL system currently on the market can exceed the Order 1 requirements set out by IHO for depths less than 100 m (Saylam, et al. 2018).

$$TVU = (a^2 + [b \times d]^2)^{1/2}$$

In order to better appreciate how the TVU varies with depth for these different IHO orders, the TVU has been calculated at typical depths achieved by shallow water lidar sensors (15 m) and deep-water sensors (20 m and greater) (Table 1).

IHO Order	***a***	***b***	**Horizontal Accuracy (m)**	**TVU (m) *d*=5m**	**TVU (m) *d*=10m**	**TVU (m) *d*=15m**	**TVU (m) *d*=20m**
Exclusive Order	0.15	0.0075	1	0.15	0.17	0.19	0.21
Special Order	0.25	0.0075	2	0.25	0.26	0.27	0.29
Order 1a	0.5	0.013	5	0.50	0.52	0.54	0.56
Order 1b	0.5	0.013	5	0.50	0.52	0.54	0.56
Order 2	1	0.023	20	1.01	1.03	1.06	1.10
Order 3	1	0.023	20	1.01	1.03	1.06	1.10

Table 1 Example of IHO orders and horizontal and vertical accuracies (95% confidence) for depths 5,10, 15, and 20 m.

7. Flood risk mapping using TB-lidar

Most flood inundation maps were based on topographic lidar alone with no details of the bathymetry. In the case of coastal flood inundation, the GIS-based still water method is often used where the sea-level is raised to determine what floods on the land based on the lidar DEM. Or alternatively for river-fluvial flood inundation mapping the Height Above Drainage (HAND) method can be used to map inundation (Johnson et al., 2019).

Although these methods produce inundation maps that have been found to be reasonably accurate, these approaches to not calculate the speed of the flood water or the time and duration of inundation. For example, some describe a hazard map as a classification of the flood water velocity times the water depth. In order to calculate the velocity, one must use a hydrodynamic model. One of the main parameters that controls the movement of water in a hydrodynamic model is the bathymetry. In many coastal areas in Canada, the population has settled along estuaries and rivers upstream of the coast. In these locations a hydrodynamic model must account for the interactions of river discharge and fluctuations in sea-level, whether it be tides or tides with an associated storm surge (McGuigan et al., 2015).

As part of this study, the River John estuary and river were surveyed on Oct. 29, 2019 using AGRG-NSCC's Leica Chiroptera-4X TB-lidar system. The survey included John Bay and the river upstream to where the east and west branches of River John join approximately 11 km inland (Figure 17). Ground truthing was conducted during August and September and the area was affected by Hurricane Dorian Sept. 7, 2019 with raised water levels, and the area experienced strong winds and heavy rain. We had hoped to survey River John much earlier in the summer, however the aircraft provider, had several delays that resulted in surveying in less than optimal conditions in late October.

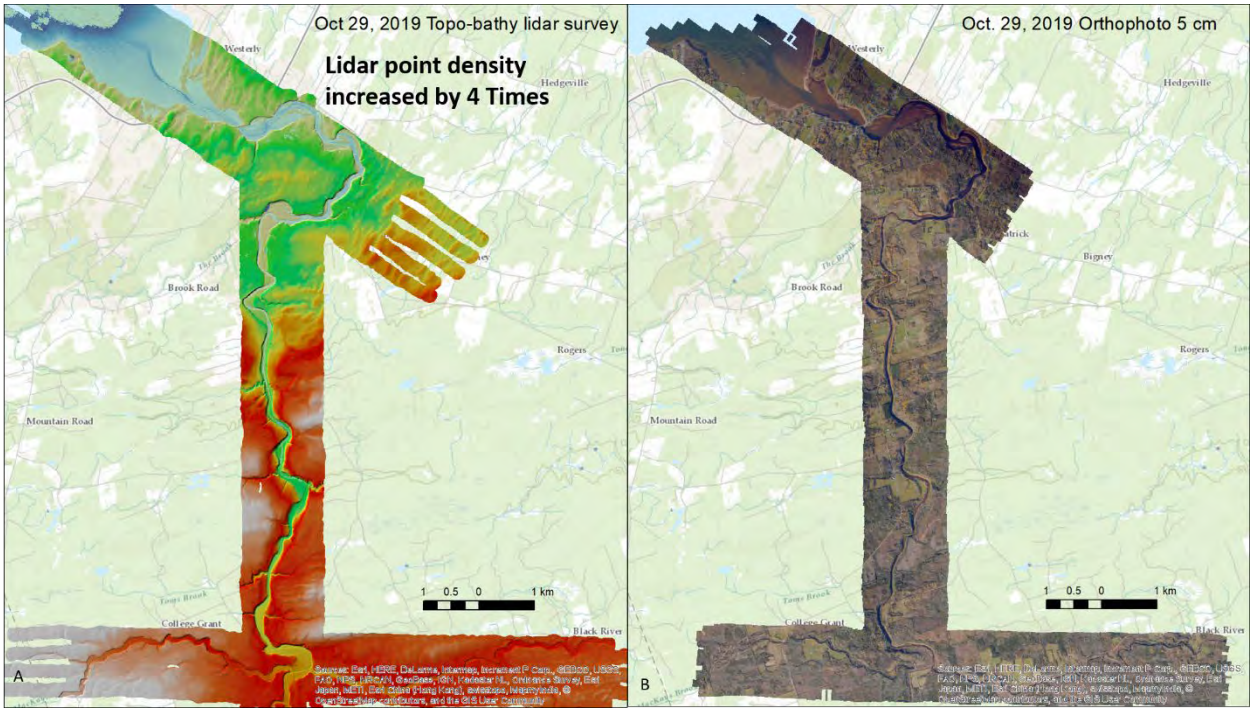

Figure 17 River John TB-lidar survey area. A - Extent of the seamless TB-lidar DEM surveyed. B - Extent of the RGB and NIR orthophoto acquired simultaneously with the TB-lidar.

7.1 Bed Roughness

As previously mentioned, the bathymetry and land elevation are key parameters in controlling the behavior of water in a hydrodynamic model. Other parameters also effect the movement of water including bed roughness, sometimes defined as Manning's Roughness Coefficient which effects the drag between the water and the bed. Webster et al. (2016) have described a method to map eelgrass in bays utilizing just the TB-lidar information and other studies where the lidar has been combined with the orthophotos captured simultaneously during the lidar survey have been used for more extensive benthic cover mapping. For the River John survey, the eelgrass beds were mapped along with spartina salt marsh vegetation and used to assign bed roughness parameters for the modelling (Figure 18, Figure 19).

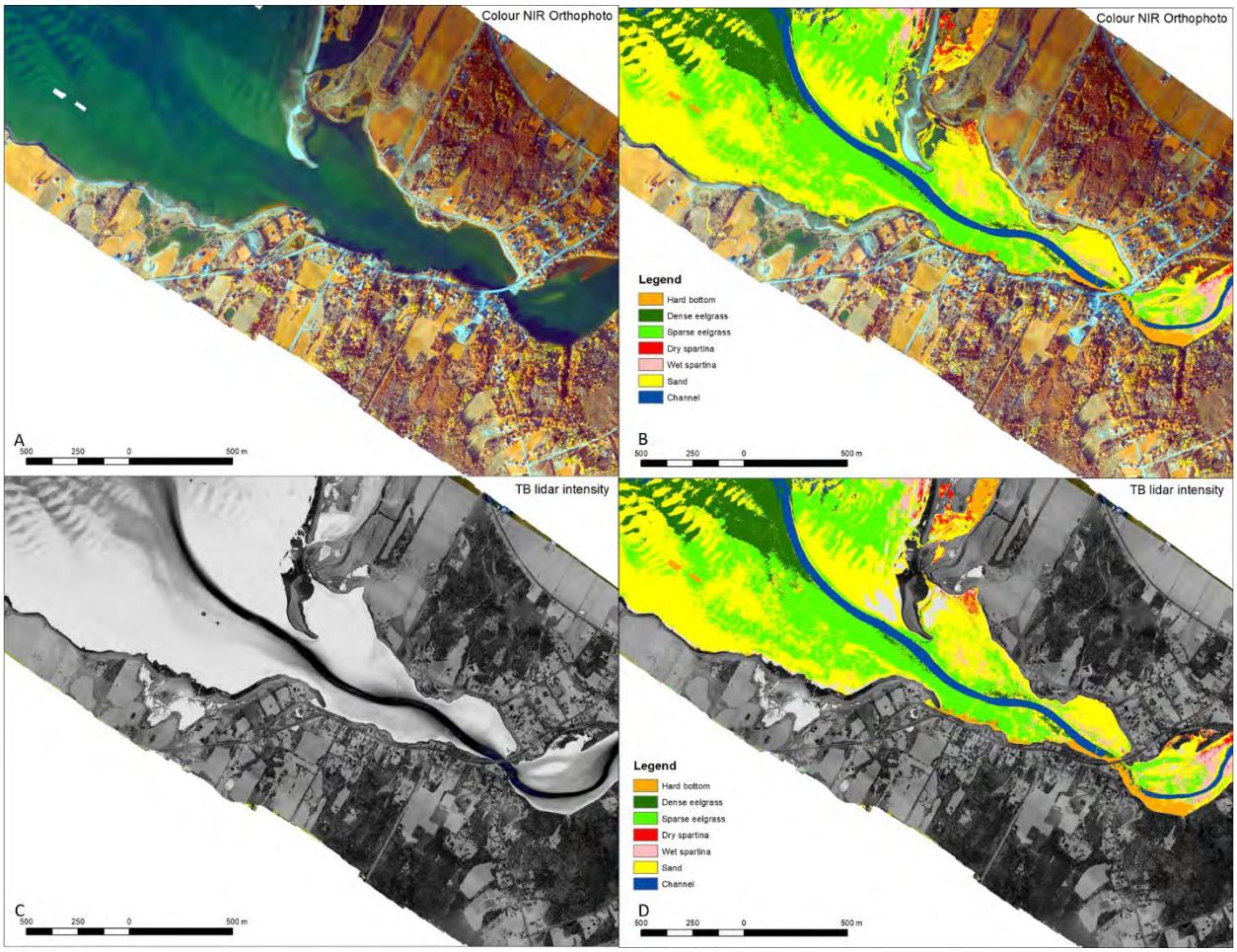

Figure 18 Aquatic vegetation and bed materials for the mouth of River John. A - Colour NIR orthophoto Oct. 29, 2019 captured during the survey. B – Derived bed cover map that can be used for roughness calculation. C – TB-lidar intensity (green laser for the seabed and NIR laser for the land). D - Derived bed cover map overlaid on the intensity map.

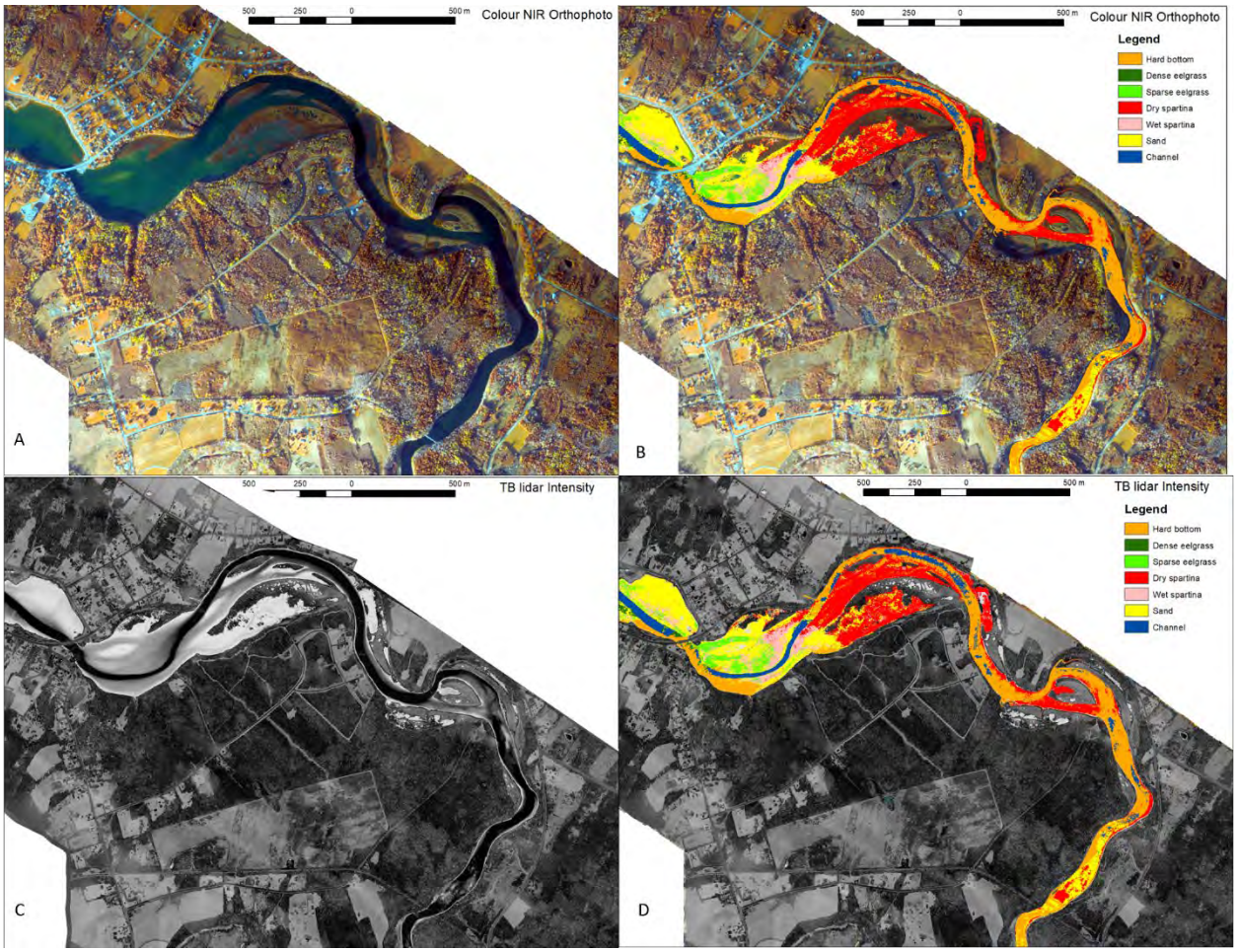

Figure 19 Aquatic vegetation and bed materials for the River John estuary. A - Colour NIR orthophoto Oct. 29, 2019 captured during the survey. B – Derived bed cover map that can be used for roughness calculation. C – TB-lidar intensity (green laser for the seabed and NIR laser for the land). D - Derived bed cover map overlaid on the intensity map.

7.2 Wave Run-up

Coastal flood risk is associated with elevated sea-levels associated with storm surges. In addition to elevated total water levels (tide+surge) waves and wave-runup can also cause additional flooding and erosion. In order to model the hydrodynamics of a storm surge event and possible wave set-up and run-up a seamless DEM is required (Figure 20). In order to calculate wave set-up and wave run-up, near shore bathymetry is required (Olabarrieta and Warner, 2016). Beach profiles have been extracted from TB-lidar data to examine the variations in the seasonal morphology utilizing the Experimental Advanced Airborne Research LIDAR (EAARL) (Klemas, 2011). This is very much an area of active research and tools to calculate 2-D wave run-up are not readily available.

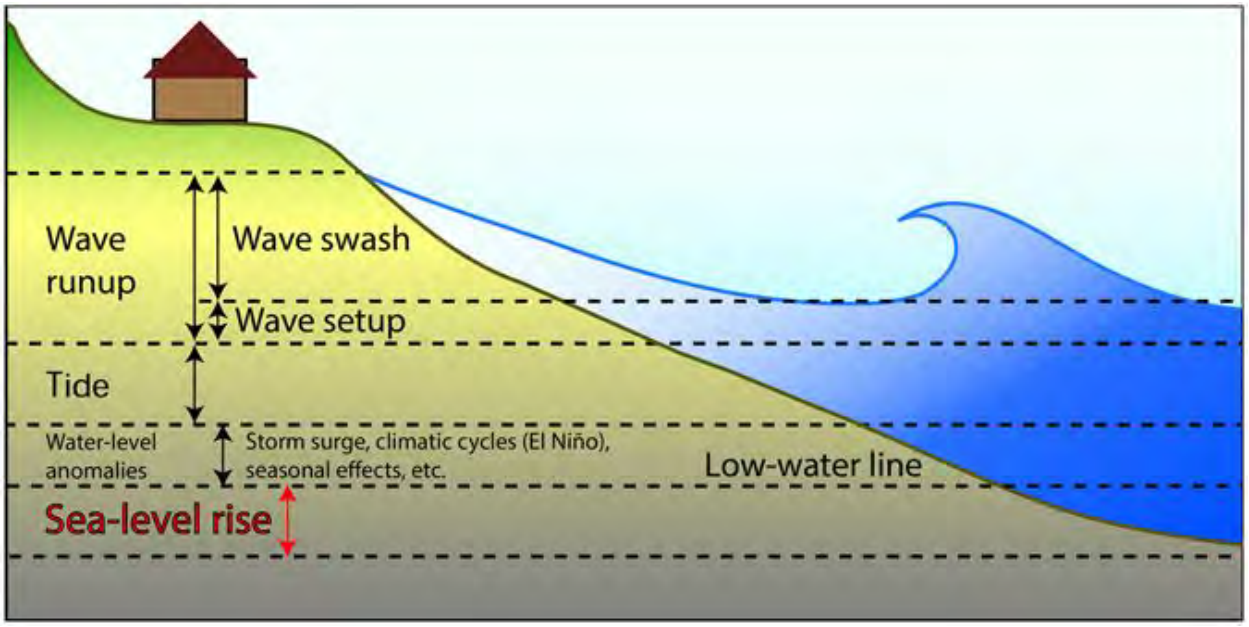

Figure 20 Diagram of storm surge and wave-runup from (From GeoGarage blog).

7.3 Hydrodynamic models for pollution tracking and flood inundation

Nearshore bathymetry has been a challenge to map prior to TB-lidar. Most techniques for mapping land elevation do not work in the coastal zone (e.g. photogrammetry, topographic lidar) and techniques to map the deep water such boat-based echo sounding are dangerous and inefficient in shallow water. The ability of TB-lidar to acquires seamless DEMs across the coastal zone into the near shore has enabled detailed hydrodynamic models to be constructed (Figure 21). These models can be used for a variety of applications including: flood hazard assessment, determining the fate of land-based pollution, determining the timing and impact of offshore contaminant spills (e.g. oil), aquaculture site selected, coastal erosion and sediment budgets. Once a hydrodynamic (HD) model is constructed and validated, particles can be added to determine their fate (Figure 21). The model can include various parameters about the particles including a time-dependent decay factor.

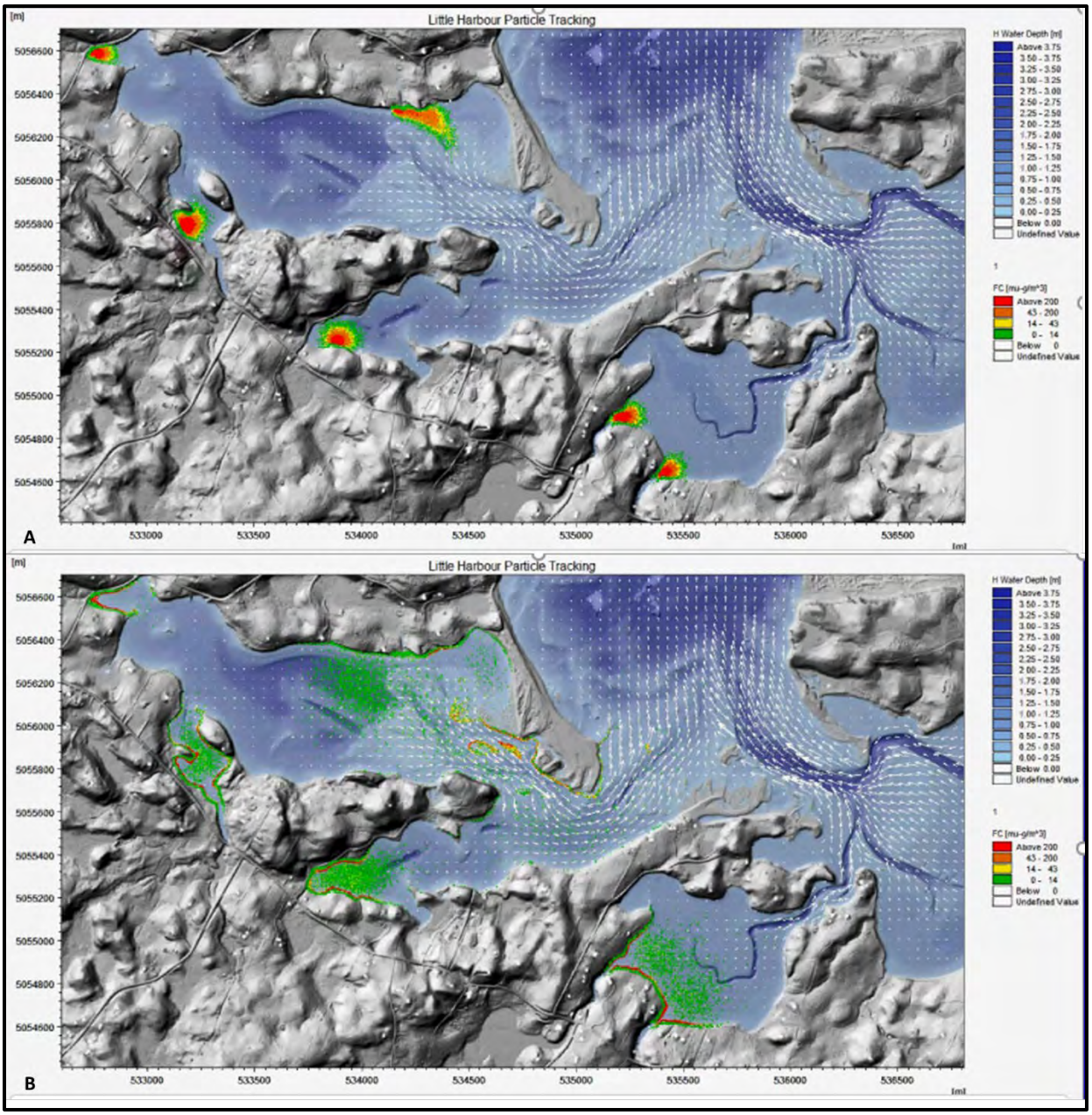

Figure 21 Example of two time-steps in a hydrodynamic model, grey is land, bathymetry in shades of blue, water current speeds represented by the white arrows for Little Harbour, NS. A – Release of land-based pollution (fecal coliform). B – Time-step in the model after a few tidal cycles showing the dispersion of pollutants and where they are concentrated in the embayment.

HD models can also be used to simulate storm surge flooding, where both the water level and current speed and direction are calculated. These HD models rely heavily on accurate seamless land-sea DEM data for their ability to produce accurate results. TB-lidar is an ideal technology to provide these required data. AGRG has conducted a few coastal studies in Nova Scotia for DFO Martimes and DFO Gulf Region for oil spill response preparedness and shellfish aquaculture studies respectively. In 2016 AGRG conducted a study for NS Fisheries and Aquaculture where they mapped Pugwash, Merigomish and Mabou using the Chiropter-2 system. They generated hydrodynamic models for calculating currents and water levels, but not storm surge flooding events. A survey was conducted in 2015 of Cow Bay near

Halifax for the Offshore Energy Research Association (OERA) and the Canadian Association of Petroleum Producers (CAPP) for oil spill preparedness. For this current study, The Cow Bay and Merigomish datasets were used to simulate storm surge events using HD modelling and compared to flooding using the still-water GIS approach.

The Cow Bay area was flooded using a total water level elevation of 5 m. This resulted in overtopping the road and protective gravel bar to the salt marsh in both models, GIS still-water and hydrodynamic modelling (Figure 22). The flood extents are similar between the results of the hydrodynamic (HD) model and the GIS still-water method for the most part. There is a small area within the salt marsh region that does not get flooded in the HD model but does in the GIS method. The GIS method tends to over-estimate the flooding, but not by a significant amount. The current speeds are depicted by the vector arrows in figure 22, C. This cannot be achieved using the GIS still-water method. The combination of water depth and current speed are sometimes used to depict flood hazard as fast-moving water can be more dangerous than deeper slow-moving water. Thus, the HD approach has this additional benefit of calculating current speeds.

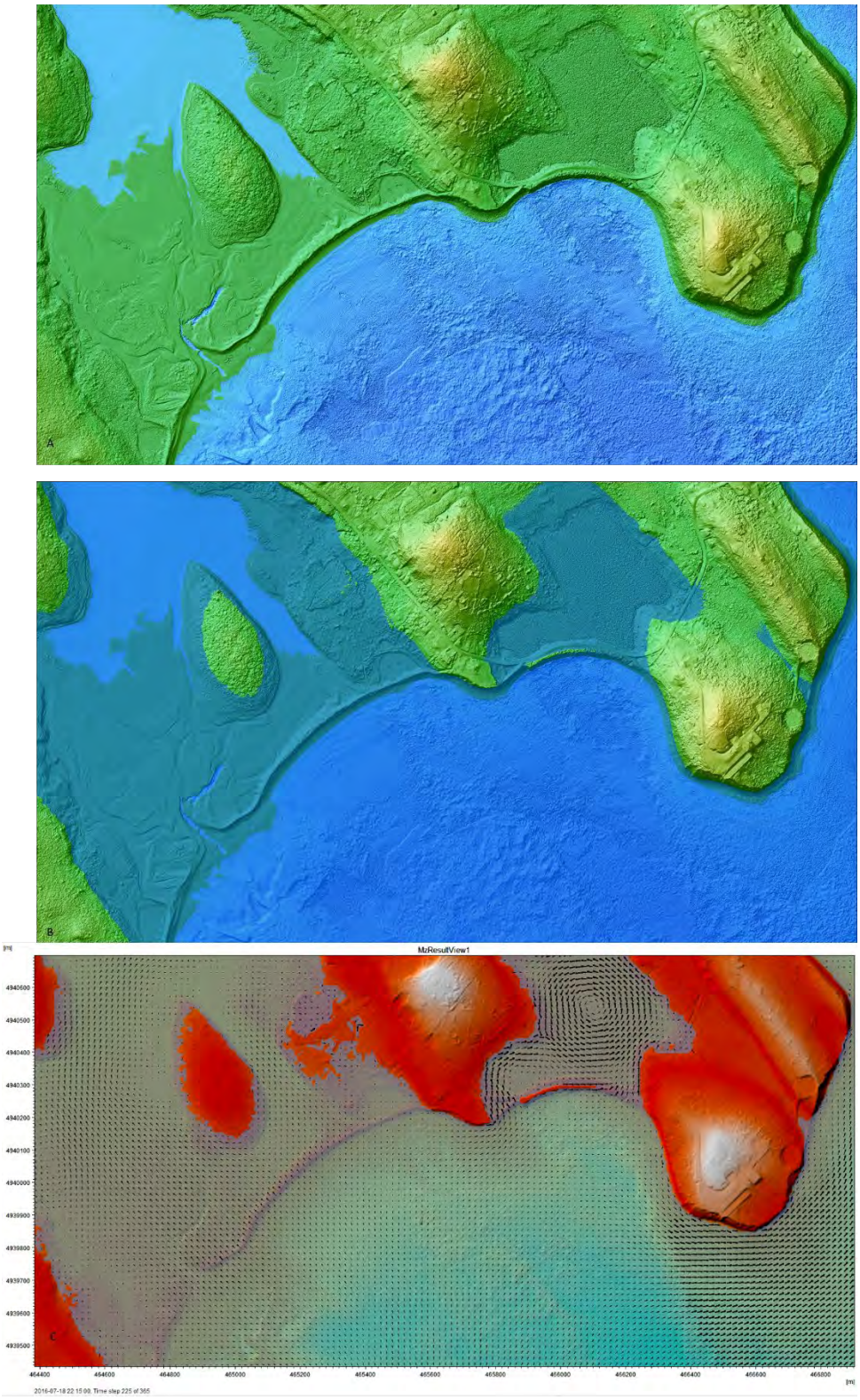

Figure 22 Example of a to still-water GIS flooding compared to hydrodynamic model simulating storm surge flooding, Cow Bay, Nova Scotia. A – Colour shaded relief model of 2015 Cow Bay seamless DEM. B – Inundation of the DEM from a total still-water level of 5 m. C – Hydrodynamic maximum water level and currents from a storm surge producing a total water level of 5 m.

As with all models, they need to be validated if possible. In the case of HD models of the coastal zone, an Acoustic Doppler Current Profiler (ADCP) can be used to collect data on water levels and current velocities which can be used as a boundary condition for a model or to validate a model. An ADCP typically sits on the seabed and directs sound pulses to the surface. Both current speeds and direction can be measured within the water column and the depth of water above the ADCP can be measured and used to parameterize the HD model (Figure 23). In Merigomish, NS AGRG surveyed the area with their Chiroptera-2 TB-lidar sensor and DFO Science Gulf Region deployed an ADCP that captured the Thanksgiving Day storm on Oct. 10, 2016. The HD model can simulate both water level and current velocities and in some cases coupled with wind in order to generate significant wave height (Figure 23, D). In the figure below the results of the TB-lidar survey were merged with lower quality elevation data landward of the coastal zone and inundation area. Note the associated flooding during the Thanksgiving Day storm in figure 23 B and C, compared to A which represents a normal high tide level.

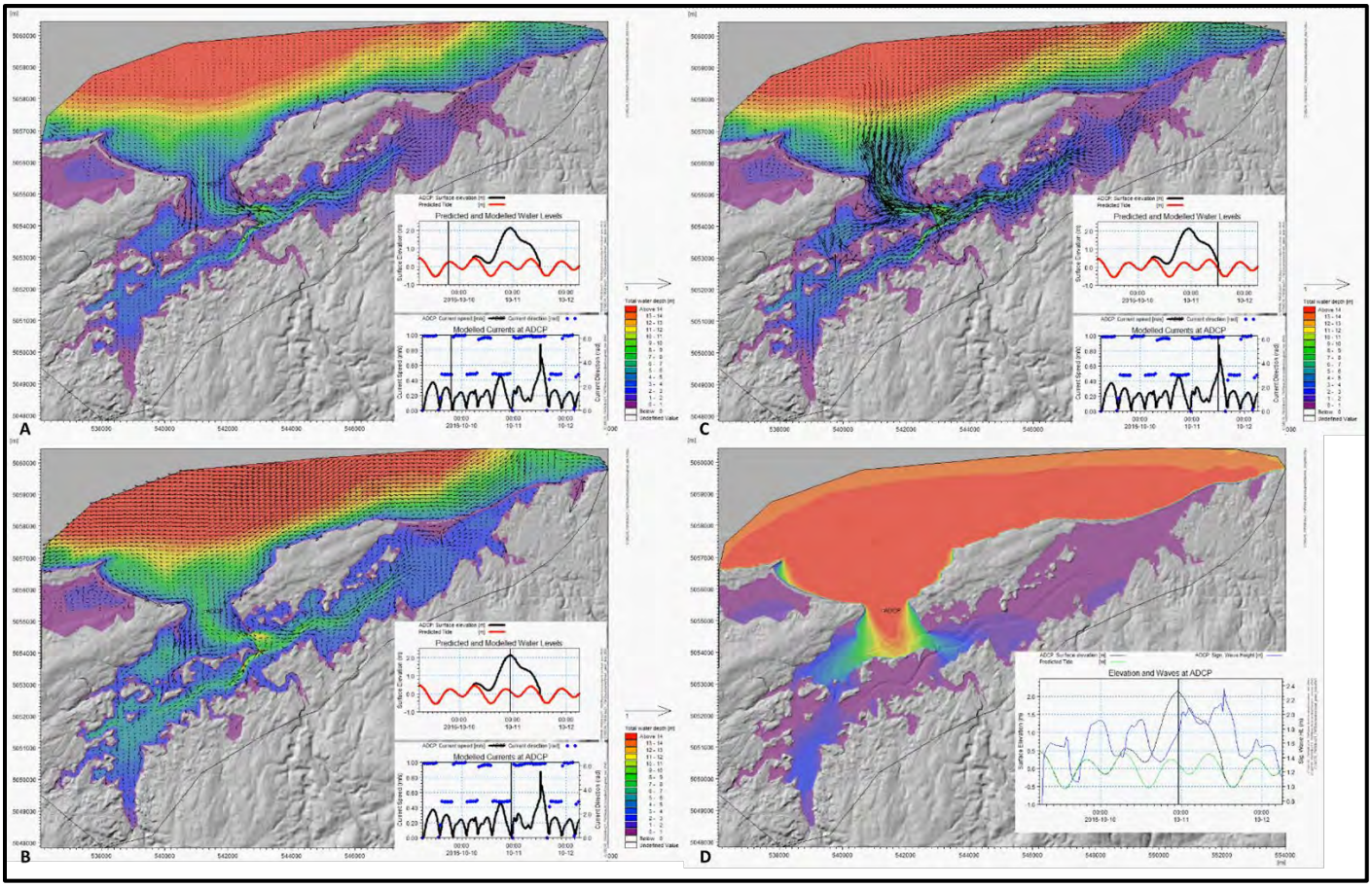

Figure 23 Example of HD model of storm surge compared to ADCP measurements, Merigomish, NS. A - Water levels prior to the storm surge event (thin black line in inset plot of water level, top inset plot-red and blackline and current speed-black line and direction-blue line), colour is water depth. B – Flooding at the time of peak total water level (storm surge) (thin black line on inset plot). C – Maximum current speeds associated with the storm surge (thin black line on inset plot). D – Comparison of model significant wave height with the ADCP measurements, ADCP location on map in the channel, colour is wave height, red = 2m waves.

The total water level of ca. 2 m was observed during the Thanksgiving Day storm of 2016 in the Merigomish. This observed water level was used as a boundary condition for this area for HD modelling

and the results of the storm surge hydrodynamic modelling and significant wave height modelling, not to be confused with wave run-up modelling, was presented in Figure 23. A comparison of flood extents between the HD model and the GIS still-water is presented in Figure 24.

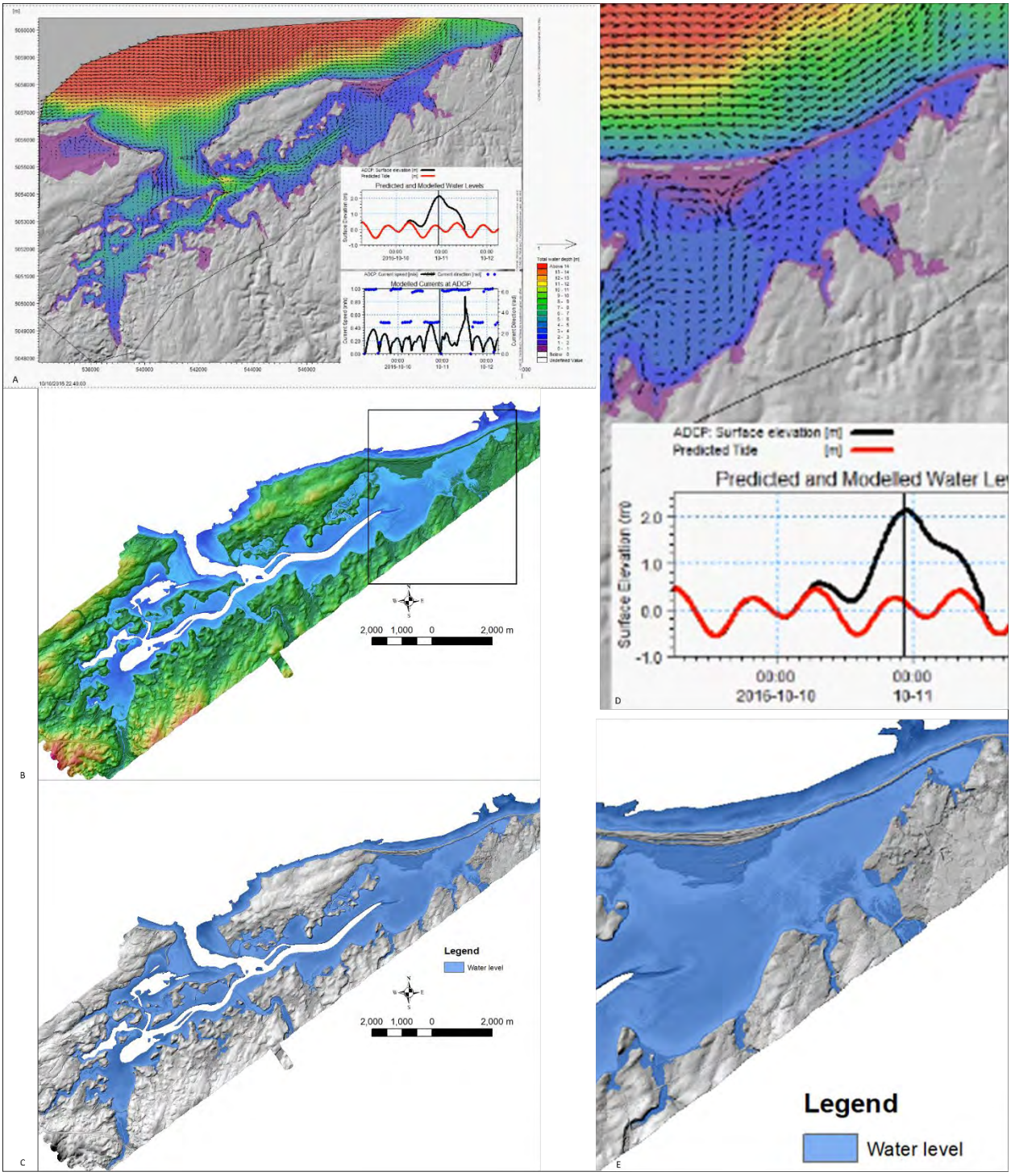

Figure 24 Comparison of HD storm surge flood model compared to GIS still-water flood model for Merigomish, NS. A - Output of HD model for 2 m total water level (tide + surge). B – Seamless DEM from TB-lidar survey (Box inset for D & E). C – Flood inundation of 2 m GIS still-water model. D – Close up HD model. E – Close up GIS still-water model with total sea level 2 m.

The flood extents of the HD model go farther inland than those of the still-water method, although very similar. This could be as a result of the water level boundary condition for the HD model being ca. 2.15 m and the still-water flood was set to 2 m. regardless these two examples show that the two methods produce very similar inundation extents with some minor discrepancies.

7.4 Inland Flood Mapping

In the case of fluvial or inland flood risk mapping, many studies have used topographic lidar to map the exposed floodplain and estimated the river channel topography. Thatcher (2019) describes how the United States Geological Survey (USGS) is investigating TB-lidar for inland bathymetry mapping to be part of the next generation of elevation and hydrography programs of the USGS. Various other researchers have begun to explore the use of TB-lidar for examining rivers including Pan et al. (2015) and Daniele et al. (2019) to assess river bathymetry, McKean et al. (2014) to examine how TB-lidar can affect flow properties in a hydrodynamic river model, Mandlburger et al. (2015) for examining instream habitat and Skinner (2009) for investigating hydrogeomorphic features in rivers using TB-lidar.

Some fluvial models are based on Two-Dimensional (2-D) HD models. However, many other studies rely on using One-Dimensional (1-D) HD models where cross-sections are extracted from the floodplain and river channel and used to calculate the momentum and mass of water moving through the section. The discharge or flow (cubic metres per second) of a river is controlled by the channel bathymetry and gradient. The discharge can be calculated by measuring the following parameters: the cross-sectional area and wetted perimeter of the channel, which can be used to define the hydraulic radius (Figure 25). The hydraulic radius and the hydraulic gradient can then be used with bed roughness to calculate the discharge. Measuring riverbed cross-sections manually (e.g. Using GNSS, or boat-based echo sounding) is expensive and time consuming and in some cases dangerous to the operators. As a result, the channel topography is only measured in a few cross-sections and the remaining areas are estimated by interpolation or using an empirical relationship based on the exposed channel geomorphology (Legleiter and Kyriakidis, 2008).

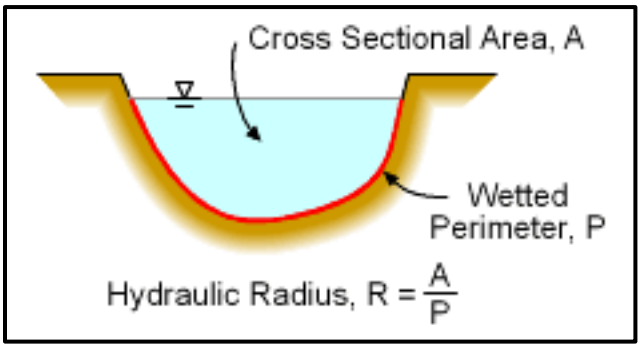

Figure 25 Schematics of river cross-section (From plainwater.com).

The ability of TB-lidar to acquire seamless elevation data of the floodplain and the river channel offers a great deal of potential to improve the accuracy of the cross-sections that are used in 1-D models and support more sophisticated 2-D models (Figure 26). Typically, the water level that is calculated for each cross-section in a 1-D model is then superimposed over the topographic DEM of the floodplain which is then used for interpolating the water level between cross-sections (Legleiter and Kyriakidis, 2008).

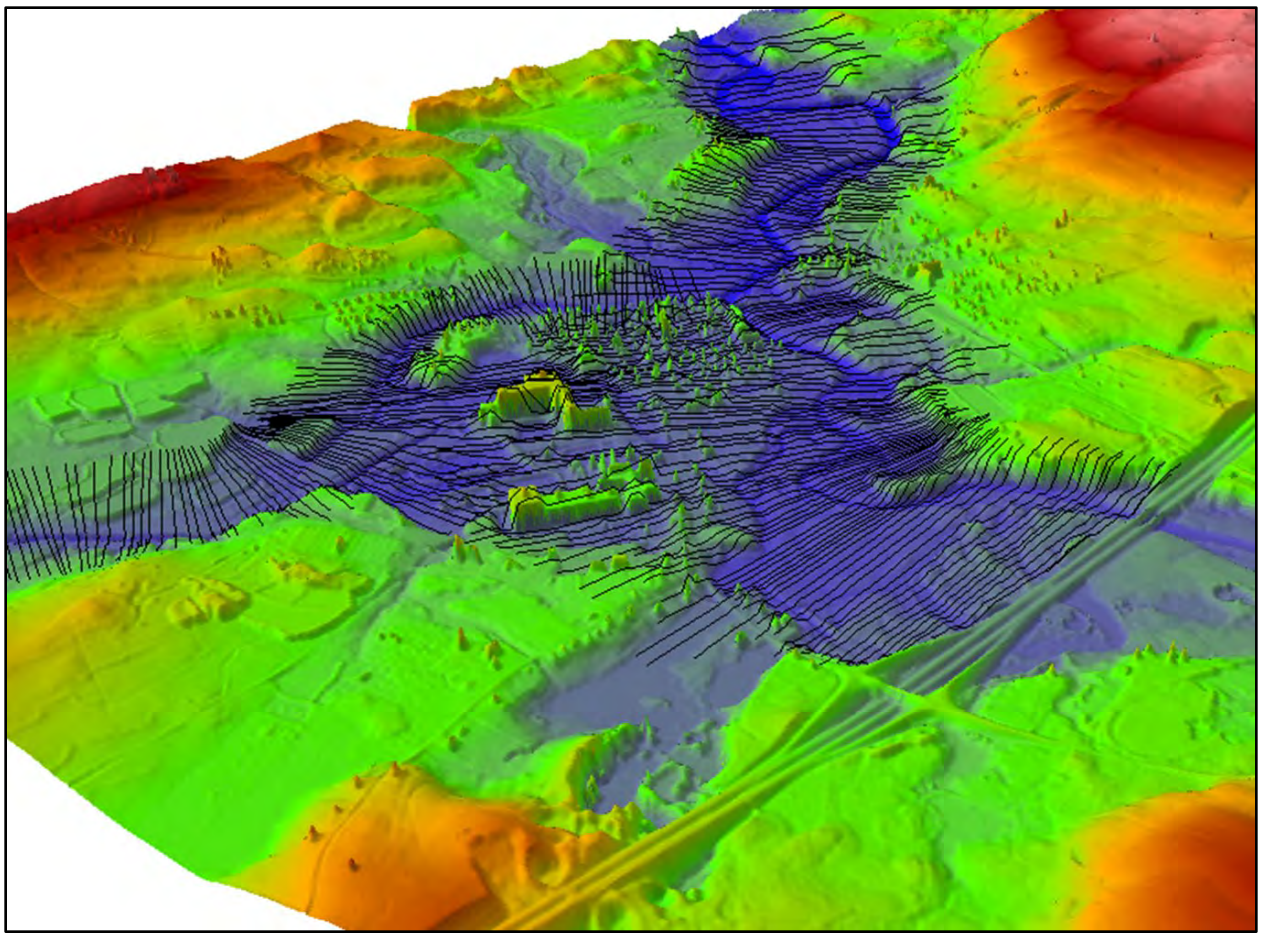

Figure 26 Example of cross-sections extracted across the floodplain and river channel from a lidar seamless-DEM.

On Oct. 29, 2019 AGRG-NSCC acquired TB-lidar for River John in norther NS to demonstrate the utility of TB-lidar for river channel mapping and subsequent floodplain mapping (Figure 17).

Having a continuous seamless land-riverbed DEM allows for more frequent and accurate cross-sections to be used in the modelling (Figure 28). The result of a TB-lidar survey is a series of lidar points from the topographic laser (NIR wavelength) and the hydrographic laser (515 nm green wavelength) as well as a series of RGB-NIR aerial photographs. The TB-lidar points are classified into measured water surface and from that a theoretical derived water surface is derived as well as points representing bathymetry and land. The bathymetry and land points can further be subdivided into classes such as submerged objects or vegetation and on land low and high vegetation and buildings for example. Seamless DEMs are built by gridding the LAS points for the bathymetry and land. A water surface grid can be constructed by gridding the measured or derived water surface (Figure 27-B). A water depth map can be constructed for the time of the survey by subtracting the bathymetric grid from the water surface grid (Figure 27-C). As can be seen in figure 27 the water surface shows the gradient of the river channel which drops approximately 2.5 m over this stretch of the river. The aerial photographs captured during the survey were processed to an RGB-NIR orthophoto mosaic at 5 cm resolution (Figure 27-D).

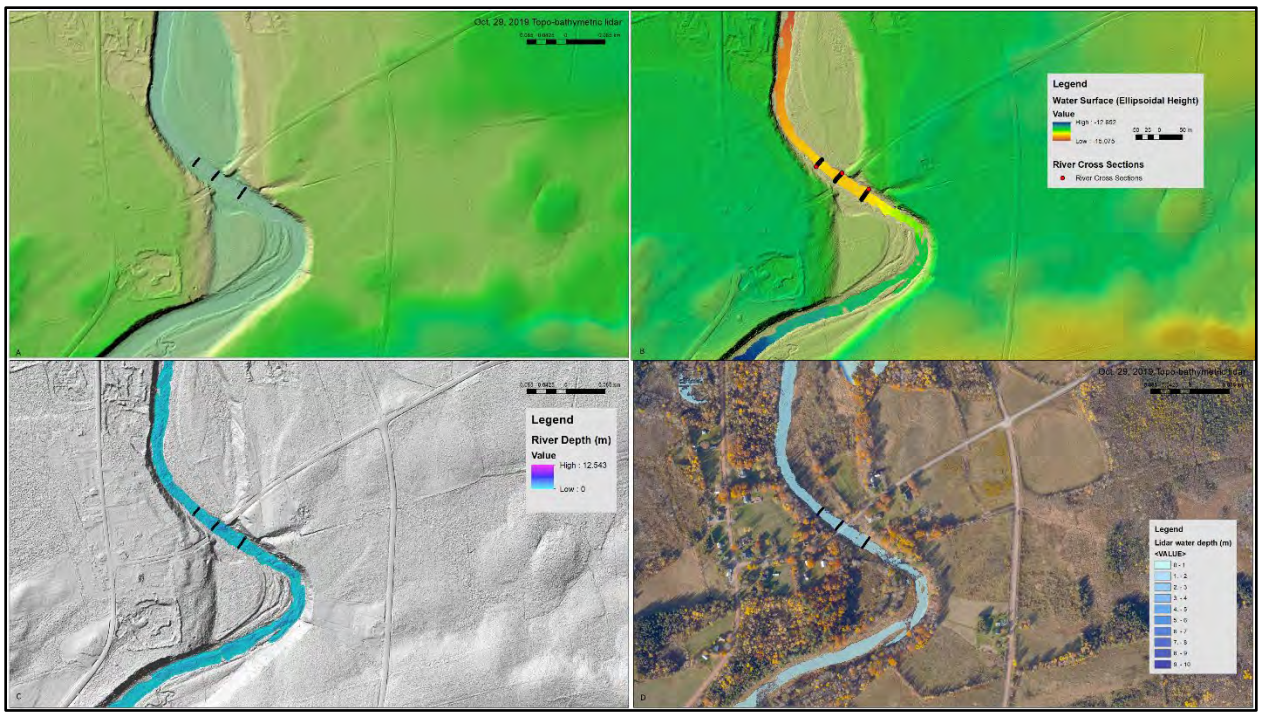

Figure 27 Example of TB-lidar survey products. A - Seamless topo-bathymetric lidar DEM with GNSS cross-section measurements. B - Seamless DEM with water surface elevation (ellipsoidal height) during the survey. C - Water depth map (water surface-DEM) with shaded relief DEM. D - Water depth superimposed over orthophoto captured during the flight.

As part of preparing for the survey, researchers at AGRG-NSCC conducted several manual cross-section surveys across the river using GNSS. These were used to validate the seamless DEM. The original lidar surface products (DEM, DSM, Water Surface, etc.) were gridded at 0.5 and 1 m resolution and voids were filled using simple interpolation of the surrounding pixels. These data were then used to construct a hydrodynamic model; however, the data volume was too much for such models and the data needed to be upscaled to 3 m. The full details of the lidar survey, processing and HD modelling effort are presented in a separated report.

An example of the level of detail the TB-lidar survey can capture and the accuracy of the results is demonstrated below (Figure 28). The top image shows the water depth map superimposed over the orthophoto with additional GNSS cross-sections measured (Figure 28-A). The middle image shows a clos-up of the river channel with four cross-sections and one highlighted by red triangles which run south to north (Figure 28-B). The GNSS points were overlaid on the seamless DEM and ellipsoidal elevations compared and plotted (Figure 28-C). The difference in elevation was calculated by subtracting the DEM from the GNSS elevation. For the cross-section (Figure 28-B), the mean difference was -0.13 m with a standard deviation of 0.04 m (Figure 28-C). The photograph (Figure 28-D) demonstrates how deep the water was during the GNSS survey.

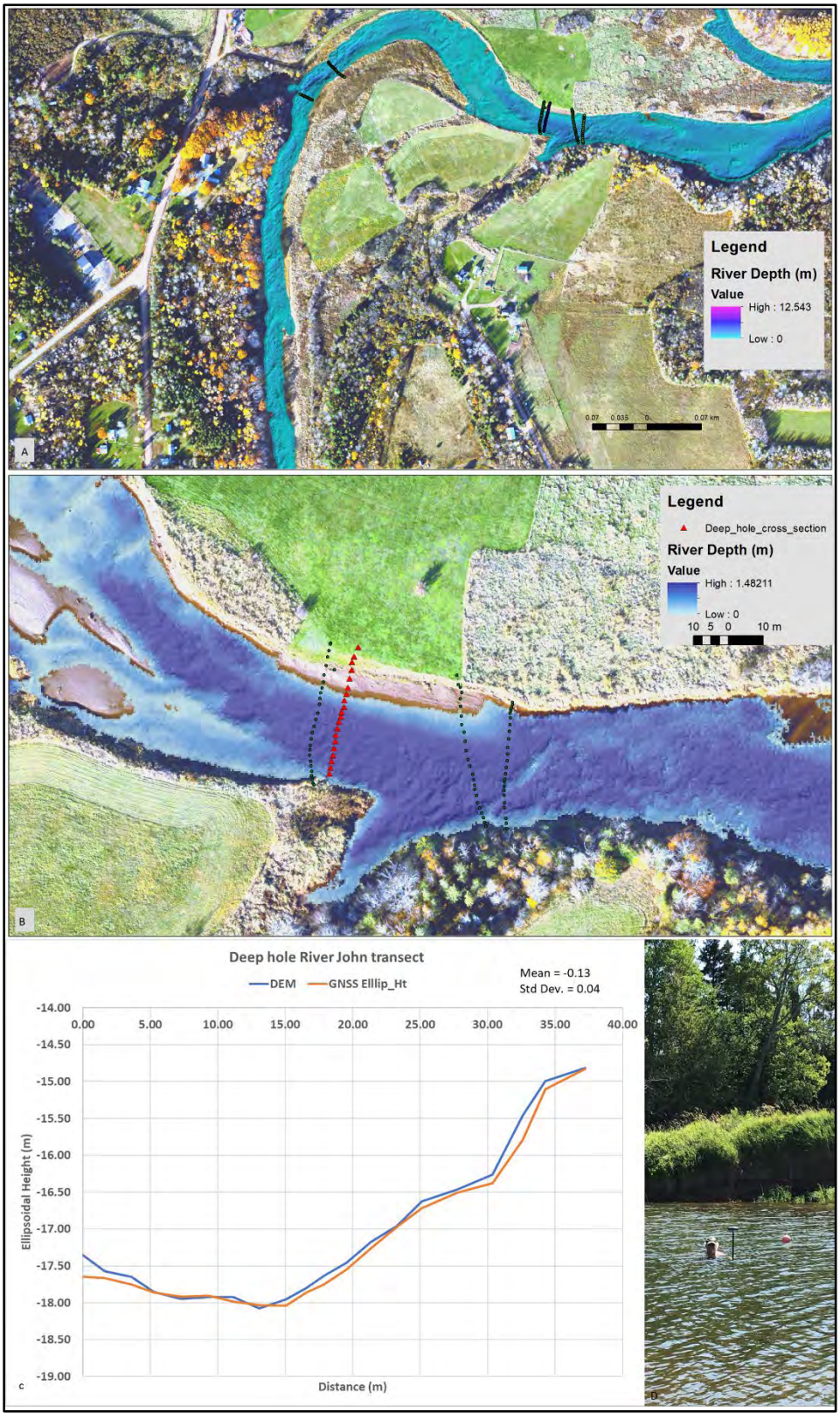

Figure 28 Example of TB-lidar for River John derived river depth. A – Orthophoto with river depth map derived from lidar. B – Close-up of river cross section GPS check points (red triangles). C - Cross-section of TB-lidar DEM compared to GPS (red triangles) including both the river channel and ground of the floodplain. D - Photograph collecting the GNSS at significant water depth.

Another example of the TB-lidar survey is at the Old Pictou Road Bridge (Figure 29). In this figure the GNSS points are depicted with larger white dots and are shown with the lidar points: bathymetry points in blue, ground in brown and vegetation in green for the cross-section shown in red triangles on the map of water depth and the orthophoto (Figure 29-A). The variability of the river channel can be seen in the water depth map. The channel is well represented by the lidar when compared to the GNSS points and the difference in elevation along this cross-section shows a mean difference of 0 m and a standard deviation of 0.08 m (Figure 29-C). The agreement between the GNSS and lidar DEM s very good for this area and as can be seen in the field photo, the water was very clear (Figure 29-D).

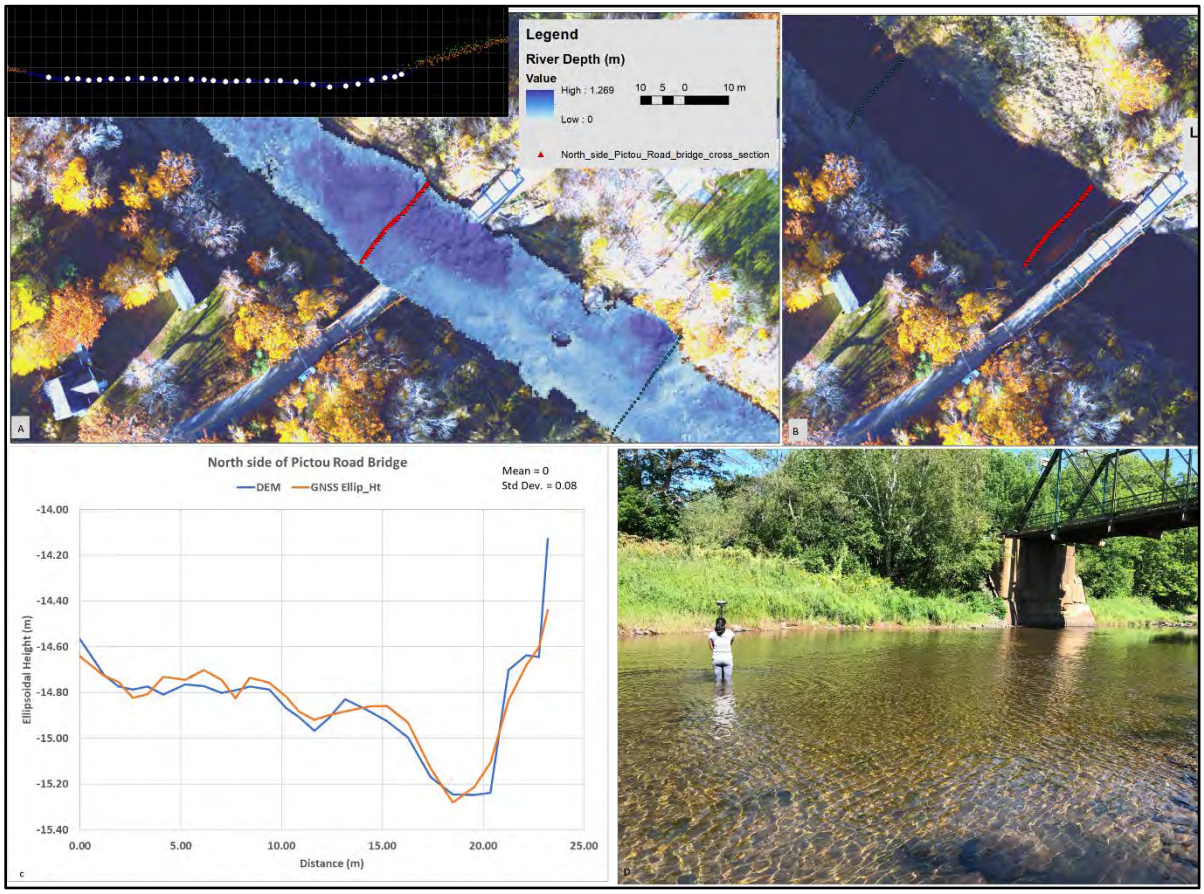

Figure 29 TB-lidar survey products from Old Pictou Road Bridge. A – Water depth map over orthophoto with GNSS points (red triangles), these GNSS points (large white dots) are compared to lidar points (smaller dots) in inset. B – orthophoto alone does not show riverbed details. C -Cross-section comparison between GNSS points and lidar DEM. D – Photo of GNSS points being measured by the bridge.

At the upper reaches of River John where the West Branch meets the East Branch of River John there is a distinct difference in the water clarity (Figure 30). This is evident by the name given to the bridge that crosses the East Branch of the river upstream of the confluence point, it is known as “Black River Bridge”. When one examines the origin of the East Branch it appears to start in a series of bogs and swamps, thus has a high level of dissolved organic carbon and the water is distinctly darker in colour compared to the West Branch of River John. In the figure below the preliminary water depth map shows an error in the pool directly downstream of where the east and west branches of River John meet. This

error is a result of the green laser pulses not reaching the riverbed in this area. We interpret this problem to be a result in the dark colour of the water coming out of the East Branch at the time of the survey in late October after several rain events. In figure 30-B one can see a higher relief area in the middle of the pool after the east and west branches of River John join. Detailed inspection of the lidar bathymetric points reveals the sensor did not penetrate to the riverbed in this area. This error has been resolved in the final product; however, it is useful to understand how local water clarity conditions can affect the survey results. The channel downstream of the confluence is well represented by the lidar when compared to the GNSS points and the difference in elevation along this cross-section shows a mean difference of -0.09 m and a standard deviation of 0.21 m. This cross-section includes the ground which is covered by low vegetation (grasses and shrubs).

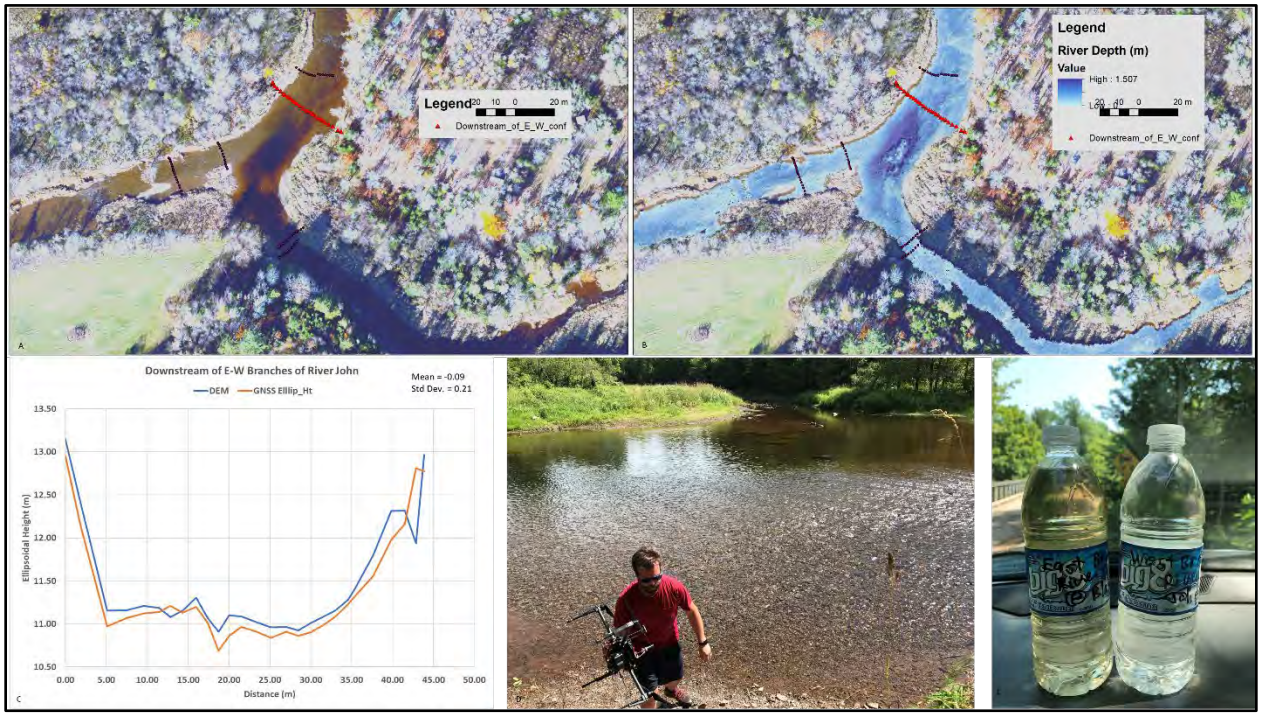

Figure 30 Analysis at the confluence of the East and West branches of River John. A – Orthophoto showing the dark water entering from the east branch with GNSS points (dots and red triangles). B - Water depth over orthophoto with GNSS points (dots and red triangles). C – Comparison of GNSS and lidar DEM for the red-triangles. D – Field photo of East Branch draining into the West Branch. E – Water samples showing the difference in water clarity of the darker East Branch (left) and clearer West Branch (right).

Another example of where the GNSS points were compared to the lidar DEM is an area where a water level pressure sensor was deployed to measure the river stage (water depth) during the study (Figure 31). In this area we compared the NIR topographic lidar returns and the 515 nm lidar returns with the topographic lidar points captured on July 5, 2018 for GeoNova for the floodplain adjacent to the river (Figure 31-A). The top image (Figure 31-A) shows the dense lidar points from the combined topographic NIR laser (operated at 500 kHz) and 515 nm laser (35 kHz) with the GNSS points (white dots) for the floodplain west of the river (see red triangles Figure 31-B) and field photos showing the dense mid-summer vegetation. The middle image (Figure 31-B) shows only the 515 nm laser returns and GNSS points. Note how these lidar returns appear to penetrate the vegetation better than the NIR lidar. The

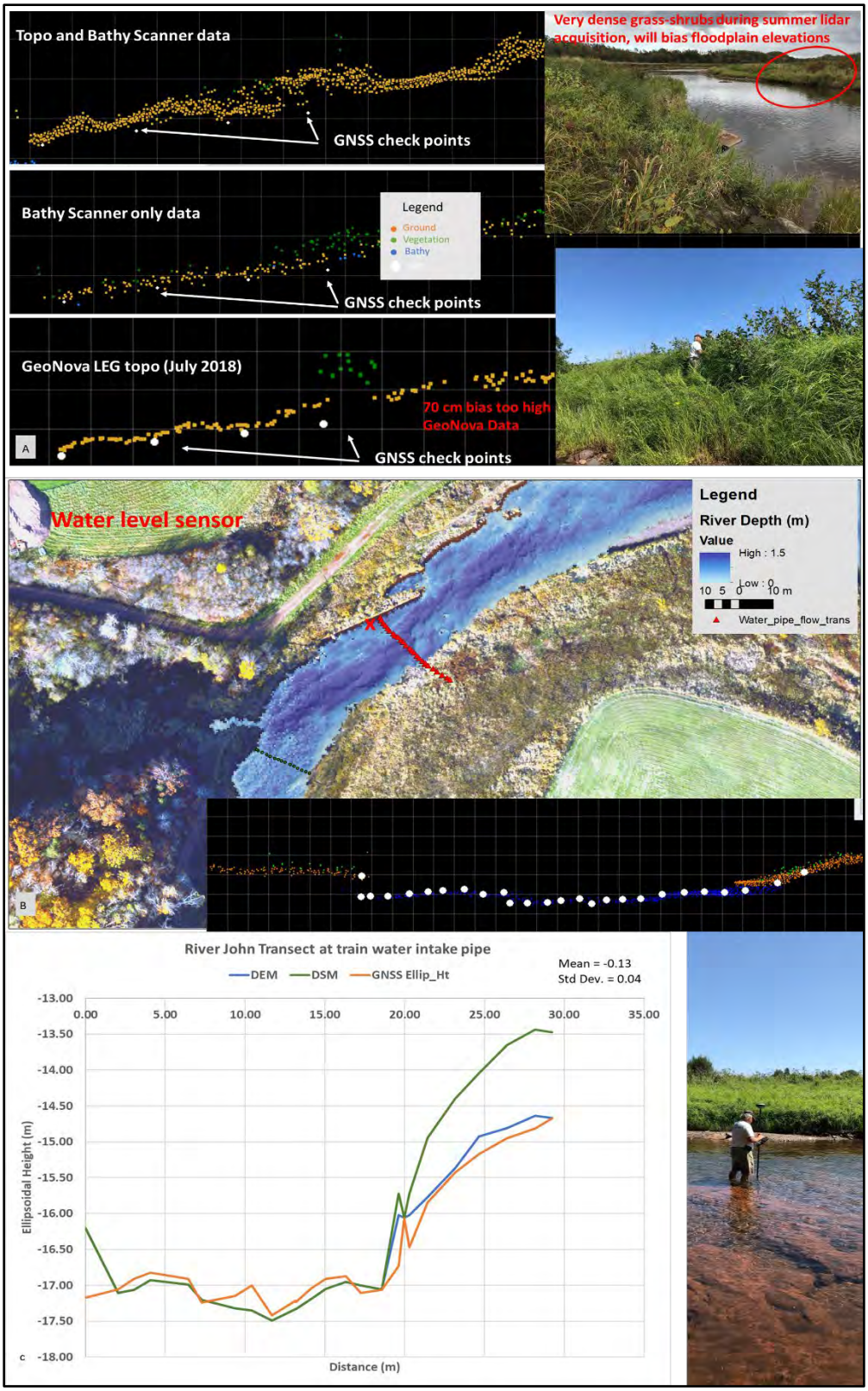

Figure 31 Comparison of GNSS with AGRG-NSCC lidar and GeoNova lidar. A – GNSS (white points) compared to lidar points and photos showing dense vegetation. B – Water depth map and pressure sensor location (red X) and GNSS points. C – Comparison of GNSS and lidar DEM. D – Field photo of GNSS points being taken across the riverbed and dense vegetation on the floodplain.

beam divergence and thus the footprint diameter of the 515 nm laser is approximately six times larger than the NIR, thus presumably allowing more energy to make it to the ground through the dense vegetation. The lower image (Figure 31-A) shows the lidar points collected by Leading Edge Geomatics with a Riegl lidar sensor under contract to GeoNova to collect data for the province. The point density is significantly lower than our TB-lidar survey. The GNSS points are in white and match the ground lidar points initially but then as one moves into the denser higher grasses (see field photos to the right) the ground is artificially too high by 70 cm. This is an important point for NS government officials to understand. The funding to fly lidar for the province was provide in part through Public Safety Canada with the intention to use these data to generate flood assessments. In order to get provincial funding the business case was made that the lidar should be flown in the summer during maximum leaf-on conditions so the data could be used by the Department of Lands and Forests to calculate forest metrics to produce a new generation forest inventory. As a result of the acquisition taking place in the summer months, this means that dense vegetation (grasses and shrubs – field photos to the right in Figure 31-A) was present along the floodplains adjacent to rivers and coastal areas, thus the ground points will be biases too high in the derived lidar maps. Even lidar as dense and precise as it is will not penetrate dense vegetation and reflect off the ground. As a result the points that are the lowest in the dense vegetation are considered ground, even though they did not reflect off the ground, and when they are used to build a bare-earth DEM it will biased too high in those locations. In turn, when these DEMs are used in flood studies, areas of dense vegetation will be too high and may not appear to flood at a given water level but in reality could flood. The end users of these data should be made aware of this limitation in the data. Figure 31-B shows the water depth map over the orthophoto of the area and the location of the water level sensor (red X) and the GNSS points (red triangles) with the inset of the GNSS points (white dots) and the TB-lidar points (blue bathymetry-riverbed, brown ground and green vegetation). Figure 31-C shows the channel is well represented by the lidar DEM when compared to the GNSS points and the difference in elevation along this cross-section shows a mean difference of -0.13 m and a standard deviation of 0.04 m. This figure also shows the GNSS (orange line) compared to the DEM (blue line) and the DSM (green line) showing the effects of vegetation along the floodplain. The field photo to the right of this graph shows the condition and water clarity in this section of the river.

A summary of all the GNSS points collected for validation is presented in Table 2. These included GNSS points collected on hard surfaces and those in the river channel. These do not include those in the floodplain. For the river channel GNSS points, two DEMs were compared, one prior to filling voids and one after voids were filled. As can be seen in Table 2 the void filling routine introduces a slight increase in the DZ error from a mean of 0.08 m to 0.16 m and a standard deviation of 0.19 m to 0.37 m.

Table 2 Summary of all GNSS validation statistics for River John TB-lidar DEM

GNSS cover type	Hard Surfaces (roads, parking lots)		River Bathymetry with voids		River Bathymetry with filled voids	
	DZ Mean	DZ StdDev	DZ Mean	DZ StdDev	DZ Mean	DZ StdDev
(m)	0.5	0.07	0.08	0.19	0.16	0.37
Number of GNSS Points	59		628		678	

We conducted a 1-D Mike-11 and simulated the Hurricane Dorian event and used the 100- year return period rainfall data IDF value in 2100 from the Case Study report prepared by WSP to simulate that event (WSP, 2020). The model setup involves a boundary condition of rainfall distributed throughout the watershed using a rainfall-runoff model within the Mike suite of software. The rainfall was based on the Cape John rain gauge. The hydrological model is then linked to the hydraulic Mike-11 1-D model where the cross-sections are utilized (Figure 32).

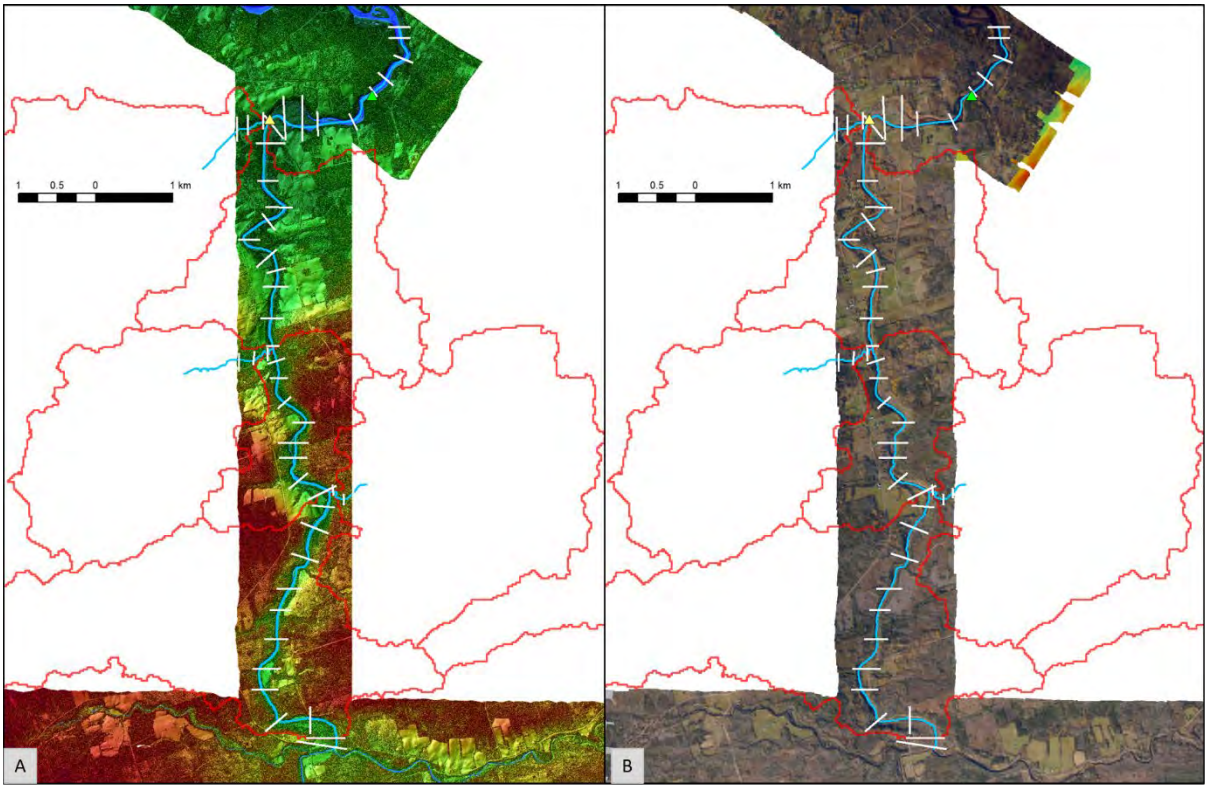

Figure 32 Mike-11 1-D model setup for the in-land flooding. A - TB-lidar DSM with cross-sections (white) and sub-watersheds (red). B - Orthophoto with cross-sections (white) and sub-watersheds (red).

The results of the Hurricane Dorian simulation do not flood the floodplain but rather raise the water level in the channel significantly (Figure 33). The model output includes flood extent, flood depth and flood water velocity (Figure 33). The model was validated by comparing the observed water levels from the Water Pipe and Iron Bridge water level sensors and the simulated water level for the Dorian event (Figure 34). The water levels simulated by the Mike-11 model agree quite well with those observed at the water level sensors.

Since the Dorian event did not overtop the bank significantly, we used the estimated 100-year rainfall event in 24 hours from the IDF curve projected to 2100 assuming a climate change scenario following RCP 8.5 from the Case Study for Pictou, River John of 107 mm (WSP, 2020) (Figure 35). The results of the 100-year rainfall simulation produced flooding the overtopped the bank but did not cover the entire geomorphic floodplain (Figure 35). This increased volume of water did overtop the bank in places and certainly increased the flood depth and velocity (Figure 35).

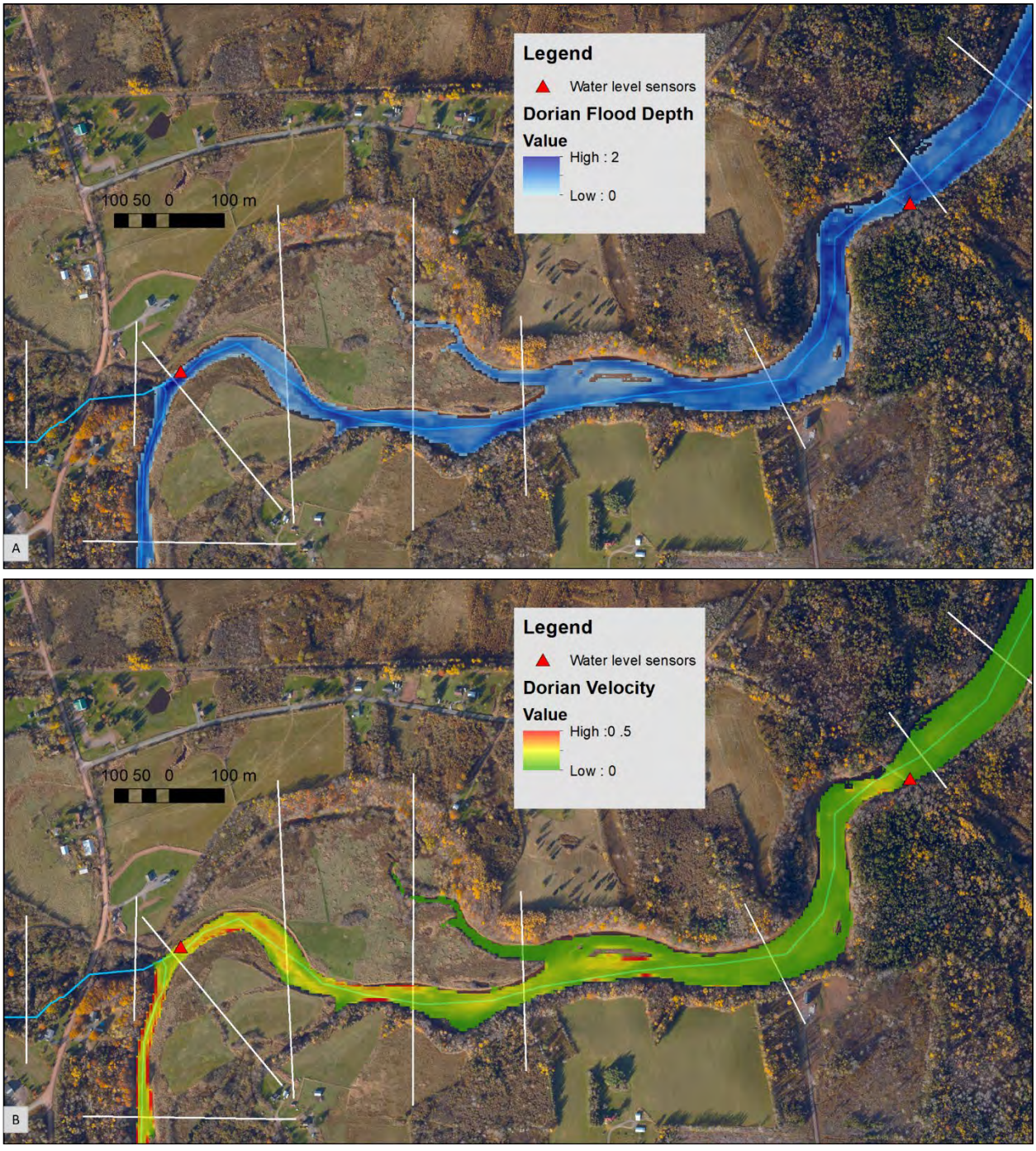

Figure 33 Mike-11 1-D model results for Hurricane Dorian. A – Orthophoto with water level sensors and simulated Dorian flood depth (m). B - Orthophoto with water level sensors and simulated Dorian flood water velocity (m/s).

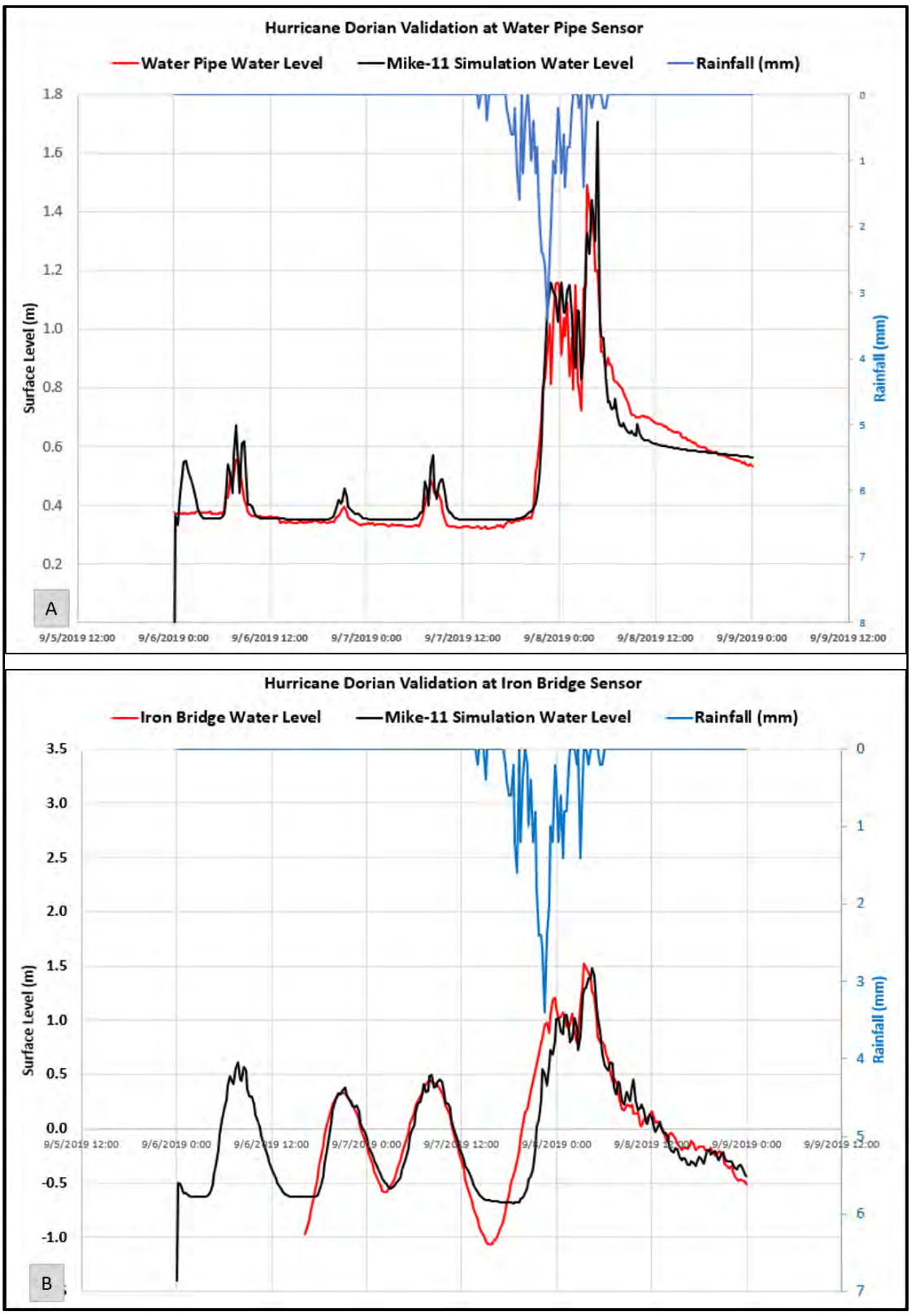

Figure 34 Validation of the Mike-11 simulation of Hurricane Dorian. A - Comparison of the water level observed at the Water Pipe and the simulated water level plus rainfall. B - Comparison of the water level observed at the Iron bridge and the simulated water level plus rainfall.

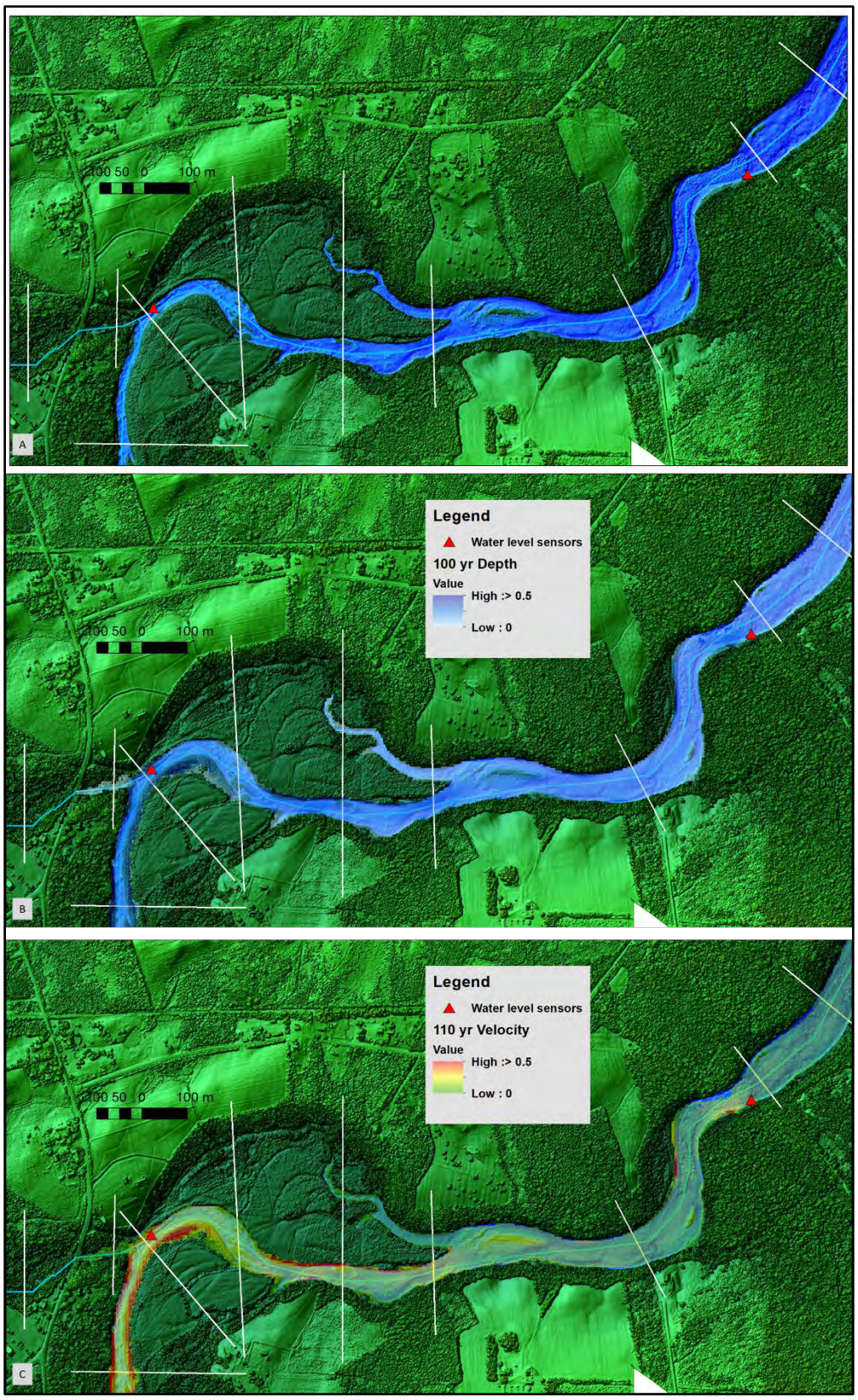

Figure 35 Simulated 100-year rainfall event. A - Normal water level and colour shaded relief TB-lidar DSM. B – 100-year flood depth (m). C – 100-year flood water velocity (m/s).

In order to increase the flooding to cover the floodplain, we multiplied the 2100 projected IDF 24 hour rainfall for the 100-year rain event by 3 times and used that to simulate flooding, which covered the floodplain (Figure 36, Figure 37).

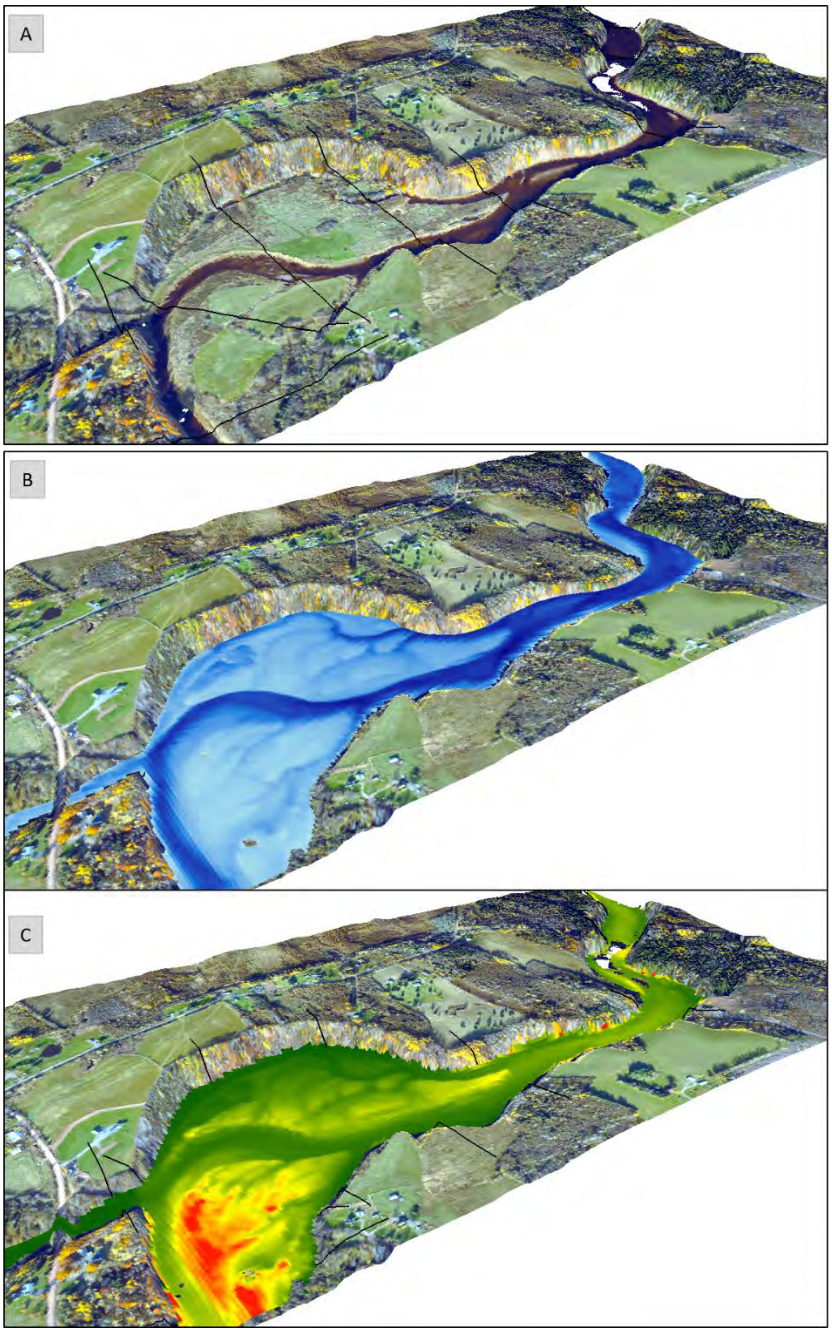

Figure 36 Simulated rainfall event to flood the geomorphic floodplain perspective views. A – Orthophoto with cross-sections (black). B – Flood depth (m), range 0 > 4 m. C – Flood water velocity (m/s) range 0 > 2.5 m/s. See Figure 37 for legend info.

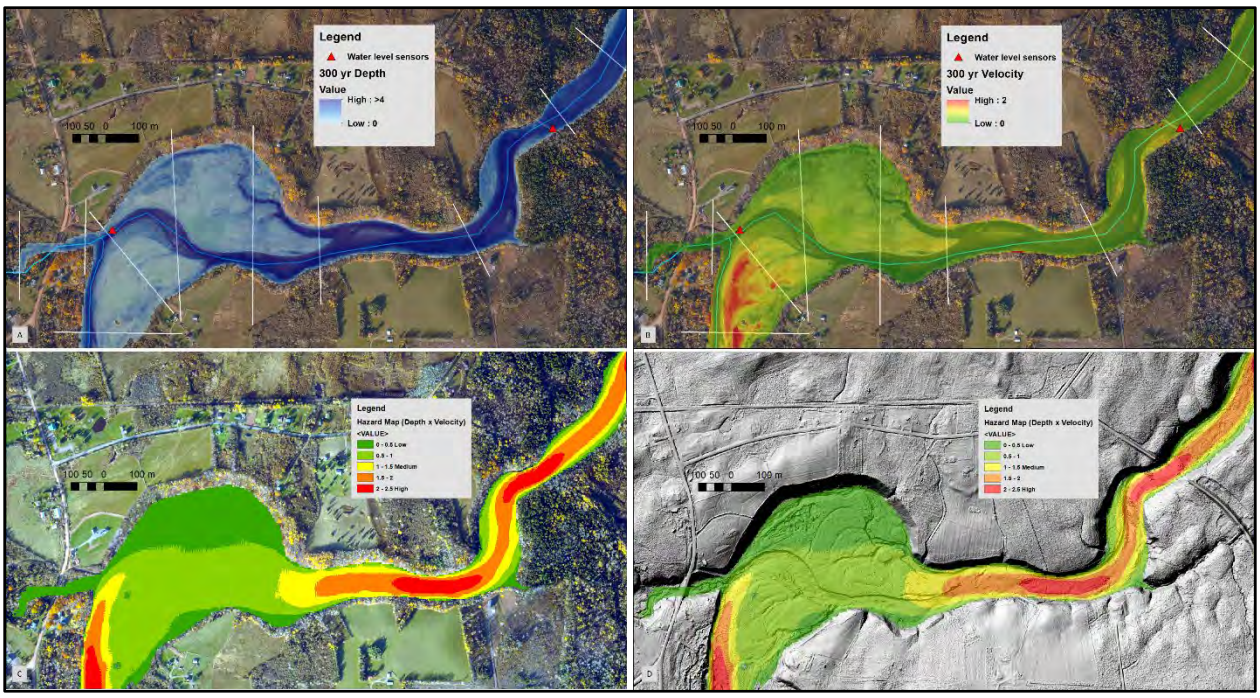

Figure 37 Simulated event to flood the entire floodplain. A – Orthophoto with cross-sections (black) with flood depth (m). B – Flood water velocity (m/s). C – Flood Hazard map (Depth X Velocity). D - Flood Hazard map (Depth X Velocity) over shaded TB-lidar DEM.

The results of the latest simulation (2100 projected 100 year IDF event under RCP8.5 climate change scenario multiplied by 3) is extreme amount of water and the probability of this happening is extremely low. This was done for illustrative purposes in order to flood the entire River John floodplain (Figure 36, Figure 37). For the simulated flood depth and flood water velocity grids, a new flood hazard grid was constructed by multiplying them together and then classifying the result into 5 classes from low hazard to high hazard (Figure 37). The combined affects of deep flood water and fast flood water are depicted in this map (Figure 37).

7.5 Couple coastal and in-land flood mapping using a 2-D hydrodynamic model

Many of the communities in Nova Scotia are located along the coast or along river systems that drain to the coast and thus have a significant part of the drainage system that has estuarine conditions (mixture of salt and fresh water). As a result, the interaction of the ocean water level and the in-land river water level must be modelled together. This modelling approach typically involves a coarser resolution ocean model, where high resolution data are rare, that is used to modulate the ocean water levels from a tidal boundary condition. The results of this model are then interfaced to a higher resolution model of the in-land area at the estuary boundary where the ocean interacts with the freshwater discharge. Elevated coastal waters can retard the discharge of river system that drain into the ocean. The interaction of the ocean and river for the River John area is used to demonstrate this modelling approach. In the case of having a seamless DEM derived from TB-lidar, a 2-D model can be supported for the entire process (ocean and in-land flooding). To demonstrate this requirement for a coupled ocean model and a river run-off model we used River John and simulated the Hurricane Dorian event which occurred on the

evening of Sept. 7 and early morning of Sept. 8, 2019. Three water level sensors were in place and captured the Dorian Hurricane event (Figure 38).

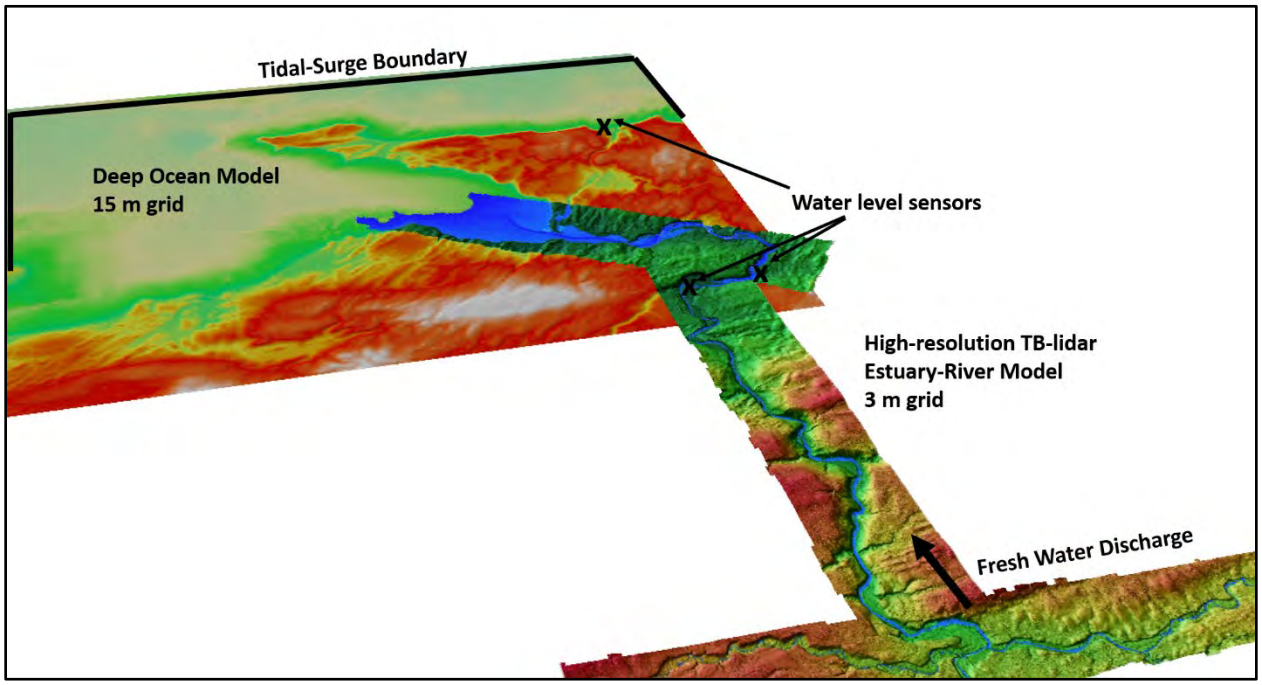

*Figure 38 Elevation models used for the coupled ocean-river model for River John. The ocean model DEM is 15 m and the river model DEM is 3 m. "**X**" marks the areas where water level pressure sensors were deployed and captured The Hurricane Dorian event. The thick black line surrounding the ocean perimeter was used a tidal-surge boundary. The thick black arrow represents a freshwater discharge boundary for the river model.*

One tide gauge at Skinner's Cove, east of Cape John where AGRG-NSCC researchers have been monitoring sea-levels since 2010 measured a 1.5 m surge. Two other water level sensors were deployed in River John for the TB-lidar survey. These included a pressure sensor at the "Iron Bridge" which is the old railway bridge abutment crossing the river and at the "Water Pipe" location, an area upstream where there is crib-work built along the river where they used to extract water from the river using a large pipe to pump it up to the tracks near the River John train station for the trains in the early part of the 20th century (Figure 39).

Figure 39 Water level sensors within River John at the "Iron Bridge" and the "Water Pipe" locations. The small dots represent river cross-section measurements.

Hurricane Dorian produced a ca. 1.5 m storm surge, which is typical of the large storm surges that have occurred, along the Northumberland Strait since AGRG-NSCC has been monitoring the sea-level at Skinner's Cove. The ocean boundary condition for the coupled model was extracted using the predicted tide with WedTide (DFO) and the residual or storm surge observed at Skinners Cove was added to the predicted tide to simulate the ocean water levels that were observed during Hurricane Dorian (Figure 38, Figure 40).

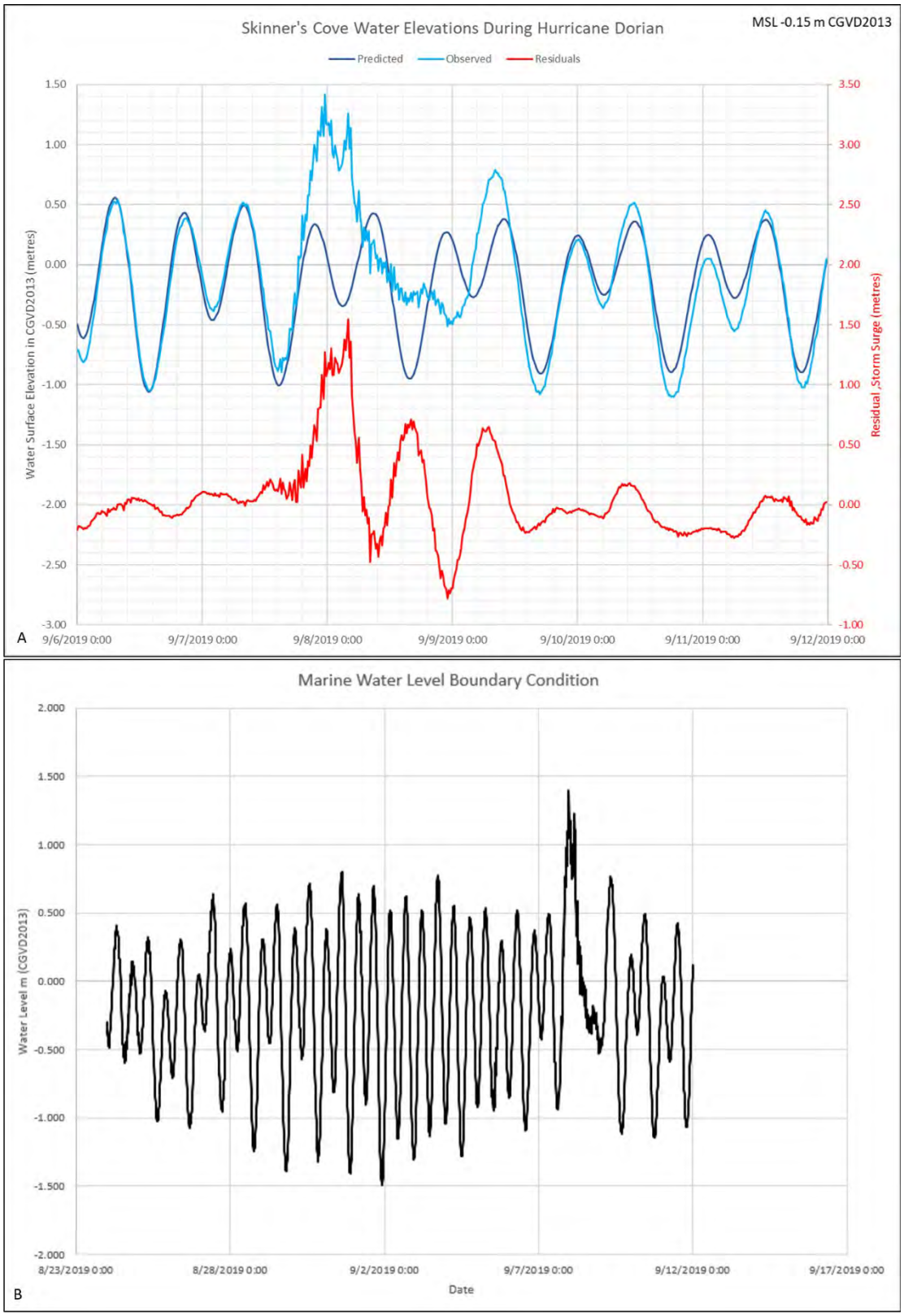

Figure 40 Hurricane Dorian ocean water levels. A- Observed water levels from Skinner's Cove tide gauge, note the 1.5 m storm surge measured. B - The ocean boundary condition derived from predicted tide from WebTide with the Dorian storm surge added.

A weather station operated by AGRG-NSCC researchers at Cape John captured the atmospheric conditions during Hurricane Dorian including wind speed and direction and precipitation. As the hurricane passed over on Sept. 7th the wind changed direction from coming from the south to coming from the east-northeast and increased to over 100 km/hr or 28 m/s and the barometric pressure dropped to 97 kPa. The total rainfall during the event Sept. 7-8 was 37.4 mm. The wind was added as another boundary condition and applied uniformly across the model (Figure 41).

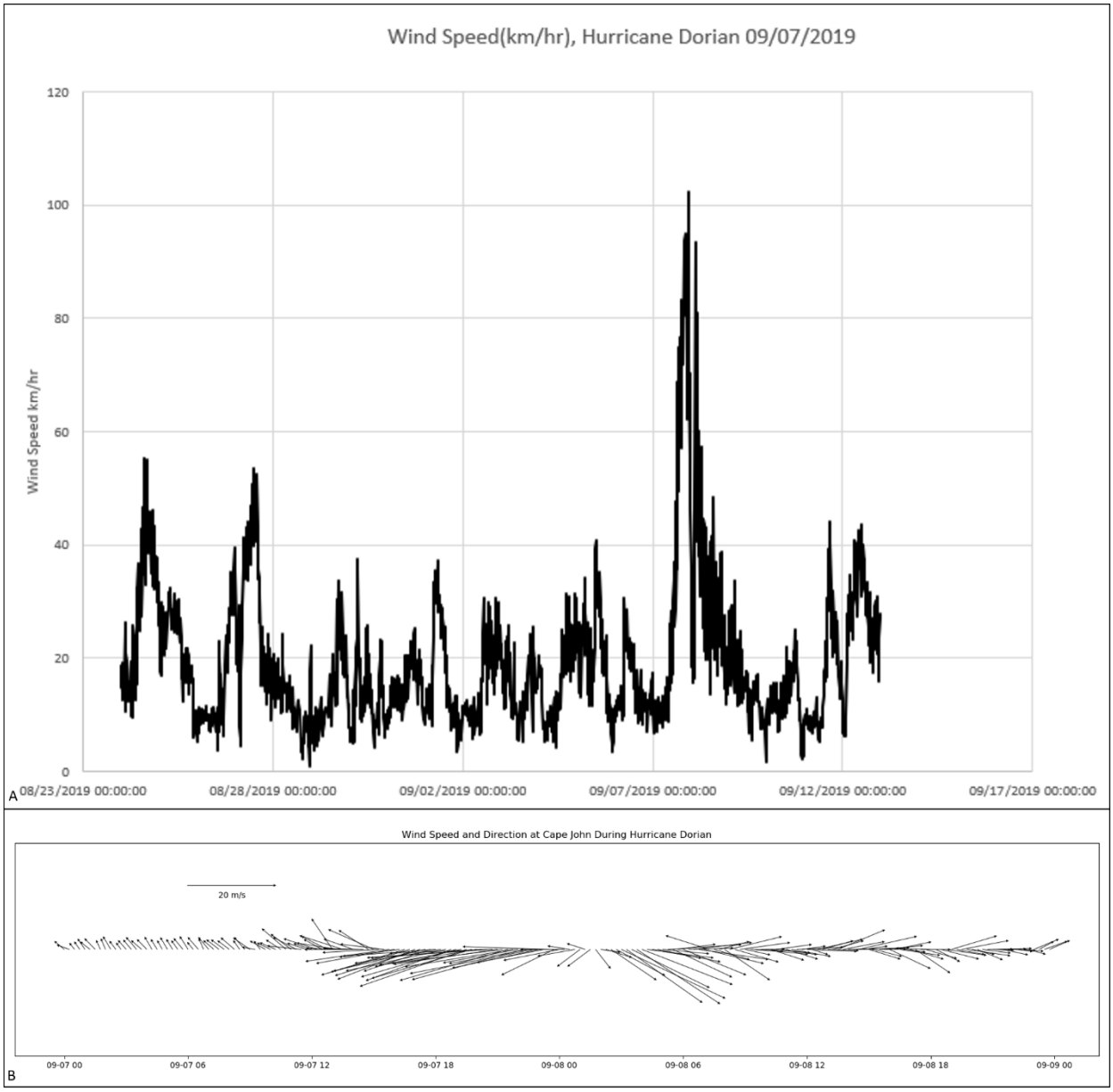

Figure 41 Observed winds (Aug. 24-Sept.12, 2019) during Hurricane Dorian at Cape John weather station. A – Wind speed in excess of 100 km/hr was reached the night of Sept. 7. Time in UTC. B – Shows the wind quiver plot for Sept.7-9, 2019. Note the strongest winds were from the east-northeast direction and then swung around to be from the west-northwest direction.

The water level sensors in River John also captured the Hurricane Dorian event and the elevated water levels. The “Iron Bridge” was known to be inter-tidal based on several visits to the site at various stages

of the tide throughout the summer and fall of 2019. However, the “Water Pipe” location upstream of the “Iron Bridge” was thought to be beyond the tidal influence of the ocean. After the water level sensor data were downloaded we observed that the Iron Bridge water level sensor behaved very similar to the Skinner’s Cove sensor which was only exposed to the effects of the ocean, and the upstream Water Pipe sensor was dominated by river runoff discharge and during higher tidal-surge events by elevated ocean levels (Figure 42). Figure 42 shows the observed water levels for the three sensors and the precipitation during the Dorian event. Note that high tide events where the water level was less than ca. 0.25 m (CGVD2013) did not influence the upstream Water Pipe elevation. However, during larger high tide events the water “backed up’ and came to the approximate same level as the tide at the Water Pipe location. It is interesting to observe the different behaviors of the three sensors during immediately after Dorian. The highest water levels were initially observed at Skinner’s Cove and the Iron Bridge as a

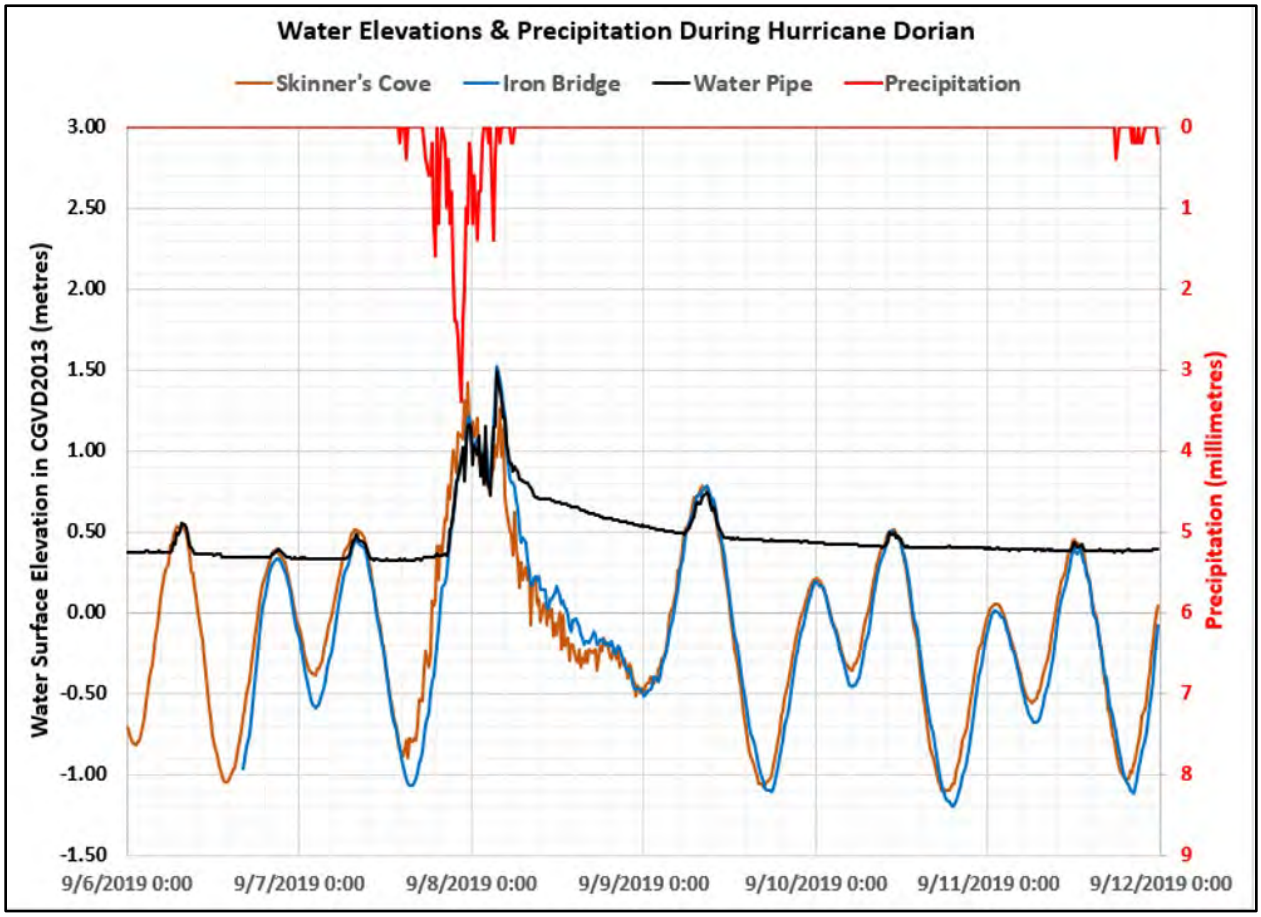

Figure 42 Observed water levels from the three pressure sensors. The Skinners Cove (brown) and Iron Bridge (blue) levels are dominated by the ocean, and Water Pipe (black) is a mixture of storm surge and river discharge from rainfall (red).

result of the storm surge (first peak in Figure 42). However, during the second peak event the water level at the and Iron Bridge was the largest followed closely by the Water Pipe which both exceeded that of Skinner’s Cove (Figure 42). Immediately following the storm surge event the water levels at the Iron Bridge and Skinner’s Cove receded while the falling limb of the Water Pipe levels declined slowly as a result of the dominance of the added freshwater input from the rainfall (Figure 42).

The result of the coupled 2-D model run show the flooding along the River John floodplain near the Water Pipe (Figure 43). The observed water level during the survey was overlaid on the orthophoto which shows several gravel bars exposed in River John near the Water Pipe sensor location (Figure 43-A). The results of the 2-D coupled modelling shows the water depth of Hurricane Dorian at

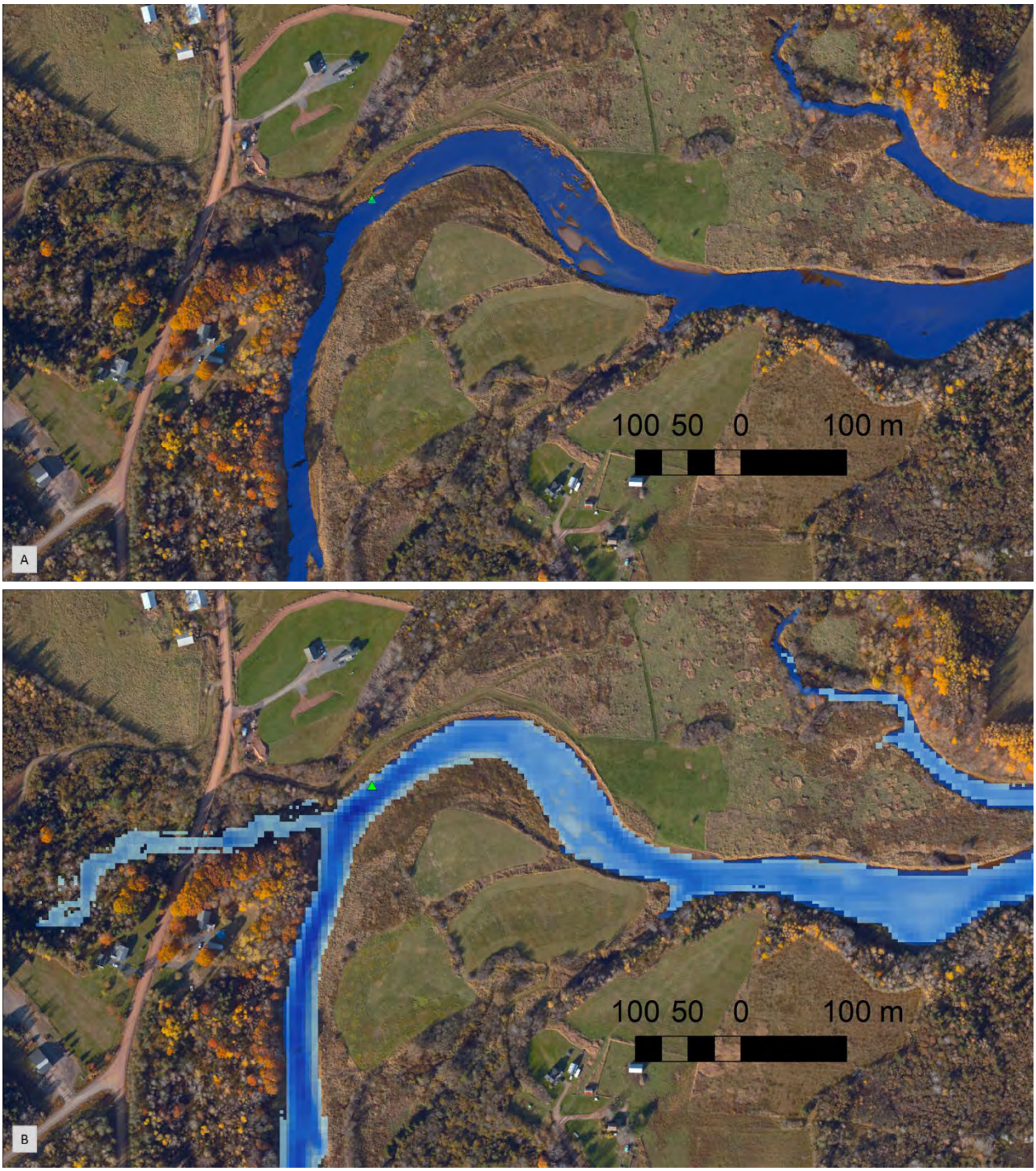

Figure 43 Results of 2-D flood simulation of Hurricane Dorian. A - Orthophoto of Water Pipe area (green triangle is the water level sensor location) with normal water levels during the TB-lidar survey. B - Modelled water depth of Hurricane Dorian levels using a 3 m seamless DEM from TB-lidar.

the same location but using a 3 m resolution seamless DEM (Figure 43-B). The elevated water level during Dorian covers the gravel bars and raised the water level approximately 1.6 m above the sensor or 0.7 m above the water level observed during the TB-lidar flight (Figure 43-A).

The 2-D model was run with and without the wind boundary condition. The best results were observed when the wind was added to the model. The model results were validated by comparing the simulated water levels and the observed water levels at the Water Pipe and Iron Bridge sensor locations (Figure 44). The model results with and without wind are not that significantly different, although the maximum wind occurred during the second peak water level and by using it as an additional boundary condition the simulated results match the observed results better (Figure 44).

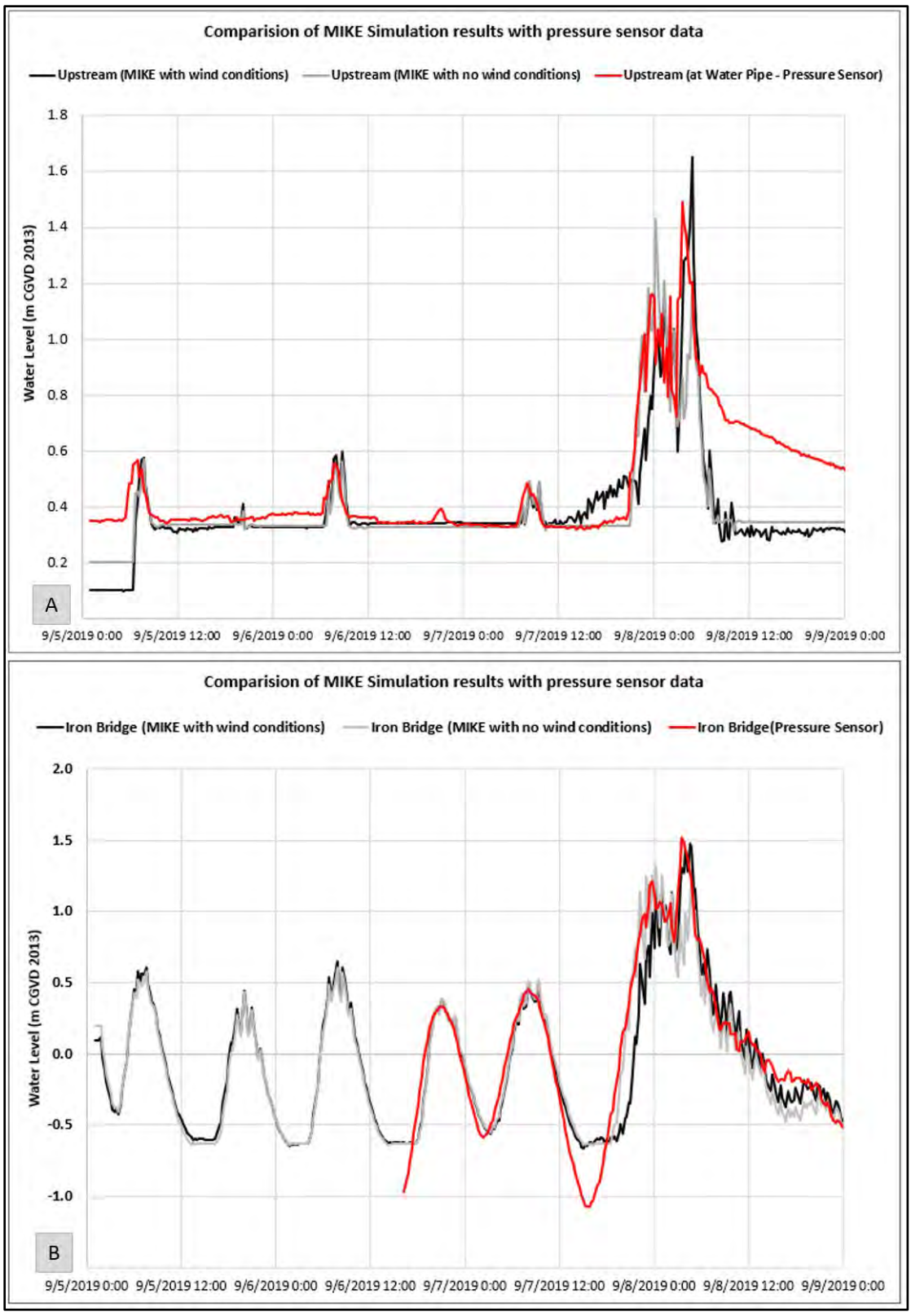

Figure 44 Comparison of 2-D model results and Hurricane Dorian simulation. A - Comparison of water levels at the Water Pipe sensor with (black) and without (grey) wind. B - Comparison of water levels at the Iron Bridge sensor with (black) and without (grey) wind.

8. Cost Assessment

Estimating the cost of any lidar project requires knowledge of specifics to the project including: ferry time to get the sensor to the study site from the airport of operations, size of the study area (can it be surveyed in one mission or will it require multiple missions), point density, ground control and validation requirements (will there need to be a ground field crew), tidal and time of day constraints (for example low tide only and light conditions suitable for aerial photography), data processing and classification requirements (minimum classes – bathymetry, land, water), deliverables – Classified LAS tiles, DSM, DEM, Intensity (normalized per flight line or not), orthophoto, report. The best approach is to ask a TB-lidar data provider to supply a quote for a given area of interest.

Similar for flood assessment, the GIS still-water or HAND approach requires pre-conditioning of the DEM to make it hydro-connected, in other worlds to ensure pathways for the water to move such as culverts and small bridges that may not be represented in the DEM must be added. In the case of using TB-lidar for hydrodynamic models, the computational requirements of such models are such that the full resolution of the lidar DEMs typically cannot be used and the models are degraded from 1 m to 3-5 m depending on the size of the study area. The HD models require more time to set up and establish boundary conditions, ensure the model is calibrated and validated, ideally against real-world observations and finally, to present the output in a clear and understandable way, ie. Flood map.

9. Recommend TB-lidar Specifications

TB-lidar can enhance flood mapping in many areas including coastal, estuarine and in-land flooding. Additional areas of enhanced capability include using the data from TB-lidar for coastal areas to begin to incorporate wave-runup into flood risk assessments. The most significant advancements of including TB-lidar in the flood assessment process are in the areas of enhanced hydrodynamic modelling, both for coastal inundation and for in-land flooding. The ability of TB-lidar to map the submerged terrain along the coast, in the riverbed and lakes makes it an ideal tool to produce the seamless DEM's required for such modelling. In addition, the data can be used to estimate bed roughness so that bed friction parameters can be assigned which influence the velocity of the water. Some of the main advantages of a hydrodynamic modelling approach over the GIS based still-water or HAND (Height Above Nearest Drainage – River GIS inundation) approach is that HD modelling produces both inundation levels and thus can derive flood water depth and current speeds which can be used to build more complex hazard maps. Another advantage of HD modelling over the still-water approach is that the still-water approach tends to overestimate the flood extent, although more study is required to exactly quantify this. The fact that most TB-lidar sensors are equipped with a camera system and aerial photos are acquired simultaneously with the lidar provides the ability to generate a high-resolution orthophoto for land use assessment, lidar error estimation and quantification and enhanced visualization of the flood event.

Recommendations for TB-lidar for coastal flood projects:

- Water clarity conditions should be monitored up to the flight
- In genera la low tide acquisition is better in that it increases the absolute depth of penetration, although there may be reasons for a high tide survey (water clarity, surf zone, time of day).
- Point density should be 2 pulses per square metre (2 pls/m^2).
- Minimum of 4 m depth should be achieved, thus allowing shallow water sensors to be used which are less expensive than deep-water ca. 1.5 X Secchi Depth specification.
- Data should be classified in standard hydrographic classes associated with LAS ver. 1.4 with the possible addition of Submerged Aquatic Vegetation (SAV).
- Deliverables include 1 m resolution grids of DEM, DSM (CGVD2013) and intensity.
- Orthophotos should be acquired simultaneously and delivered at ca. 5 cm resolution (RGB and NIR ideally).
- Report of flight parameters, including the aircraft trajectory and data acquisition parameters, processing steps and validation results.
- Vertical accuracy for topographic open features RMS < 15 cm, bathymetric non-vegetated features RMS < 15 cm.

Recommendations for TB-lidar for in-land projects:

- For best representation of the ground surface of the terrestrial floodplain the flight should be with leaf-off conditions (the spring is better than the fall as the dense grasses and shrubs typically have been flattened from the winter snowpack).
- Water clarity conditions should be monitored up to the flight, which is typically related with rainfall events
- If the river system drains to the ocean, the survey extent should extend into the estuary and coastal environment to allow coupled coastal-inland modelling
- Point density should be 2 pulses per square metre (2 pls/m^2).
- Minimum of 4 m depth should be achieved, thus allowing shallow water sensors to be used which are less expensive than deep-water ca. 1.5 X Secchi Depth specification.
- Data should be classified in standard hydrographic classes associated with LAS ver. 1.4 with the possible addition of Submerged Aquatic Vegetation (SAV).
- Deliverables include 1 m resolution grids of DEM, DSM (CGVD2013) and intensity.
- Orthophotos should be acquired simultaneously and delivered at ca. 5 cm resolution (RGB and NIR ideally).
- Report of flight parameters, including the aircraft trajectory and data acquisition parameters, processing steps and validation results.
- Vertical accuracy for topographic open features RMS < 15 cm, bathymetric non-vegetated features RMS < 15 cm.

10. Conclusions

The emergence of the latest generation of shallow water TB-lidar systems now allow for seamless land-water DEMs to be constructed, even in shallow areas less than 30 cm in depth. This technology allows the near-shore coastal bathymetry to be captured, which is critical as input into hydrodynamic models for assessing storm surge flooding and the impacts of long-term sea-level rise. The ability to capture the

near-shore topography also provides the critical data that is required to better understand and model the behavior and impacts of waves, including wave run-up.

The ability of the TB-lidar systems to seamlessly map the river floodplain and river channel perhaps offers the greatest advancements in improving our ability for fluvial flood risk assessment. In the past topographic lidar has been utilized to map the floodplain, however the river channels typically have been approximated or ignored because of the expense and time required to survey the channels manually. The ability to survey the river channel directly from the TB-lidar survey has the potential to vastly improve 2-D and 1-D hydrodynamic models that are typically employed for such flood assessments. The ability to construct seamless DEMs of the channel and floodplain may allow fluvial modelling to move from 1-D models into the more sophisticated and computationally intensive 2-D models where there is no interpolation between cross-section outputs to define the flood inundation extents. The ability of improved HD models will allow us to estimate both flood depth and current velocity, which play an important factor in determining the level of hazard a flood may pose to the critical infrastructure and people's lives. As with all models they depend on high quality bathymetric data as in input source and should be calibrated against known observations.

11. References

Allouis, T., Bailly, J.-S., Pastol, Y., Le Roux, C. (2010). Comparison of LiDAR waveform processing methods for very shallow water bathymetry using Raman, near-infrared and green signals. Earth Surf. Process. Landf. 35, 640–650. doi:10.1002/esp.1959.

Arifin, R.R., Kennedy, A.B. (2011). The evolution of large scale crescentic bars on the northern Gulf of Mexico coast. Mar. Geol. 285, 46–58. doi:10.1016/j.margeo.2011.04.003.

Brock and Perkins (2009). Brock, J.C., Purkis, S.J., 2009. The Emerging Role of Lidar Remote Sensing in Coastal Research and Resource Management. J. Coast. Res. 1–5. doi:10.2112/SI53-001.1

Canadian Hydrographic Services (2019). https://www.dfo-mpo.gc.ca/science/hydrography-hydrographie/data-acquisition-eng.html

Canadian Hydrographic Services (2013). Standards for Hydrographic Surveys. Edition 2.

Collin, A.; Long, B.; Archambault, P. (2011). Benthic Classifications Using Bathymetric LIDAR Waveforms and Integration of Local Spatial Statistics and Textural Features. J. Coast. Res. 2011, 86–98.

Collin, A.; Long, B.; Archambault, P. (2012). Merging land-marine realms: Spatial patterns of seamless coastal habitats using a multispectral LiDAR. Remote Sens. Environ. 2012, 123, 390–399.

Daniele, T. et al. (2019) Mapping river bathymetries: evaluating topobathymetric LiDAR survey. Earth Surface Processes and Landforms., Vol. 44 (2), 507-520. https://doi.org/10.1002/esp.4513.

International Hydrographic Organization (2008). IHO Standards for Hydrographic Surveys (Special Publication No. 44). Pp. 1-28. Monaco: International Hydrographic Bureau.

Johnson, Mike & Munasinghe, Dinuke & Eyelade, Damilola & Cohen, Sagy. (2019). An integrated evaluation of the National Water Model (NWM)–Height Above Nearest Drainage (HAND) flood mapping methodology. Natural Hazards and Earth System Sciences. 1-17. 10.5194/nhess-2019-82.

Kennedy, A.B., Slatton, K.C., Hsu, T.-J., Starek, M.J., Kampa, K. (2008). Ephemeral sand waves in the hurricane surf zone. Mar. Geol. 250, 276–280. doi:10.1016/j.margeo.2008.01.015.

Klemas, V. (2011) Beach Profiling and LIDAR Bathymetry: An Overview with case studies. Journal of Coastal research 27(6), 1019-1028. http://doi.org/10.3390/rs70505133.

Legleiter, C. J., & Kyriakidis, P. C. (2008). Spatial prediction of river channel topography by kriging. Earth Surface Processes and Landforms, 33, 155–161. http://doi.org/10.1002/esp.1579.

Mandlburger, G., Hauer, C., Wieser, M. and Pfeifer, N. (2015). Topo-Bathymetric LiDAR for Monitoring River Morphology and Instream Habitats- A Case Study at the Pielach River. Remote Sensing, 7, 6160-6195; doi:10.3390/rs70506160.

McKean, J., Tonina, D., Bohn, C., & Wright, C. W. (2014). Effects of bathymetric lidar errors on flow properties predicted with a multi-dimensional hydraulic model. Journal of Geophysical Research : Earth Surface, 119, 644–664. http://doi.org/10.1002/2013JF002897

McKean, J., Nagel, D., Tonina, D., Bailey, P., Wright, C. W., Bohn, C., & Nayegandhi, A. (2009). Remote Sensing of Channels and Riparian Zones with a Narrow-Beam Aquatic-Terrestrial LIDAR. Remote Sensing, (1), 1065–1096. http://doi.org/10.3390/rs1041065

National Science Technology Council (2016). National Coastal Mapping Strategy 1.0: Coastal Lidar Elevation for a 3-D Nation. https://iocm.noaa.gov/reports/IWG-OCM-Natl-Coastal-Mapping-Strat-DRAFT-PUBLIC-COMMENT-4.29.16.pdf.

Olabarrieta, M. and Warner, J.C. (2016) Inwave: The Infragagravity Wave Driver of Coast. COAWST Workshop. Woods Hole 2016.

Pan, Z., Glennie, C., Hartzell, P., Fernandez-diaz, J. C., Legleiter, C., & Overstreet, B. (2015). Performance Assessment of High Resolution Airborne Full Waveform LiDAR for Shallow River Bathymetry. Remote Sensing, 7, 5133–5159. http://doi.org/10.3390/rs70505133

Philpot and William (2019). Airborne Laser Hydrography II. https://doi.org/10.7298/jxm9-g971 https://ecommons.cornell.edu/handle/1813/58722

Reif, M.K., Wozencraft, J.M., Dunkin, L.M., Sylvester, C.S., Macon, C.L. (2013). A review of U.S. Army Corps of Engineers airborne coastal mapping in the Great Lakes. J. Gt. Lakes Res. 39, Supplement 1, 194–204. doi:10.1016/j.jglr.2012.11.002.
Paine, J.G., Andrews, J.R., Saylam, K., Tremblay, T.A. (2015). Airborne LiDAR-Based Wetland and Permafrost-Feature Mapping on an Arctic Coastal Plain, North Slope, Alaska, in: Remote Sensing of Wetlands: Applications and Advances. CRC Press, Boca Raton, FL, pp. 413–434.

Saylam, K., Hupp, J.R., Averett, A.R., Gutelius, W.F., and Gelhar, B.W. (2018). Airborne lidar bathymetry: assessing quality assurance and quality control methods with Leica Chiroptera examples. International Journal of Remote Sensing. Vo. 30 No. 8; doi: 10.1080/01431161.2018.1430916 pp. 2518-2542.

Skinner, K. (2009) Evaluation of LiDAR-Acquired Bathymetric and Topographic Data Accuracy in Various Hydrogeomorphic Settings in the Lower Boise River, Southwestern Idaho, 2007. USGS Scientific Investigations Report 2009-5260.

Thatcher, C. (2019) 3DEP Inland Bathymetry Mapping-Part of the Next Generation of Elevation & Hydrography Programs. USGS presentation.

Tulldahl, H.M., Wikström, S.A. (2012). Classification of aquatic macrovegetation and substrates with airborne lidar. Remote Sens. Environ. 121, 347–357. doi:10.1016/j.rse.2012.02.004.

Velasco, J., Molina, I., Martinez, E., Arquero, A., Prieto, J.F. (2014). Sea Bottom Classification by Means of Bathymetric LIDAR Data. Lat. Am. Trans. IEEE Rev. IEEE Am. Lat. 12, 590–595. doi:10.1109/TLA.2014.6868859.

Webster, T., McGuigan, K., Crowell, N., Collins, K. and MacDonald, C. (2016). Optimization of data collection and refinement of post-processing techniques for Maritime Canada's first shallow water topographic-bathymetric lidar survey. Journal of Coastal Research. Special issue on Advances in Topo-Bathymetric lidar. Vol 76: doi:10.2112/SI76-004, pp. 31-43.

Webster, T., McGuigan, K., Crowell, N., Collins, K. and MacDonald, C (2016). The use of Topo-bathymetric lidar to enhance Geological Structural Mapping in Maritime Canada. GeoScience Canada. Vol. 43; doi:10.12789/geocanj.2016.43.099, pp.199-210.

WSP (2020). Nova Scotia Flood Line Mapping: Test Case # 1: Pictou, River John. Report submitted to NS Department of Municipal Affairs.

Whyte, C. (2019). GeoGaragre Blog. Rising seas could double the number of severe coastal floods. https://blog.geogarage.com/2017/05/rising-seas-could-double-number-of.html?m=0

Zavalas, R., Ierodiaconou, D., Ryan, D., Rattray, A., Monk, J. (2014). Habitat Classification of Temperate Marine Macroalgal Communities Using Bathymetric LiDAR. Remote Sens. 6, 2154–2175. doi:10.3390/rs6032154.

12. Acknowledgements

The authors would like to thank the staff at AGRG-NSCC who assisted in some of the data processing of the River John Survey including Kevin McGuigan and Matt Roscoe. We would like to thank the various research assistance for their field work. We would like to thank Colin MacDonald of Internal Services for overseeing this research agreement between the province of NS and the NSCC. We would also like to acknowledge the staff at Municipal Affairs for their interest in and funding the project including Gordan Smith, Eva Wright, Daniel Bryce and Peter Horn.